iScience

CellPress
OPEN ACCESS

Article

Antispasmodic Drug Drofenine as an Inhibitor of Kv2.1 Channel Ameliorates Peripheral Neuropathy in Diabetic Mice

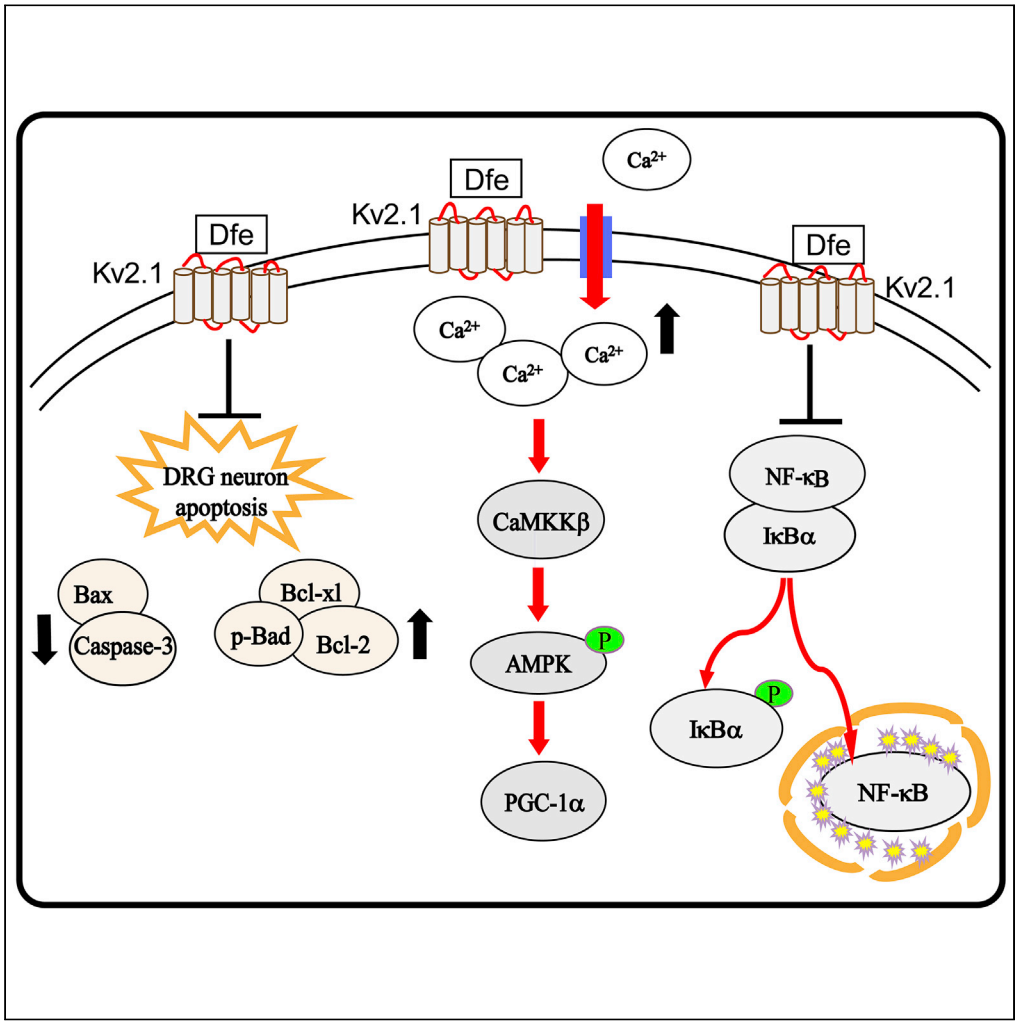

Xiaoju Xu, Xu Xu, Yanping Hao, ..., Yang Li, Jiaying Wang, Xu Shen

liyang@simm.ac.cn (Y.L.)
wangjy@njucm.edu.cn (J.W.)
xshen@njucm.edu.cn (X.S.)

HIGHLIGHTS

Antispasmodic drug drofenine (Dfe) ameliorates DPN-like pathology in diabetic mice

Dfe inhibits Kv2.1 channel and/or Kv2.1 mRNA and protein expression level

Dfe represses inflammation, apoptosis, and mitochondrial dysfunction in DPN mice

Kv2.1 inhibition is a therapeutic tactic and Dfe shows therapeutic potential for DPN

Xu et al., iScience *23*, 101617
October 23, 2020
https://doi.org/10.1016/j.isci.2020.101617

iScience

CellPress
OPEN ACCESS

Article

Antispasmodic Drug Drofenine as an Inhibitor of Kv2.1 Channel Ameliorates Peripheral Neuropathy in Diabetic Mice

Xiaoju Xu,[1,4] Xu Xu,[1,4] Yanping Hao,[2,3,4] Xialin Zhu,[1] Jian Lu,[1] Xingnan Ouyang,[1] Yin Lu,[1] Xi Huang,[1] Yang Li,[2,3,*] Jiaying Wang,[1,*] and Xu Shen[1,5,*]

SUMMARY

Diabetic peripheral neuropathy (DPN) is a common diabetic complication and has yet no efficient medication. Here, we report that antispasmodic drug drofenine (Dfe) blocks Kv2.1 and ameliorates DPN-like pathology in diabetic mice. The underlying mechanisms are investigated against the DPN mice with *in vivo* Kv2.1 knockdown through adeno associated virus AAV9-Kv2.1-RNAi. Streptozotocin (STZ) induced type 1 or *db/db* type 2 diabetic mice with DPN exhibited a high level of Kv2.1 protein in dorsal root ganglion (DRG) tissue and a suppressed neurite outgrowth in DRG neuron. Dfe promoted neurite outgrowth by inhibiting Kv2.1 channel and/or Kv2.1 mRNA and protein expression level. Moreover, it suppressed inflammation by repressing IκBα/NF-κB signaling, inhibited apoptosis by regulating Kv2.1-mediated Bcl-2 family proteins and Caspase-3 and ameliorated mitochondrial dysfunction through Kv2.1/CaMKKβ/AMPK/PGC1α pathway. Our work supports that Kv2.1 inhibition is a promisingly therapeutic strategy for DPN and highlights the potential of Dfe in treating this disease.

INTRODUCTION

Diabetic peripheral neuropathy (DPN) is a microvascular complication of diabetes afflicting more than two-thirds of diabetic patients (Liu et al., 2017; Hur et al., 2015; Vincent et al., 2011). Clinical characteristics of DPN include pain, paresthesia, and sensory loss, which are the risk factors for burns, injuries, and foot ulceration (Tesfaye et al., 2012; Bönhof et al., 2019). DPN severely affects the life quality of diabetic patients (Tesfaye et al., 2012; Boulton et al., 2005), but there is yet no efficient treatment against this disease.

DPN is a complicated disease with complex pathological mechanisms. For example, mitochondrial dysfunction is closely linked to the occurrence and development of DPN, and it occurs in sensory neurons and contributes to distal axonopathy in animal models of diabetic neuropathy (Roy Chowdhury et al., 2012). In addition, apoptosis is also associated with DPN, as exemplified by the finding that apoptosis is increased in acutely dissociated DRG neuron from 3- to 6-week-old diabetic rats (Srinivasan et al., 2000). Besides, inflammation is severely implicated in DPN, as indicated by the published reports that patients with DPN have high levels of TNF-α and IL-6 in plasma and rodents with DPN show increased levels of these two proinflammatory cytokines in sciatic nerve (Nguyen et al., 2012; Wilson, 2011; Duksal et al., 2016). Currently, dozens of clinical medications are available, including antioxidant alfa lipoic acid, aldose reductase inhibitor epalrestat, neurotrophic agent mecobalamin, and vasoactive drug alprostadil, but they only can alleviate the symptoms of DPN (Zhao et al., 2018; Hotta et al., 2006; Jiang et al., 2015, 2016). Thus, it is full of challenges to design new generation of anti-DPN drugs based on new therapeutic strategies.

Voltage-gated potassium (Kv) channels participate in varied physiological events, such as neuronal discharge pattern, synaptic integration, and neurotransmitter release (Yang et al., 2018; Romer et al., 2016; Wei et al., 2018). In structure, Kv channels are tetramers consisting of six transmembrane helixes and one pore subunit. Abnormal structure and dysfunction of Kv channel are tightly linked to many kinds of diseases, including neurodegenerative diseases (Chao et al., 2017; Frazzini et al., 2016). Kv channel family is divided into 12 subfamilies, including Kv1-12. Among them, Kv2 family mainly has two members, Kv2.1 and Kv2.2 (Johnson et al., 2018). Kv2.1 is enriched in varied tissues and organs such as brain tissue,

[1]Jiangsu Key Laboratory for Pharmacology and Safety Evaluation of Chinese Materia Medica, Nanjing University of Chinese Medicine, Nanjing 210023, China

[2]CAS Key Laboratory of Receptor Research, Shanghai Institute of Materia Medica, Chinese Academy of Sciences, 555 Zuchongzhi Road, Shanghai 201203, China

[3]University of Chinese Academy of Sciences, No. 19A Yuquan Road, Beijing 100049, China

[4]These authors contributed equally

[5]Lead Contact

*Correspondence: liyang@simm.ac.cn (Y.L.), wangjy@njucm.edu.cn (J.W.), xshen@njucm.edu.cn (X.S.)

https://doi.org/10.1016/j.isci.2020.101617

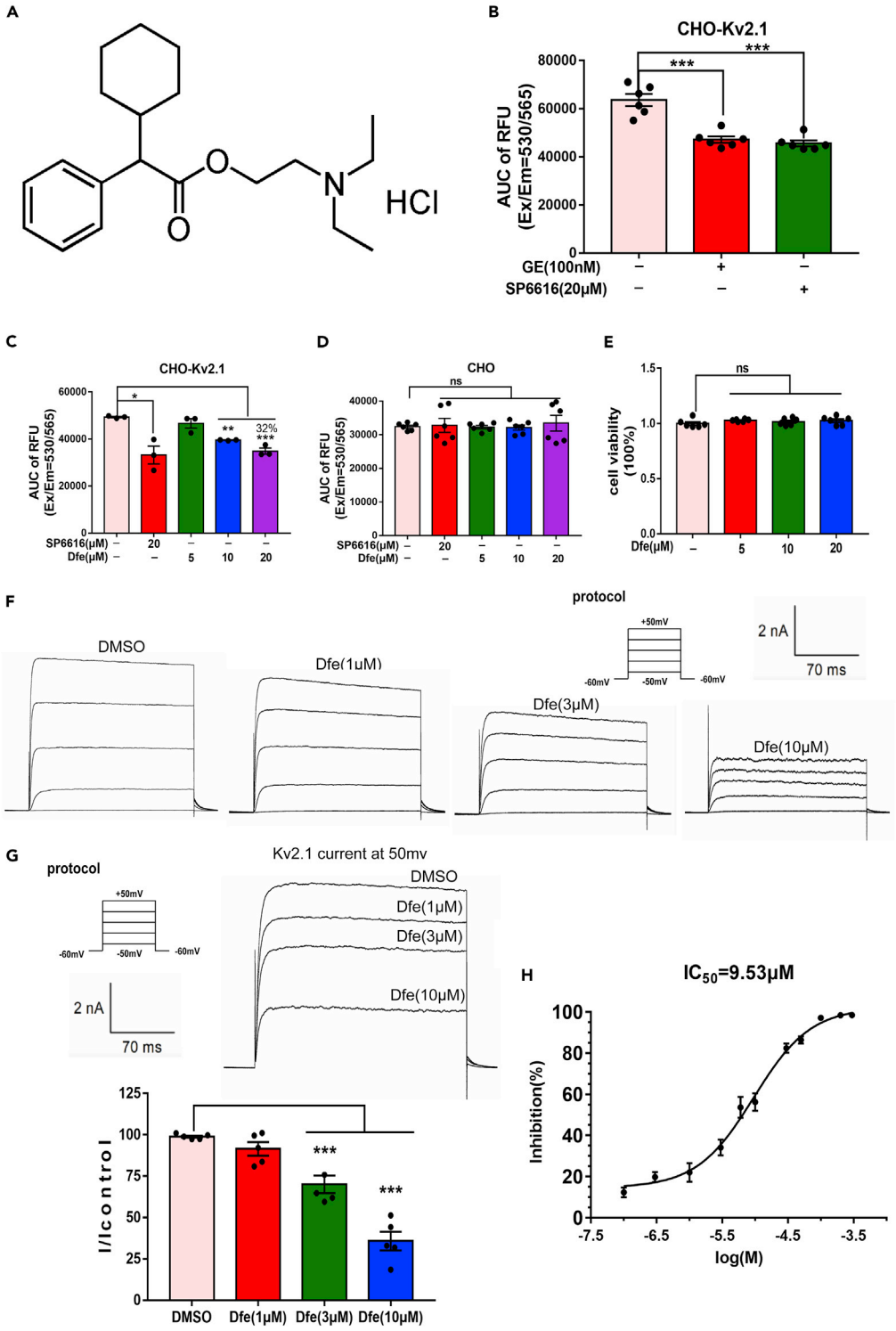

Figure 1. Dfe Was an Inhibitor of Kv2.1 Channel

SP6616 or GxTx-1E (GE) was used as a positive control.

(A) Chemical structure of Dfe.

(B) CHO-Kv2.1 cell was incubated with SP6616 (20 μM) or GxTx-1E (GE, 100 nM) and membrane potential dye for 30 min, and signal was recorded. Data were shown as area under the curve (AUC). N = 6. SP6616 versus DMSO by Student's t test: ***p < 0.001. GE versus DMSO by Student's t test: ***p < 0.001.

Figure 1. *Continued*

(C) CHO-Kv2.1 cell was incubated with SP6616 (20 μM) or Dfe (5, 10, 20 μM) and membrane potential dye for 30 min, and signal was recorded. Data were shown as area under the curve (AUC). N = 3. SP6616 versus DMSO by Student's t test: *p < 0.05. Dfe (5, 10, 20 μM) versus DMSO by one-way ANOVA with Dunnett's post hoc test: F (3, 8) = 29.5. **p < 0.01; ***p < 0.001.

(D) Membrane potential assay in CHO cell was conducted using the similar procedure to that in CHO-Kv2.1 cell. N = 6. SP6616 versus DMSO by Student's t test: ns. Dfe (5, 10, 20 μM) versus DMSO by one-way ANOVA with Dunnett's post hoc test: F (3, 20) = 0.2102. ns.

(E) Effect of Dfe (5, 10, 20 μM) on cell viability in CHO-Kv2.1 cell was detected by MTT assay. N = 6. Dfe (5, 10, 20 μM) versus DMSO by one-way ANOVA with Dunnett's post hoc test: F (3, 20) = 0.9416. ns.

(F) The whole-cell patch-clamp technique was used to detect the inhibitory effect of different concentrations of Dfe on Kv2.1 current in different cells, and the current curve of CHO-Kv2.1 cell was recorded.

(G) The electrophysiological data of multiple concentrations of Dfe on the same cell. N = 5. Dfe (1, 3, 10 μM) versus DMSO by one-way ANOVA with Dunnett's post hoc test: F (3, 16) = 41.48. ***p < 0.001.

(H) The 50% inhibitory concentration (IC50) of Dfe at 9.53 μM was detected by whole-cell patch-clamp technique. N = 4–9. All data were presented as means ± SEM.

peripheral tissue, retina, heart, and pancreas (Frolov et al., 2014; Jacobson et al., 2007; MacDonald, 2002). It has been also reported recently that Kv2.1 is also expressed in dorsal root ganglion (DRG) tissue (Tsantoulas et al., 2014) together with other Kv channels, including Kv1.1, Kv1.2, Kv1.4, Kv2.2, Kv3.4, Kv4.2, Kv4.3 (Cao et al., 2010). Kv2.2 is mainly distributed in brain tissue and participates in the periodic physiological processes of sleep and wakefulness (Hermanstyne et al., 2013).

Kv2.1 channel is involved in multiple functions of neuron, including cell discharge, classical delayed rectifier potassium current encoding, and neuronal action potential repolarization (Pathak et al., 2016). Abnormal sensory symptoms of DPN include pain and hypoalgesia in late stage of DPN (Liu et al., 2017), and Kv2.1 channel may function potently as an excitatory brake that can be compromised under chronic pain conditions (Cao et al., 2010). Demyelination is one of the mainly pathophysiological features of DPN, which can be relieved by protecting and promoting the neurite outgrowth of sensory neuron (Calcutt et al., 2017). Recently, it has been reported that Kv2.1 is essential for the excitability of neuron and functions of afferent myelination (Jensen et al., 2017). Abnormal Kv2.1 regulation may cause outflow of potassium ions resulting in apoptotic reaction cascades and further mitochondrial dysfunction and inflammation reaction (Ramirez et al., 2016; Pal et al., 2003). Thus, it is suggested that Kv2.1 channel be associated with demyelination, apoptosis, mitochondrial dysfunction, and inflammation, further addressing the mediation of Kv2.1 channel in the pathological process of DPN.

In the current work, we reported that antispasmodic drug drofenine (Dfe, drofenine hydrochloride was here used for better solubility. Figure 1A) as a Kv2.1 inhibitor efficiently ameliorated DPN-like pathology of diabetic mice. The mechanisms underlying the Kv2.1 inhibition-mediated amelioration have been intensively investigated by *in vivo* Kv2.1 knockdown assay with adeno associated virus AAV9-Kv2.1-RNAi in diabetic mice with DPN. Our work has highly supported that Kv2.1 inhibition is a promising therapeutic strategy for DPN and shed light on the potential of Dfe in the treatment of this disease.

RESULTS

Dfe Inhibits the Kv2.1 Channel

Dfe inhibited membrane potential in CHO-Kv2.1 cell: Kv2.1 inhibitor candidate was assayed by evaluating its inhibition against the membrane potential in CHO-Kv2.1 cell according to our previously published approach (Zhou et al., 2016). As indicated in Figures 1B and 1C, the known Kv2.1 inhibitors GxTx-1E (GE, 100 nM) (Lee et al., 2010) and SP6616 (20 μM) (Zhou et al., 2016) as well as Dfe could inhibit the membrane potential in CHO-Kv2.1 cell, F (3, 8) = 29.5. Furthermore, Dfe could neither inhibit the membrane potential in normal CHO cell (Figure 1D) (F (3, 20) = 0.2102) nor affect the cell viability of CHO-Kv2.1 cell (Figure 1E) (F (3, 20) = 0.9416).

Thus, all data revealed that Dfe might inhibit the Kv2.1 channel (Zhou et al., 2016).

Patch-clamp assay confirmed the inhibition of Dfe against Kv2.1 channel: We performed whole-cell patch-clamp on Kv2.1 channel stably expressed in CHO cells. As indicated in Figure 1H, Dfe blocked the channel

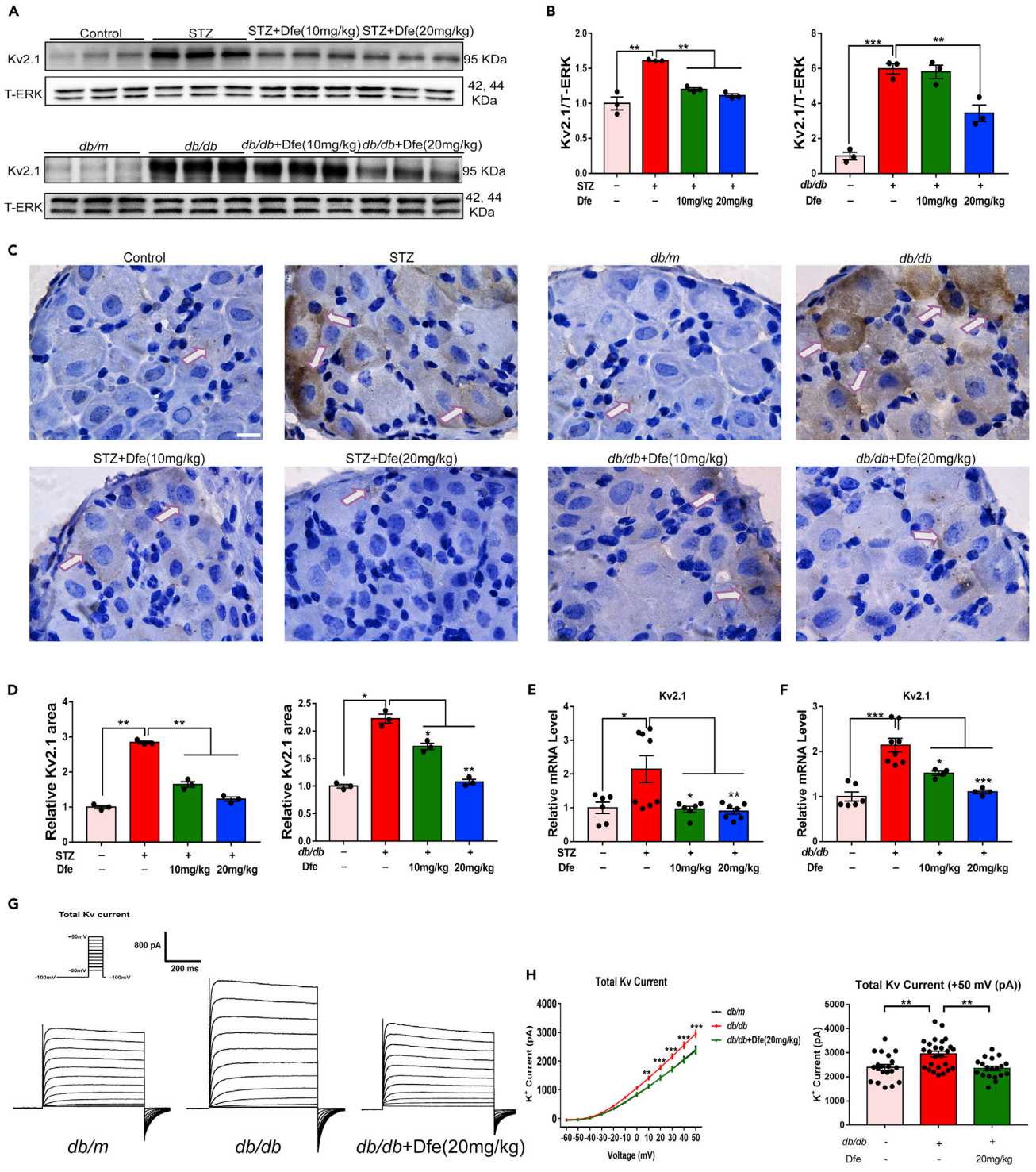

Figure 2. Dfe Reduced Kv2.1 Expression in DPN Mice

(A) Western blot results of Kv2.1 protein expression in control mice (Control, age-matched C57BL/6 mice as control in the related assay for STZ-induced type 1 diabetic mice with DPN; db/m, age-matched heterozygotes mice with nonpenetrant genotype as control in the related assay for db/db type 2 diabetic mice with DPN; the same hereinafter), DPN mice (STZ, type 1 diabetic mice with DPN; db/db, type 2 diabetic mice with DPN), and Dfe (10, 20 mg/kg)-treated DPN mice (STZ + Dfe, db/db + Dfe). T-ERK served as the loading control. N = 3.

Figure 2. *Continued*

(B) Quantitative analyses for (A). STZ versus Control by Student's t test: **p < 0.01. Dfe (10, 20 mg/kg) versus STZ by one-way ANOVA with Dunnett's post hoc test: F (2, 6) = 162.2. ***p < 0.001; db/db versus db/m by Student's t test: ***p < 0.001. Dfe (10, 20 mg/kg) versus db/db by one-way ANOVA with Dunnett's post hoc test: F (2, 6) = 13.31. **p < 0.01.

(C and D) Representative micrographs stained by Kv2.1 (brown) and quantitative analysis results based on Image (J) Scale bar: 25 μm. N = 3. STZ versus Control by Student's t test: ***p < 0.001. Dfe (10, 20 mg/kg) versus STZ by one-way ANOVA with Dunnett's post hoc test: F (2, 6) = 183.7. ***p < 0.001; db/db versus db/m by Student's t test: ***p < 0.001. Dfe (10, 20 mg/kg) versus db/db by one-way ANOVA with Dunnett's post hoc test: F (2, 6) = 79.87. **p < 0.01. ***p < 0.001.

(E and F) The qPCR result of Kv2.1 mRNA level in (E) control, STZ or Dfe (10, 20 mg/kg)-treated STZ mice (STZ + Dfe) and (F) db/m, db/db or Dfe (10, 20 mg/kg)-treated db/db mice (db/db + Dfe). N = 4–8. STZ versus Control by Student's t test: *p < 0.05. Dfe (10, 20 mg/kg) versus STZ by one-way ANOVA with Dunnett's post hoc test: F (2, 18) = 7.103. *p < 0.05, **p < 0.01; db/db versus db/m by Student's t test: ***p < 0.001. Dfe (10, 20 mg/kg) versus db/db by one-way ANOVA with Dunnett's post hoc test: F (2, 13) = 15.26. *p < 0.05. ***p < 0.001.

(G) Example traces of whole-cell currents in DPN mice were recorded by the whole-cell patch clamp. N = 19–26.

(H) Whole-cell currents changes of DRG neuron from DPN mice under different voltages and the current value at the highest voltage +50 mv was recorded by the whole-cell patch clamp. N = 19–26. db/db versus db/m by Student's t test: **p < 0.01. Dfe (20 mg/kg) versus db/db by Student's t test: **p < 0.01. ***p < 0.001. All data were presented as means ± SEM.

with an IC_{50} of 9.53 μM. Shown in Figures 1F and 1G were the example traces of Dfe in patch-camp electrophysiological recordings at 1, 3, and 10 μM (F (3, 16) = 41.48).

Dfe exhibits selectivity for Kv2.1 over Kv2.2: Since Kv2.1 is similar in sequence to Kv2.2 (Johnson et al., 2018; IUPHAR Ion Channel Database, https://www.guidetopharmacology.org/GRAC/ObjectDisplayForward?objectId=547&familyId=81&familyType=IC), we tested Dfe on the Kv2.2 channel by measuring membrane potential in CHO cells transfected with the pcDNA3.1a-Kv2.2 plasmid (Zhou et al., 2016) (Figure S1C). In whole-cell patch clamp, Dfe exhibited minimal inhibition of Kv2.2 at 1, 3, and 10 μM (Figures S1A and S1B) (F (3, 32) = 12.64). Taken together, Dfe is a weak (micromolar potency) inhibitor of Kv2.1 with selectivity over Kv2.2. However, it modulates butyrylcholinesterase and TRPV3 (Bodur et al., 2001; Deering-Rice et al., 2014) at the same low micromolar concentrations as that it blocks Kv2.1, indicating that it is not a selective Kv2.1 inhibitor. Actually, further studies are needed to determine if Dfe inhibits other Kv channels expressed in DRG neurons (Cao et al., 2010).

Dfe Treatment Suppressed Protein and mRNA Expressions of Kv2.1 in the DRG Tissue of DPN Mice

Next, we investigated the protein level of Kv2.1 channel in DRG tissue from DPN mice by western blot assay. As indicated in Figures 2A and 2B, Kv2.1 level in DRG tissue from either type 1 (STZ) or type 2 (*db/db*) DPN mice was obviously increased compared with that from normal mice (Control: age-matched C57BL/6 mice as a control in STZ mice-related assay; *db/m*: age-matched heterozygotes mice with nonpenetrant genotype as a control in *db/db* mice-related assay; the same hereinafter). Notably, the DRG tissue from the Dfe-treated DPN mice (STZ + Dfe, *db/db* + Dfe) exhibited lower level of Kv2.1 protein compared with that from the vehicle-treated DPN mice (STZ, *db/db*) (F (2, 6) = 162.2 for STZ mice, 13.31 for *db/db* mice).

In addition, immunohistochemistry (IHC)-based assay was also applied to investigate Kv2.1 expression in the DRG tissue from DPN mice by micrographs stained with Kv2.1 protein (brown) (Figure 2C), and the quantitation was indicated in Figure 2D by ImageJ. Similarly, the results also demonstrated the high level of Kv2.1 protein in the DRG tissue from either type of DPN mice (STZ, *db/db*) and Dfe treatment efficiently suppressed Kv2.1 protein level in DPN mice (Figures 2C and 2D) (F (2, 6) = 183.7 for STZ mice, 79.87 for *db/db* mice).

Moreover, qPCR assay results (Figures 2E and 2F, Figure S7) demonstrated that mRNA level of Kv2.1 was elevated in the DRG tissue of DPN mice compared with that of control mice and Dfe treatment obviously decreased the mRNA level of Kv2.1 (Figures 2E and 2F) (F (2, 18) = 7.103 for STZ mice, F (2, 13) = 15.26 for *db/db* mice).

Finally, we investigated the effect of Dfe on potassium flow in the DRG neuron from DPN mice by whole-cell patch clamp-related assay. As indicated in Figures 2G and 2H, the level of the total voltage-gated potassium current was upregulated in the DRG neuron from DPN mice compared with that from normal mice, and Dfe treatment efficiently suppressed such a level in DPN mice. These results are consistent with the above-mentioned western blot, IHC, and qPCR results.

Taken together, Dfe treatment suppressed protein and mRNA expression of Kv2.1 in the DRG tissue of DPN mice. The mechanism underlying this suppression remains to be determined but may not be related to Dfe's block of Kv2.1 current. Future studies are needed to determine whether Dfe treatment suppresses the expression of other Kv channels reported in DRG tissue. It must be noted here that, in a study of diabetic rats, the mRNA level of Kv2.1 was unchanged in DRGs, whereas mRNA levels of Kv1.4, Kv3.4, Kv4.2, and Kv4.3 were decreased (Cao et al., 2010). The reason for the difference between their results and ours is not clear.

Dfe Treatment Promoted Neurite Outgrowth of DRG Neurons in DPN Mice by Modulating Kv2.1 Channel

Dfe treatment promoted the neurite outgrowth of DRG neuron in DPN mice: By considering that neurodegeneration is highly related to the pathology of DPN (Jia et al., 2016), we detected the potential effect of Dfe treatment on the neurite outgrowth of DRG neuron in DPN mice.

As indicated in Figures 3A and 3B, the total neurite outgrowth of DRG neuron from either type of DPN mice (STZ, *db/db*) was repressed compared with that from the control mice (Control, *db/m*). Obviously, the total neurite outgrowth of DRG neuron was promoted from the Dfe-treated DPN mice (STZ + Dfe, *db/db* + Dfe) compared with that from the vehicle-treated DPN mice (STZ, *db/db*) (Figures 3C and 3D) ($F(2, 6) = 197.8$ for STZ mice, 215 for *db/db* mice). These results thus implied that Dfe treatment promoted the neurite outgrowth of DRG neuron in DPN mice.

Dfe treatment promoted the neurite outgrowth of DRG neuron in DPN mice by inhibiting Kv2.1 channel: Next, to verify that the above-mentioned Dfe-mediated promotion on the neurite growth of DRG neuron was via Kv2.1 inhibiting, *in vivo* Kv2.1 knockdown assay was carried out by injection of adeno associated virus AAV9-Kv2.1-RNAi into STZ mice. As indicated in Figures 3E and 3F, the neurite outgrowth of DRG neuron was enhanced from AAV9-Kv2.1-RNAi-injected STZ mice (STZ + AAV9-Kv2.1) compared with that from AAV9-negative control (NC) injected STZ mice (STZ + AAV9-NC). Notably, no significant difference was determined in neurite outgrowth of DRG neuron between Dfe-treated AAV9-Kv2.1-RNAi-injected STZ mice (STZ + AAV9-Kv2.1 + Dfe) and vehicle-treated AAV9-Kv2.1-RNAi-injected STZ mice (STZ + AAV9-Kv2.1) ($F(2, 6) = 0.06414$).

Given that Dfe was also ever reported to be M1 receptor antagonist (Kunysz et al., 1988), butyrylcholinesterase blocker (Bodur et al., 2001), and TRPV3 inhibitor (Deering-Rice et al., 2014), we also performed related assays to inspect whether or not the above-mentioned Dfe-mediated promotion on neurite outgrowth of DRG neuron was also through any of these three targets. As indicated in Figures S4A–S4G, none of M1 inhibitor Pirenzepine, TRPV3 si-RNA, and BCHE si-RNA could block the capability of Dfe in promoting the neurite growth of DRG neuron. These results thereby demonstrated that Dfe promoted the neurite growth of DRG neuron independent of any of these three targets.

Therefore, all results demonstrated that Dfe treatment enhanced neurite outgrowth of DRG neuron in DPN mice by inhibiting Kv2.1 channel.

Dfe Treatment Ameliorated Nerve Conduction Deficiency and Hypoalgesia of DPN Mice by Inhibiting Kv2.1 Channel

Next, the behavioral indicators (tactile allodynia and thermal sensitivity) and motor nerve conduction velocity of STZ and *db/db* mice were detected. As shown in Figure 4A and 4B, orange wide arrows above axis indicated Dfe injection, orange triangle below axis indicated behavioral tests (tactile allodynia and thermal sensitivity), orange pentacles indicated motor nerve conduction velocity (MNCV). The following neurological changes were found in DPN mice (STZ and *db/db*): nerve conduction deficiency, hypoalgesia, impairment in motor nerve conduction velocity (MNCV) (Figures 4C and 4D; $F(2, 33) = 9.92$ for STZ mice, 20.87 for *db/db* mice), enhanced sensitivity to mechanical stimuli (Figures 4E and 4F; $F(2, 33) = 130.2$ for STZ mice, 70.06 for *db/db* mice), and augmented thermal response (Figures 4G and 4H; $F(2, 33) = 6.211$ for STZ mice, 13.3 for *db/db* mice). Dfe treatment (10, 20 mg/kg) attenuated these pathological features in DPN mice (Figures 4C–4H).

Next, AAV9-Kv2.1-RNAi-based *in vivo* Kv2.1 knockdown assay against STZ mice was carried out to verify that the above-mentioned Dfe-mediated improvement on DPN-like pathology of DPN mice

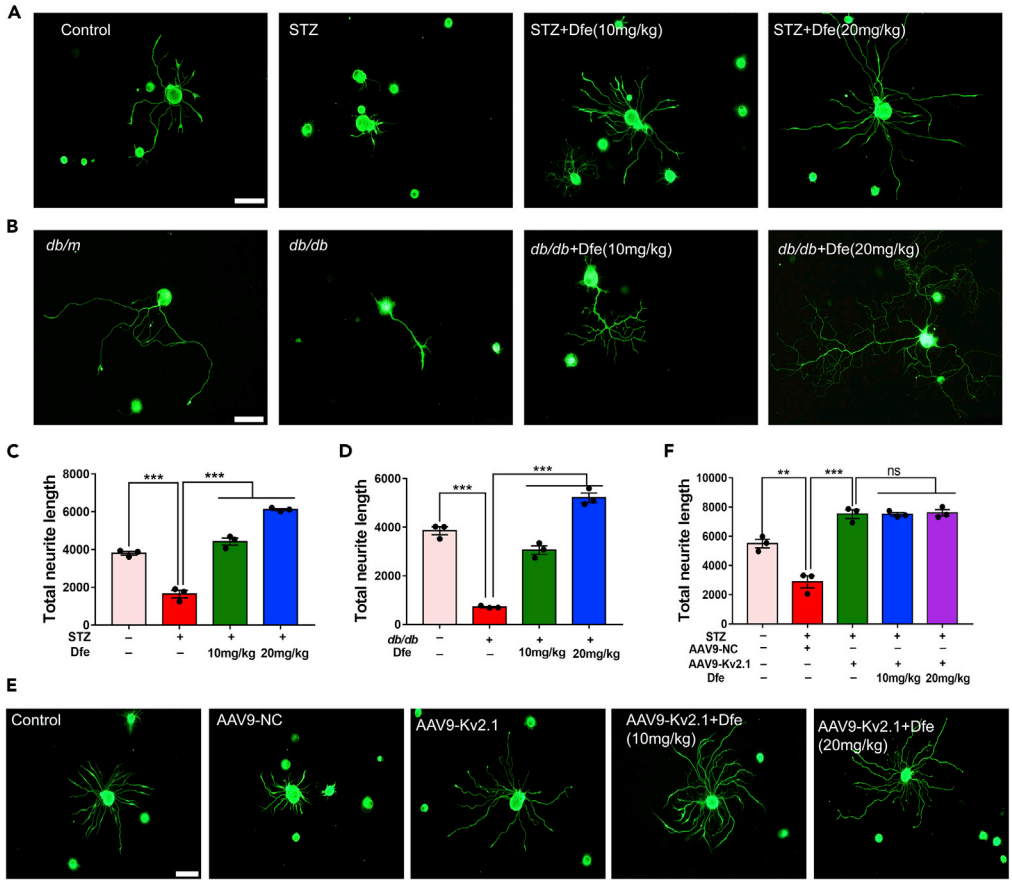

Figure 3. Dfe Treatment Promoted Neurite Outgrowth of DRG Neuron in DPN Mice by Inhibiting Kv2.1 Channel

(A and B) β-Tubulin III-immunostained sensory neurons from: (A) Control, STZ or Dfe (10, 20 mg/kg)-treated STZ mice (STZ + Dfe) and (B) db/m, db/db or Dfe (10, 20 mg/kg)-treated db/db mice (db/db + Dfe). Scale bar: 100 μm.

(C and D) Quantitative analyses of total neurite outgrowth for (A, B). N = 3. STZ versus Control by Student's t test: ***$p < 0.001$. Dfe (10, 20 mg/kg) versus STZ by one-way ANOVA with Dunnett's post hoc test: $F(2, 6) = 197.8$. ***$p < 0.001$; db/db versus db/m by Student's t test: ***$p < 0.001$. Dfe (10, 20 mg/kg) versus db/db by one-way ANOVA with Dunnett's post hoc test: $F(2, 6) = 215$. ***$p < 0.001$.

(E) β-Tubulin III immunofluorescence analyses in DRG neuron from Control, AAV9-NC-injected STZ mice (STZ + AAV9-NC), AAV9-Kv2.1-RNAi-injected STZ (STZ + AAV9-Kv2.1) and Dfe (10, 20 mg/kg)-treated AAV9-Kv2.1-RNAi-injected STZ mice (STZ + AAV9-Kv2.1 + Dfe). Scale bar: 100 μm.

(F) Quantitative analyses of total neurite outgrowth for (E). N = 3. STZ + AAV9-NC versus Control by Student's t test: **$p < 0.01$. STZ + AAV9-Kv2.1 versus STZ + AAV9-NC by Student's t test: ***$p < 0.001$. Dfe (10, 20 mg/kg) versus STZ + AAV9-Kv2.1 by one-way ANOVA with Dunnett's post hoc test: $F(2, 6) = 0.06414$. ns. All data were presented as means ± SEM.

was through inhibiting Kv2.1 channel. As expected, the results in Figures 4I–4K demonstrated that AAV9-Kv2.1-RNAi-injected STZ mice (STZ + AAV9-Kv2.1) exhibited improvements on MNCV, sensitivity to mechanical stimuli, and thermal response compared with AAV9-NC-injected STZ mice (STZ + AAV9-NC). Notably, no significant difference was determined in any of the potential improvements on the mentioned pathological behaviors between Dfe-treated AAV9-Kv2.1-RNAi-injected STZ mice (STZ + AAV9-Kv2.1 + Dfe) and vehicle-treated AAV9-Kv2.1-RNAi-injected STZ mice (STZ + AAV9-Kv2.1) ($F(2, 33) = 0.3592$ for MNCV, $F(2, 33) = 0.6631$ for tactile allodynia test, $F(2, 33) = 1.486$ for thermal sensitivity measurement).

Moreover, Dfe was also applied in the assay against normal (non-DPN) animals by performing the same behavioral tests as DPN mice (motor nerve conduction velocity test, tactile allodynia test, and thermal sensitivity measurement). As shown in Figure S11, Dfe treatment for 4 weeks rendered no effects on normal animals in terms of any of these behavioral activities.

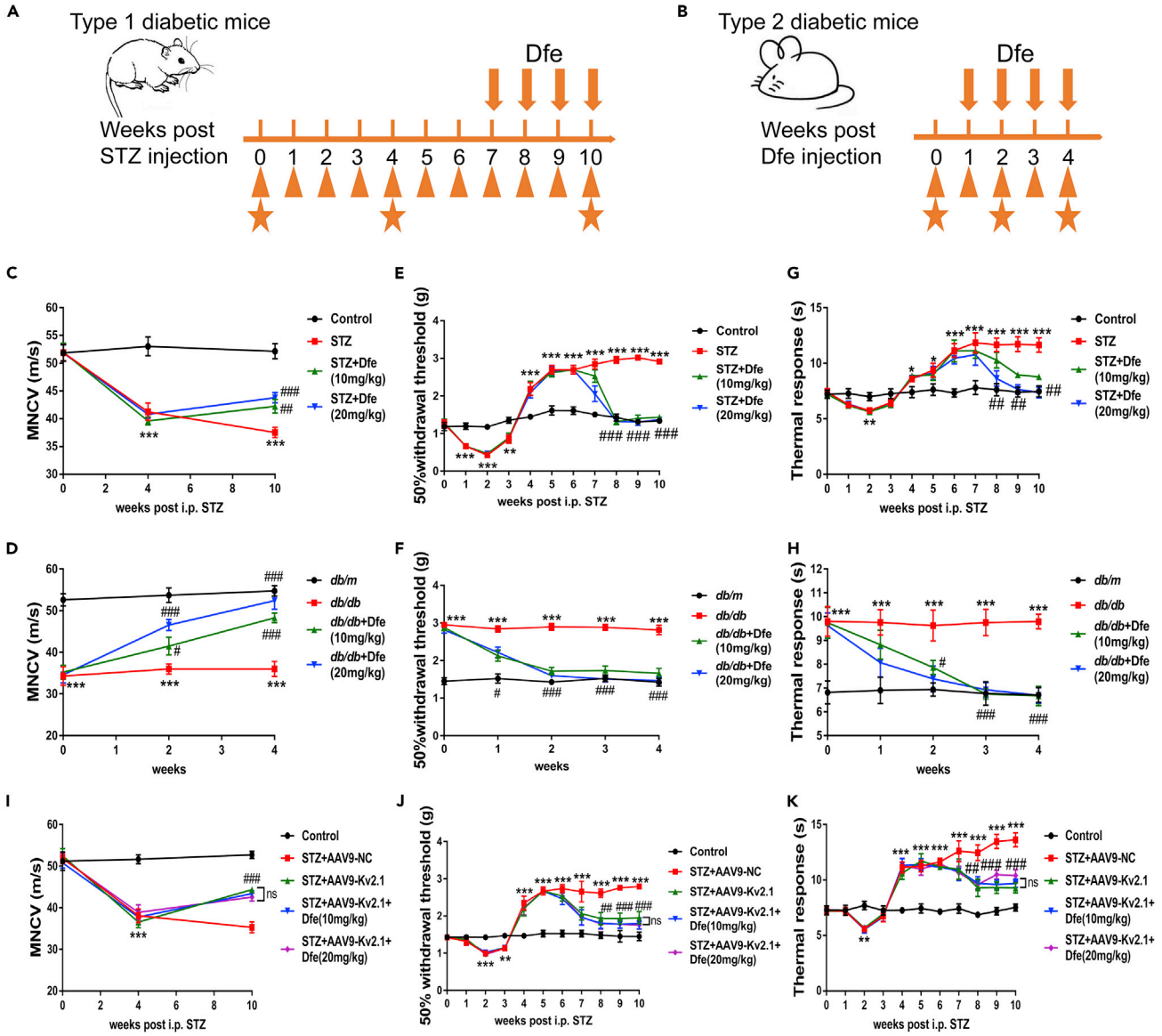

Figure 4. Dfe Treatment Ameliorated Nerve Conduction Deficiency and Hypoalgesia in DPN Mice by Inhibiting Kv2.1 Channel

(A and B) Experimental schedule of STZ and db/db mice. Orange wide arrows above axis indicated Dfe injection, orange triangle below axis indicated behavioral tests (tactile allodynia and thermal sensitivity), orange pentacles indicated motor nerve conduction velocity (MNCV).

(C and D) MNCV was assayed to detect nerve function of (C) STZ mice and (D) db/db mice. N = 12. STZ versus Control by Student's t test: ***p < 0.001. Dfe (10, 20 mg/kg) versus STZ by one-way ANOVA with Dunnett's post hoc test: F (2, 33) = 9.92. ##p < 0.01. ###p < 0.001; db/db versus db/m by Student's t test: ***p < 0.001. Dfe (10, 20 mg/kg) versus db/db by one-way ANOVA with Dunnett's post hoc test: F (2, 33) = 20.87. ###p < 0.001.

(E and F) Tactile allodynia test was used to evaluate neurological function of (E) STZ mice and (F) db/db mice. N = 12. STZ versus Control by Student's t test: ***p < 0.001. Dfe (10, 20 mg/kg) versus STZ by one-way ANOVA with Dunnett's post hoc test: F (2, 33) = 130.2. ###p < 0.001; db/db versus db/m by Student's t test: ***p < 0.001. Dfe (10, 20 mg/kg) versus db/db by one-way ANOVA with Dunnett's post hoc test: F (2, 33) = 70.06. ###p < 0.001.

(G and H) radial heat plate test was performed to evaluate neurological function of (G) STZ mice and (H) db/db mice. N = 12. STZ versus Control by Student's t test: ***p < 0.001. Dfe (10, 20 mg/kg) versus STZ by one-way ANOVA with Dunnett's post hoc test: F (2, 33) = 6.211. ##p < 0.01; db/db versus db/m by Student's t test: ***p < 0.001. Dfe (10, 20 mg/kg) versus db/db by one-way ANOVA with Dunnett's post hoc test: F (2, 33) = 13.3. ###p < 0.001.

(I–K) (I) MNCV assay, (J) tactile allodynia test, and (K) radial heat plate test were carried out in Control, AAV9-NC or AAV9-Kv2.1-RNAi-injected STZ (STZ + AAV9-NC, STZ + AAV9-Kv2.1) and Dfe (10, 20 mg/kg)-treated AAV9-Kv2.1-RNAi-injected STZ (STZ + AAV9-Kv2.1 + Dfe) mice. N = 12. In MNCV assay, STZ + AAV9-NC versus Control by Student's t test: ***p < 0.001, STZ + AAV9-Kv2.1 versus STZ + AAV9-NC by Student's t test: ###p < 0.001, Dfe (10, 20 mg/kg) versus STZ + AAV9-Kv2.1 by one-way ANOVA with Dunnett's post hoc test: F (2, 33) = 0.3592. ns; In tactile allodynia test, STZ + AAV9-NC versus Control by

Figure 4. *Continued*

Student's t test: ***p < 0.001, STZ + AAV9-Kv2.1 versus STZ + AAV9-NC by Student's t test: ###p < 0.001, Dfe (10, 20 mg/kg) versus STZ + AAV9-Kv2.1 by one-way ANOVA with Dunnett's post hoc test: F (2, 33) = 0.6631. ns; In radial heat plate test, STZ + AAV9-NC versus Control by Student's t test: ***p < 0.001, STZ + AAV9-Kv2.1 versus STZ + AAV9-NC by Student's t test: ###p < 0.001, Dfe (10, 20 mg/kg) versus STZ + AAV9-Kv2.1 by one-way ANOVA with Dunnett's post hoc test: F (2, 33) = 1.486. ns. All data were presented as means ± SEM.

Therefore, all data verified that Dfe treatment ameliorated nerve conduction deficiency and hypoalgesia of DPN mice by inhibiting Kv2.1 channel.

Dfe Treatment Improved Mitochondrial Dysfunction of DRG Neuron in DPN Mice through Kv2.1/CaMKKβ/AMPK/PGC-1α Pathway

Given that mitochondrial dysfunction is tightly linked to diabetic neuropathy and the lesion of peripheral sensory neuron (Chowdhury et al., 2013), we investigated the potential of Dfe treatment in ameliorating mitochondrial dysfunction of DRG neuron in DPN mice.

Dfe treatment improved mitochondrial dysfunction of DRG neuron in DPN mice by inhibiting Kv2.1 channel: In the assay, oxygen consumption rate (OCR) was investigated to evaluate mitochondrial respiratory function of DRG neuron from DPN mice. To our expect, Dfe treatment improved ATP production, maximal respiration, basal respiration, and spare respiratory capacity of DRG neuron from either STZ (Figures 5A and 5B) or *db/db* (Figures 5C and 5D) mice. Notably, no significant difference was found in the improvement on OCR of DRG neuron between Dfe-treated AAV9-Kv2.1-RNAi-injected STZ mice (STZ + AAV9-Kv2.1 + Dfe) and vehicle-treated AAV9-Kv2.1-RNAi-injected STZ mice (STZ + AAV9-Kv2.1) (Figures 5E and 5F).

By considering that downregulation of mitochondrial membrane potential (MMP) features mitochondrial apoptosis (Srinivasan et al., 2000), we also investigated the potential amelioration of Dfe treatment on MMP of DRG neuron in DPN mice by commercial MMP kit. As indicated in Figures 5G and 5H, MMP level of DRG neuron from either type of DPN mice (STZ, *db/db*) was expectedly reduced compared with that from normal mice (Control, *db*/m) but reversed by Dfe treatment as comparing the corresponding results from the Dfe-treated DPN mice (STZ + Dfe, *db/db* + Dfe) with those from the vehicle-treated DPN mice (STZ, *db/db*) (F (2, 6) = 40.94 for STZ mice, 7.388 for *db/db* mice). Obviously, these results implied that Dfe protected mitochondria from apoptosis in DRG neuron of DPN mice.

Together, all results demonstrated that Dfe treatment improved mitochondrial dysfunction of DRG neuron in DPN mice by inhibiting Kv2.1 channel.

Dfe treatment improved mitochondrial dysfunction through Kv2.1/CaMKKβ/AMPK/PGC-1α pathway: Given the pivotal role of AMPK/PGC-1α signaling in mitochondrial energy homeostasis (Calcutt et al., 2017; Herzig et al., 2018; Hashem et al., 2017), we detected the potential of Dfe treatment in regulating AMPK/PGC-1α signaling in DRG tissue of DPN mice by western blot. The results demonstrated that the levels of phosphorylated AMPK and PGC-1α were decreased from DPN mice (STZ, *db/db*) compared with those from control mice (Control, *db*/m) but increased from the Dfe-treated DPN mice (STZ + Dfe, *db/db* + Dfe) compared with the vehicle-treated DPN mice (STZ, *db/db*) (Figures 5I–5L) (for p-AMPK, F (2, 6) = 91.83 in STZ mice, 56.34 in *db/db* mice; for PGC1-α, F (2, 6) = 79.92 in STZ mice, 20.91 in *db/db* mice; for AMPK, F (2, 6) = 3.235 in STZ mice, 1.179 in *db/db* mice; for p-ACC, F (2, 6) = 3.615 in STZ mice, 4.675 in *db/db* mice).

It was noticed that AMPK can be phosphorylated then activated by Ca^{2+}/CaM-dependent protein kinase Came β (CaMKKβ) or the tumor suppressor LKB1 (Shaw et al., 2005). Since western blot results revealed that Dfe rendered no effects on LKB1 as comparing the LKB1 protein level in DRG tissue from Dfe-treated DPN mice (STZ + Dfe, *db/db* + Dfe) with that from vehicle-treated DPN mice (STZ, *db/db*) (Figure S2) (F (2, 6) = 0.6136 for STZ mice, 0.3575 for *db/db* mice), we here focused on the study on CaMKKβ in response to Dfe-mediated Kv2.1 regulation. To our expect, the results in Figures 5I–5L demonstrated that Dfe treatment promoted the level of CaMKKβ protein in DRG tissue from either type of DPN mice (F (2, 6) = 22.41 for STZ mice, 10.58 for *db/db* mice).

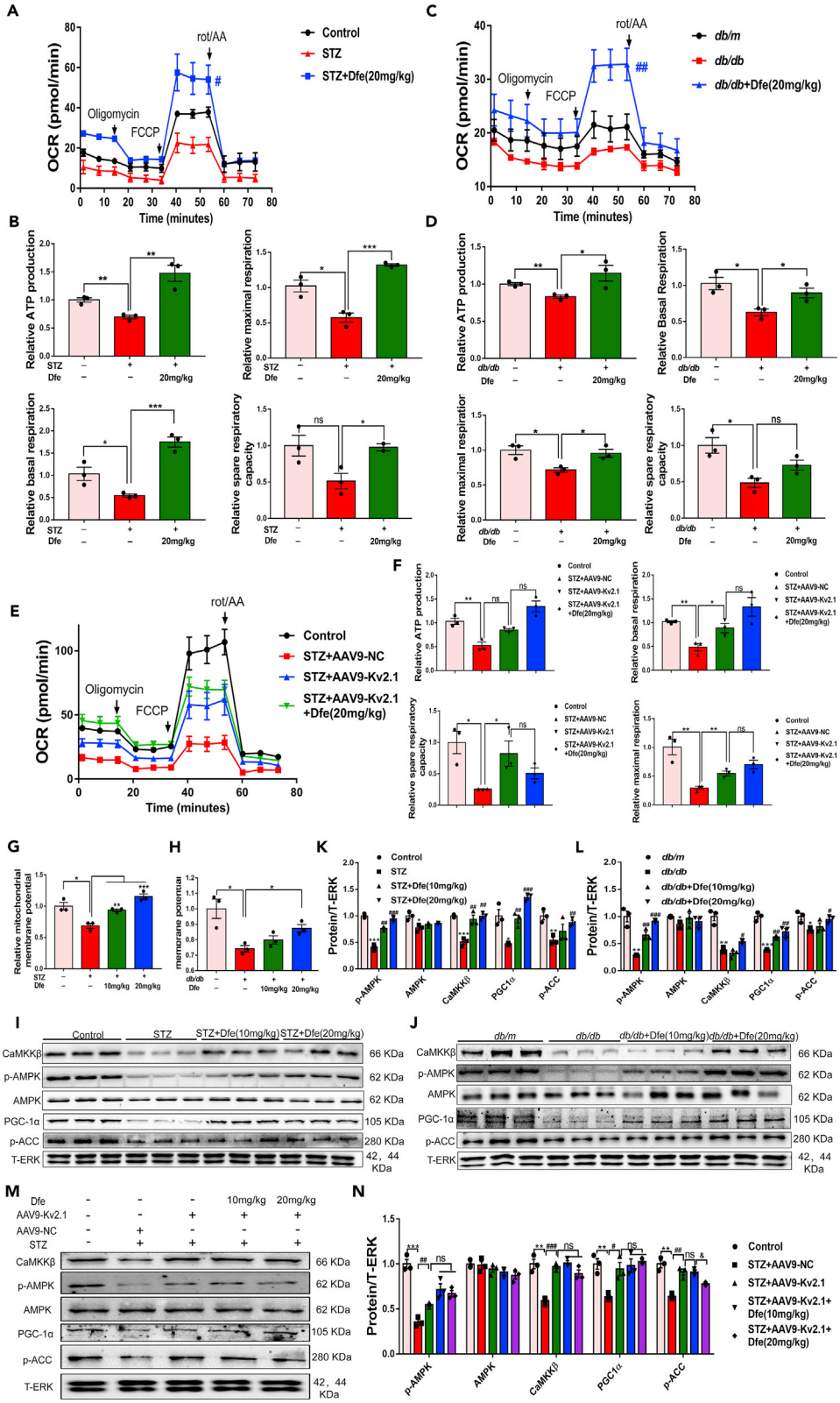
A
OCR (pmol/min)
Time (minutes)
rot/AA
Oligomycin
FCCP
Control
STZ
STZ+Dfe(20mg/kg)
C
db/m
db/db
db/db+Dfe(20mg/kg)
B
Relative ATP production
Relative maximal respiration
Relative basal respiration
Relative spare respiratory capacity
D
Relative Basal Respiration
E
STZ+AAV9-NC
STZ+AAV9-Kv2.1
STZ+AAV9-Kv2.1 +Dfe(20mg/kg)
F
G
Relative mitochondrial membrane potential
H
K
Protein/T-ERK
STZ+Dfe(10mg/kg)
STZ+Dfe(20mg/kg)
L
p-AMPK
AMPK
CaMKKβ
PGC1α
p-ACC
I
CaMKKβ
T-ERK
66 KDa
62 KDa
105 KDa
280 KDa
42, 44 KDa
J
M
Dfe
AAV9-Kv2.1
AAV9-NC
STZ
10mg/kg
20mg/kg
N

Figure 5. Dfe Improved Mitochondrial Dysfunction of DRG Neuron in DPN Mice through Kv2.1/CaMKKβ/AMPK/PGC-1α Pathway

(A and C) Oxygen consumption rate (OCR) was measured in DRG neuron from (A) Control, STZ or Dfe (20 mg/kg)-treated STZ mice (STZ + Dfe 20 mg/kg) and (C) db/m, db/db or Dfe (20 mg/kg)-treated db/db mice (db/db + Dfe 20 mg/kg) using XF96 analyzer. N = 4–7. STZ + Dfe (20 mg/kg) versus STZ by Student's t test: #p < 0.05; db/db + Dfe (20 mg/kg) versus db/db by Student's t test: ##p < 0.01.

(B and D) ATP production, basal respiration, spare respiratory capacity, and maximal respiration were measured in DRG neuron from (B) Control, STZ or Dfe (20 mg/kg)-treated STZ mice (STZ + Dfe 20 mg/kg) and (D) db/m, db/db or Dfe (20 mg/kg)-treated db/db mice (db/db + Dfe 20 mg/kg). N = 3. For ATP production, STZ versus Control by Student's t test: **p < 0.01, STZ + Dfe (20 mg/kg) versus STZ by Student's t test: **p < 0.01; db/db versus db/m by Student's t test: **p < 0.01, db/db + Dfe (20 mg/kg) versus db/db by Student's t test: *p < 0.05. For basal respiration, STZ versus Control by Student's t test: *p < 0.05, STZ + Dfe (20 mg/kg) versus STZ by Student's t test: ***p < 0.01; db/db versus db/m by Student's t test: *p < 0.05, db/db + Dfe (20 mg/kg) versus db/db by Student's t test: *p < 0.05. For spare respiratory capacity, STZ versus Control by Student's t test: ns, STZ + Dfe (20 mg/kg) versus STZ by Student's t test: *p < 0.05; db/db versus db/m by Student's t test: *p < 0.05, db/db + Dfe (20 mg/kg) versus db/db by Student's t test: ns. For maximal respiration, STZ versus Control by Student's t test: *p < 0.05, STZ + Dfe (20 mg/kg) versus STZ by Student's t test: ***p < 0.01; db/db versus db/m by Student's t test: *p < 0.05, db/db + Dfe (20 mg/kg) versus db/db by Student's t test: *p < 0.05.

(E) OCR data in DRG neuron from Control, AAV9-NC or AAV9-Kv2.1-RNAi-injected STZ (STZ + AAV9-NC, STZ + AAV9-Kv2.1) and Dfe (20 mg/kg)-treated AAV9-Kv2.1-RNAi-injected STZ mice (STZ + AAV9-Kv2.1 + 20 mg/kg) were obtained. N = 5–7. STZ + AAV9-Kv2.1 + Dfe versus STZ + AAV9-Kv2.1 by Student's t test: ns.

(F) ATP production, basal respiration, spare respiratory capacity, and maximal respiration were measured in DRG neuron from Control, AAV9-NC or AAV9-Kv2.1-RNAi-injected STZ (STZ + AAV9-NC, STZ + AAV9-Kv2.1) and Dfe (10, 20 mg/kg)-treated AAV9-Kv2.1-RNAi-injected STZ mice (STZ + AAV9-Kv2.1 + Dfe). N = 3. For ATP production, STZ + AAV9-NC versus Control by Student's t test: **p < 0.01, STZ + AAV9-Kv2.1 versus STZ + AAV9-NC by Student's t test: *p < 0.05. Dfe (20 mg/kg) versus STZ + AAV9-Kv2.1 by Student's t test: ns; For basal respiration, STZ + AAV9-NC versus Control by Student's t test: **p < 0.01, STZ + AAV9-Kv2.1 versus STZ + AAV9-NC by Student's t test: *p < 0.05. Dfe (20 mg/kg) versus STZ + AAV9-Kv2.1 by Student's t test: ns; For spare respiratory capacity, STZ + AAV9-NC versus Control by Student's t test: *p < 0.05, STZ + AAV9-Kv2.1 versus STZ + AAV9-NC by Student's t test: *p < 0.05. Dfe (20 mg/kg) versus STZ + AAV9-Kv2.1 by Student's t test: ns; For maximal respiration, STZ + AAV9-NC versus Control by Student's t test: **p < 0.01, STZ + AAV9-Kv2.1 versus STZ + AAV9-NC by Student's t test: **p < 0.01. Dfe (20 mg/kg) versus STZ + AAV9-Kv2.1 by Student's t test: ns.

(G and H) Mitochondrial membrane potential levels in DRG neuron from (G) Control, STZ or Dfe (10, 20 mg/kg)-treated STZ mice (STZ + Dfe) and (H) db/m, db/db and Dfe (10, 20 mg/kg)-treated db/db mice (db/db + Dfe). N = 3. STZ versus Control by Student's t test: *p < 0.05. Dfe (10, 20 mg/kg) versus STZ by one-way ANOVA with Dunnett's post hoc test: F (2, 6) = 40.94. **p < 0.01, ***p < 0.001; db/db versus db/m by Student's t test: *p < 0.05. Dfe (10, 20 mg/kg) versus db/db by one-way ANOVA with Dunnett's post hoc test: F (2, 6) = 7.388. *p < 0.05.

(I and J) Western blot results of CaMKKβ, AMPK, p-AMPK, PGC-1α and p-ACC in DRG homogenates from (I) Control, STZ or Dfe (10, 20 mg/kg)-treated STZ mice (STZ + Dfe) and (J) db/m, db/db or Dfe (10, 20 mg/kg)-treated db/db mice (db/db + Dfe). T-ERK was used as an internal control. N = 3.

(K and L) Quantitative analyses for (I) and (J). p-AMPK (STZ versus Control by Student's t test: ***p < 0.001, Dfe (10, 20 mg/kg) versus STZ by one-way ANOVA with Dunnett's post hoc test: F (2, 6) = 91.83. ##p < 0.01, ###p < 0.001; db/db versus db/m by Student's t test: **p < 0.01, Dfe (10, 20 mg/kg) versus db/db by one-way ANOVA with Dunnett's post hoc test: F (2, 6) = 56.34. ##p < 0.01, ###p < 0.001), AMPK (STZ versus Control by Student's t test: *p < 0.05, Dfe (10, 20 mg/kg) versus STZ by one-way ANOVA with Dunnett's post hoc test: F (2, 6) = 3.235. ns; db/db versus db/m by Student's t test: *p < 0.05, Dfe (10, 20 mg/kg) versus db/db by one-way ANOVA with Dunnett's post hoc test: F (2, 6) = 1.179. ns), CaMKKβ (STZ versus Control by Student's t test: ***p < 0.001, Dfe (10, 20 mg/kg) versus STZ by one-way ANOVA with Dunnett's post hoc test: F (2, 6) = 22.41. ##p < 0.01; db/db versus db/m by Student's t test: **p < 0.01, Dfe (10, 20 mg/kg) versus db/db by one-way ANOVA with Dunnett's post hoc test: F (2, 6) = 10.58. #p < 0.05), PGC1-α (STZ versus Control by Student's t test: *p < 0.05, Dfe (10, 20 mg/kg) versus STZ by one-way ANOVA with Dunnett's post hoc test: F (2, 6) = 79.92. ##p < 0.01, ###p < 0.001; db/db versus db/m by Student's t test: **p < 0.01, Dfe (10, 20 mg/kg) versus db/db by one-way ANOVA with Dunnett's post hoc test: F (2, 6) = 20.91. ##p < 0.01), p-ACC (STZ versus Control by Student's t test: **p < 0.01, Dfe (10, 20 mg/kg) versus STZ by one-way ANOVA with Dunnett's post hoc test: F (2, 6) = 3.615. ##p < 0.01; db/db versus db/m by Student's t test: *p < 0.05, Dfe (10, 20 mg/kg) versus db/db by one-way ANOVA with Dunnett's post hoc test: F (2, 6) = 4.675. #p < 0.05).

(M) Western blot results of CaMKKβ, AMPK, p-AMPK, PGC-1α, and p-ACC in DRG homogenates from Control, AAV9-NC or AAV9-Kv2.1-RNAi-injected STZ (STZ + AAV9-NC, STZ + AAV9-Kv2.1), and Dfe (10, 20 mg/kg)-treated AAV9-Kv2.1-RNAi-injected STZ mice (STZ + AAV9-Kv2.1 + Dfe). T-ERK was used as an internal control. DRG tissue isolated from three mice per group was mixed and homogenized.

(N) Quantitative analysis for (M). p-AMPK (STZ + AAV-NC versus Control by Student's t test: ***p < 0.001. STZ + AAV-Kv2.1 versus STZ + AAV-NC by Student's t test: ##p < 0.01. Dfe (10, 20 mg/kg) versus STZ + AAV-Kv2.1 by one-way ANOVA with Dunnett's post hoc test: F (2, 6) = 3.97. ns), AMPK (STZ + AAV-NC versus Control by Student's t test: ns. STZ + AAV-Kv2.1 versus STZ + AAV-NC by Student's t test: ns. Dfe (10, 20 mg/kg) versus STZ + AAV-Kv2.1 by one-way ANOVA with

Figure 5. *Continued*
Dunnett's post hoc test: F (2, 6) = 1.121. ns), CaMKKβ (STZ + AAV-NC versus Control by Student's t test: **p < 0.01. STZ + AAV-Kv2.1 versus STZ + AAV-NC by Student's t test: ###p < 0.001. Dfe (10, 20 mg/kg) versus STZ + AAV-Kv2.1 by one-way ANOVA with Dunnett's post hoc test: F (2, 6) = 3.787. ns), PGC1-α (STZ + AAV-NC versus Control by Student's t test: **p < 0.01. STZ + AAV-Kv2.1 versus STZ + AAV-NC by Student's t test: #p < 0.05. Dfe (10, 20 mg/kg) versus STZ + AAV-Kv2.1 by one-way ANOVA with Dunnett's post hoc test: F (2, 6) = 0.4457. ns), p-ACC (STZ + AAV-NC versus Control by Student's t test: **p < 0.01. STZ + AAV-Kv2.1 versus STZ + AAV-NC by Student's t test: ##p < 0.01. Dfe (10, 20 mg/kg) versus STZ + AAV-Kv2.1 by one-way ANOVA with Dunnett's post hoc test: F (2, 6) = 10.19. &p < 0.05). All data were presented as means ± SEM.

Moreover, western blot results (Figures 5M and 5N) indicated that the DRG tissue from AAV9-Kv2.1-RNAi-injected STZ mice (STZ + AAV9-Kv2.1) exhibited increased levels of CaMKKβ, p-AMPK, and PGC-1α proteins compared with that from AAV9-NC-injected STZ mice (STZ + AAV9-NC) and no significant difference was found in the regulation of any of these three proteins (CaMKKβ, p-AMPK, and PGC-1α) in DRG tissue between Dfe-treated AAV9-Kv2.1-RNAi-injected STZ mice (STZ + AAV9-Kv2.1 + Dfe) and vehicle-treated AAV9-Kv2.1-RNAi-injected STZ mice (STZ + AAV9-Kv2.1) (F (2, 6) = 3.97 for p-AMPK, F (2, 6) = 1.121 for AMPK, F (2, 6) = 3.787 for CaMKKβ, F (2, 6) = 0.4457 for PGC-1α, F (2, 6) = 10.19 for p-ACC).

Thus, all findings indicated that Dfe treatment improved mitochondrial dysfunction by regulating Kv2.1/CaMKKβ/AMPK/PGC-1α signaling. Additional studies will have to be undertaken to elucidate the molecular mechanisms coupling Kv2.1 to CaMKKβ/AMPK/PGC-1α signaling and to determine if Dfe-mediated suppression of Kv2.1 expression or blockade of Kv2.1 current by Dfe underlies this modulatory effect.

Dfe Treatment Alleviated Apoptosis of DRG Neuron in DPN Mice Involving Regulation of Bcl-2 Family Proteins and Caspase-3 by Inhibiting Kv2.1 Channel

Dfe treatment alleviated apoptosis of DRG neuron in DPN mice: As apoptosis was also tightly linked to DPN (Srinivasan et al., 2000), we detected the potential of Dfe treatment in preventing against apoptosis of DRG neuron in DPN mice (STZ, *db/db*). In the assay, images of double immune-fluorescent staining were detected to inspect the Annexin V-FITC and PI-labeled early and late apoptosis of DRG neuron from mice.

As indicated in Figures 6A–6C, the number of early or late apoptotic cells of DRG neuron from DPN mice (STZ, *db/db*) was increased compared with that from normal mice (Control, *db/m*) and the apoptotic response was markedly decreased nearly to normal level in DRG neuron from Dfe-treated DPN mice (STZ + Dfe, *db/db* + Dfe) compared with that from vehicle-treated DPN mice (STZ, *db/db*) (F (2, 6) = 27.24 for STZ mice, 14.77 for *db/db* mice).

In addition, we also investigated the prevention of Dfe treatment against the apoptosis of DRG neuron from DPN mice by IHC assay. Paraffin sections of DRG tissue were used, and DRG neuron was located by NeuN antibody and apoptotic cells were labeled by tunnel. As shown in Figures 6D–6F, the level of green fluorescence marked by tunnel (apoptotic cells) in DRG neuron was increased from DPN mice (STZ, *db/db*) compared with that from control mice (Control, *db/m*), and reduced from the Dfe-treated DPN mice (STZ + Dfe, *db/db* + Dfe) compared with the vehicle-treated DPN mice (STZ, *db/db*) (F (2, 6) = 54.09 for STZ mice, 41.48 for *db/db* mice).

Dfe treatment alleviated apoptosis of DRG neuron in DPN mice involving regulation of Bcl-2 family proteins and Caspase-3 by inhibiting Kv2.1 channel: Next, we investigated the potential regulation of Dfe against Bcl-2 family proteins (Bcl-xl, Bcl-2, p-Bad, and Bax) and Caspase-3 in response to the Dfe-mediated suppression against DRG neuron apoptosis in DPN mice by western blot assay.

As shown in Figures 6G–6J, the levels of anti-apoptotic (Bcl-xl, Bcl-2 and p-Bad) and pro-apoptotic (Bax and cleaved Caspase-3) proteins in DRG tissue were, respectively, decreased and increased from DPN mice (STZ, *db/db*) compared with those from control mice (Control, *db*/m), indicative of the apoptosis of DRG neuron in DPN mice. Obviously, the levels of these anti-apoptotic and pro-apoptotic proteins of DRG tissue were, respectively, increased and decreased from the Dfe-treated DPN mice (STZ + Dfe, *db/db* + Dfe) compared with those from the vehicle-treated DPN mice (STZ, *db/db*) (for Bcl-xl, F (2, 6) = 14.33 in STZ mice, 4.535 in *db/db* mice; for Bcl-2, F (2, 6) = 4.205 in STZ mice, 15.61 in *db/db* mice; for Bax, F (2, 6) = 11.06 in STZ mice, 8.733 in *db/db* mice; for p-Bad, F (2, 6) = 5.134 in STZ mice, 5.357 in *db/db* mice; for cleaved Caspase-3, F (2, 6) = 4.543 in STZ mice, 20.9 in *db/db* mice). All results

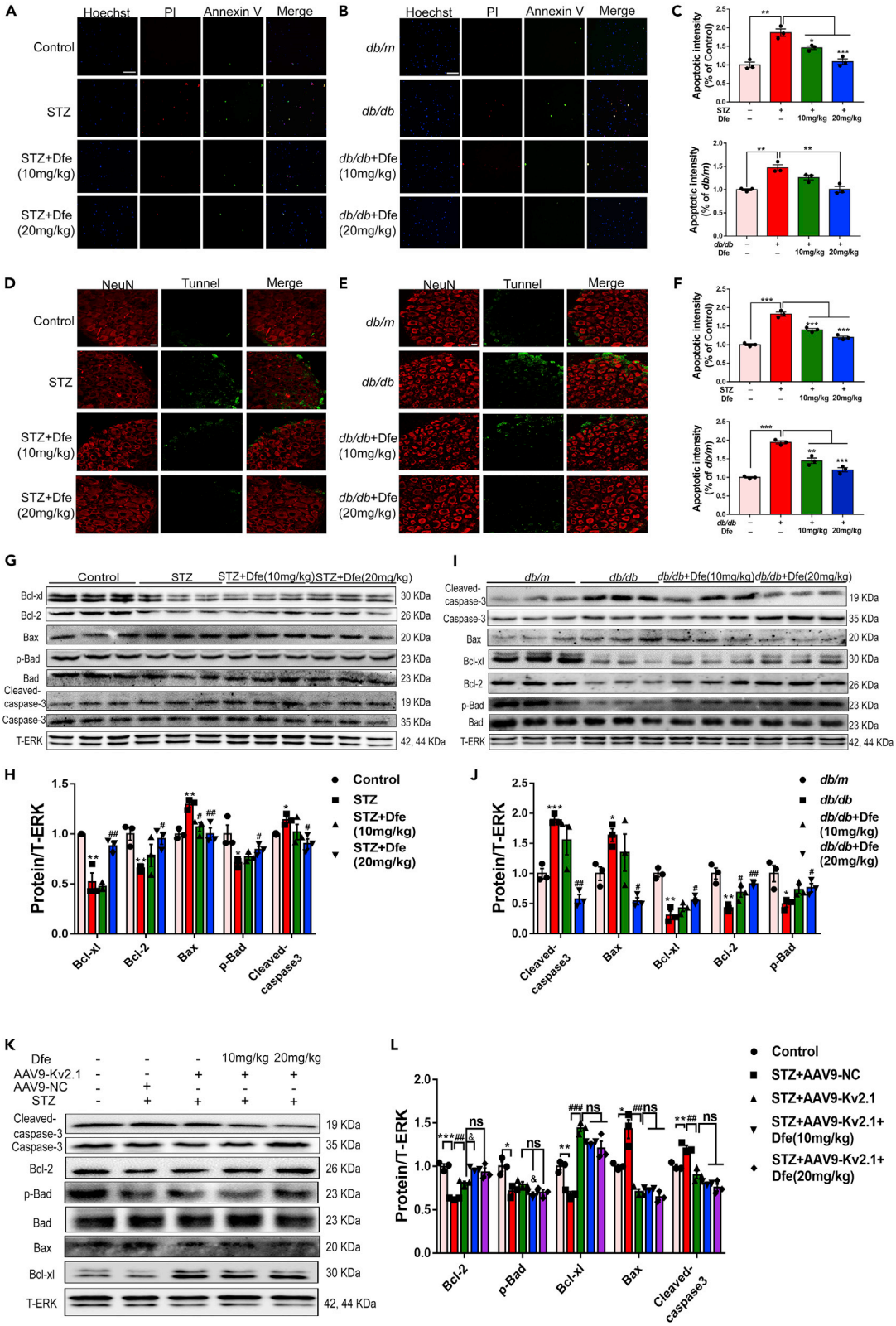
A
Hoechst
PI
Annexin V
Merge
Control
STZ
STZ+Dfe (10mg/kg)
STZ+Dfe (20mg/kg)
B
db/m
db/db
db/db+Dfe (10mg/kg)
db/db+Dfe (20mg/kg)
C
Apoptotic intensity (% of Control)
Apoptotic intensity (% of db/m)
STZ
Dfe
10mg/kg
20mg/kg
D
NeuN
Tunnel
Merge
E
F
G
Control
STZ
STZ+Dfe(10mg/kg)
STZ+Dfe(20mg/kg)
Bcl-xl
Bcl-2
Bax
p-Bad
Bad
Cleaved-caspase-3
Caspase-3
T-ERK
30 KDa
26 KDa
20 KDa
23 KDa
23 KDa
19 KDa
35 KDa
42, 44 KDa
I
db/m
db/db
db/db+Dfe(10mg/kg)
db/db+Dfe(20mg/kg)
19 KDa
35 KDa
20 KDa
30 KDa
26 KDa
23 KDa
23 KDa
42, 44 KDa
H
Protein/T-ERK
Control
STZ
STZ+Dfe (10mg/kg)
STZ+Dfe (20mg/kg)
Bcl-xl
Bcl-2
Bax
p-Bad
Cleaved-caspase3
J
db/m
db/db
db/db+Dfe (10mg/kg)
db/db+Dfe (20mg/kg)
K
Dfe
AAV9-Kv2.1
AAV9-NC
STZ
10mg/kg
20mg/kg
L
Control
STZ+AAV9-NC
STZ+AAV9-Kv2.1
STZ+AAV9-Kv2.1+ Dfe(10mg/kg)
STZ+AAV9-Kv2.1+ Dfe(20mg/kg)
ns

Figure 6. Dfe Treatment Alleviated Apoptosis of DRG Neuron in DPN Mice Involving Regulation of Bcl-2 Family Proteins and Caspase-3 by Inhibiting Kv2.1 Channel

(A and B) Representative images of double immune-fluorescent staining showing Annexin V-FITC and PI labeled early and late stage of apoptosis of DRG neuron from (A) Control, STZ or Dfe (10, 20 mg/kg)-treated STZ mice (STZ + Dfe) and (B) db/m, db/db or Dfe (10, 20 mg/kg)-treated db/db mice (db/db + Dfe). Hoechst was used to mark nuclei. Scale bar: 250 μm.

(C) Quantitative analyses for (A, B). N = 3. STZ versus Control by Student's t test: **p < 0.01. Dfe (10, 20 mg/kg) versus STZ by one-way ANOVA with Dunnett's post hoc test: F (2, 6) = 27.24. *p < 0.05, ***p < 0.001; db/db versus db/m by Student's t test: **p < 0.01. Dfe (10, 20 mg/kg) versus db/db by one-way ANOVA with Dunnett's post hoc test: F (2, 6) = 14.77. **p < 0.01.

(D and E) The paraffin sections of DRG tissue from (D) Control, STZ or Dfe (10, 20 mg/kg)-treated STZ mice (STZ + Dfe) and (E) db/m, db/db or Dfe (10, 20 mg/kg)-treated db/db mice (db/db + Dfe) were fluorescently stained for IHC assay. Neurons were located by NeuN and apoptotic cells were labeled by tunnel. Scale bar: 25 μm.

(F) Quantitative analyses for (D, E). N = 3. STZ versus Control by Student's t test: ***p < 0.001. Dfe (10, 20 mg/kg) versus STZ by one-way ANOVA with Dunnett's post hoc test: F (2, 6) = 54.09. ***p < 0.001; db/db versus db/m by Student's t test: ***p < 0.001. Dfe (10, 20 mg/kg) versus db/db by one-way ANOVA with Dunnett's post hoc test: F (2, 6) = 41.48. **p < 0.01, ***p < 0.001.

(G and I) Western blot results demonstrated that Kv2.1 inhibitor Dfe reduced apoptosis in DRG neuron from (G) Control, STZ or Dfe (10, 20 mg/kg)-treated STZ mice (STZ + Dfe) and (I) db/m, db/db or Dfe (10, 20 mg/kg)-treated db/db mice (db/db + Dfe) by regulating apoptosis-related proteins. T-ERK was used as loading control. N = 3.

(H and J) Quantitative analyses for (G, I). Bcl-xl (STZ versus Control by Student's t test: **p < 0.01, Dfe (10, 20 mg/kg) versus STZ by one-way ANOVA with Dunnett's post hoc test: F (2, 6) = 14.33. ##p < 0.01; db/db versus db/m by Student's t test: **p < 0.01, Dfe (10, 20 mg/kg) versus db/db by one-way ANOVA with Dunnett's post hoc test: F (2, 6) = 4.535. #p < 0.05), Bcl-2 (STZ versus Control by Student's t test: **p < 0.01, Dfe (10, 20 mg/kg) versus STZ by one-way ANOVA with Dunnett's post hoc test: F (2, 6) = 4.205. #p < 0.05; db/db versus db/m by Student's t test: **p < 0.01, Dfe (10, 20 mg/kg) versus db/db by one-way ANOVA with Dunnett's post hoc test: F (2, 6) = 15.61. #p < 0.05, ##p < 0.01), Bax (STZ versus Control by Student's t test: **p < 0.01, Dfe (10, 20 mg/kg) versus STZ by one-way ANOVA with Dunnett's post hoc test: F (2, 6) = 11.06. #p < 0.05. ##p < 0.01; db/db versus db/m by Student's t test: *p < 0.05, Dfe (10, 20 mg/kg) versus db/db by one-way ANOVA with Dunnett's post hoc test: F (2, 6) = 8.733. #p < 0.05), p-Bad (STZ versus Control by Student's t test: *p < 0.05, Dfe (10, 20 mg/kg) versus STZ by one-way ANOVA with Dunnett's post hoc test: F (2, 6) = 5.134. #p < 0.05; db/db versus db/m by Student's t test: *p < 0.05, Dfe (10, 20 mg/kg) versus db/db by one-way ANOVA with Dunnett's post hoc test: F (2, 6) = 5.357. #p < 0.05), Cleaved-caspase-3 (STZ versus Control by Student's t test: *p < 0.05, Dfe (10, 20 mg/kg) versus STZ by one-way ANOVA with Dunnett's post hoc test: F (2, 6) = 4.543. #p < 0.05; db/db versus db/m by Student's t test: ***p < 0.001, Dfe (10, 20 mg/kg) versus db/db by one-way ANOVA with Dunnett's post hoc test: F (2, 6) = 20.9. ##p < 0.01).

(K and L) Western blot assays in DRG tissue from Control, AAV9-NC or AAV9-Kv2.1-RNAi-injected STZ (STZ + AAV9-NC, STZ + AAV9-Kv2.1) and Dfe (10, 20 mg/kg)-treated AAV9-Kv2.1-RNAi-injected STZ mice (STZ + AAV9-Kv2.1 + Dfe). DRG tissue from three mice per group was mixed and homogenized. Bcl-xl (STZ + AAV-NC versus Control by Student's t test: **p < 0.01. STZ + AAV-Kv2.1 versus STZ + AAV-NC by Student's t test: ###p < 0.001. Dfe (10, 20 mg/kg) versus STZ + AAV-Kv2.1 by one-way ANOVA with Dunnett's post hoc test: F (2, 6) = 5.186. ns), Bcl-2 (STZ + AAV-NC versus Control by Student's t test: ***p < 0.001. STZ + AAV-Kv2.1 versus STZ + AAV-NC by Student's t test: ##p < 0.01. Dfe (10, 20 mg/kg) versus STZ + AAV-Kv2.1 by one-way ANOVA with Dunnett's post hoc test: F (2, 6) = 6.773. ns. #p < 0.05), Bax (STZ + AAV-NC versus Control by Student's t test: *p < 0.05. STZ + AAV-Kv2.1 versus STZ + AAV-NC by Student's t test: ##p < 0.01. Dfe (10, 20 mg/kg) versus STZ + AAV-Kv2.1 by one-way ANOVA with Dunnett's post hoc test: F (2, 6) = 2.492. ns), p-Bad (STZ + AAV-NC versus Control by Student's t test: *p < 0.05. STZ + AAV-Kv2.1 versus STZ + AAV-NC by Student's t test: ns. Dfe (10, 20 mg/kg) versus STZ + AAV-Kv2.1 by one-way ANOVA with Dunnett's post hoc test: F (2, 6) = 5.101. &p < 0.05, ns), Cleaved caspase-3 (STZ + AAV-NC versus Control by Student's t test: **p < 0.01. STZ + AAV-Kv2.1 versus STZ + AAV-NC by Student's t test: ##p < 0.01. Dfe (10, 20 mg/kg) versus STZ + AAV-Kv2.1 by one-way ANOVA with Dunnett's post hoc test: F (2, 6) = 4.272. &p < 0.05, ns). All data were presented as means ± SEM.

demonstrated that Dfe treatment alleviated apoptosis of DRG neuron in DPN mice involving regulation of Bcl-2 family proteins and Caspase-3.

As indicated in Figures 6K and 6L by western blot, DRG tissue from AAV9-Kv2.1-RNAi-injected STZ mice (STZ + AAV9-Kv2.1) exhibited, respectively, increased and decreased levels of the above-mentioned anti-apoptotic and pro-apoptotic proteins compared with those from AAV9-NC-injected STZ mice (STZ + AAV9-NC). However, no significant difference was determined in the levels of any anti-apoptotic or pro-apoptotic proteins in DRG tissue between Dfe-treated AAV9-Kv2.1-RNAi-injected STZ mice (STZ + AAV9-Kv2.1 + Dfe) and vehicle-treated AAV9-Kv2.1-RNAi-injected STZ mice (STZ + AAV9-Kv2.1) (F (2, 6) = 5.186 for Bcl-xl, 6.773 for Bcl-2, 2.492 for Bax, 5.101 for p-Bad, and 4.272 for cleaved Caspase-3).

Therefore, all data demonstrated that Dfe treatment alleviated apoptosis of DRG neurons from DPN mice involving regulation of Bcl-2 family proteins and Caspase-3 by inhibiting the Kv2.1 channel. It must be noted here that Kv2.1 has been identified as the channel responsible for the pro-apoptotic K^+ current increase in cortical, hippocampal, and cerebellar granule neurons; increased phosphorylation of Kv2.1, enhanced plasma membrane delivery of Kv2.1, and larger Kv2.1 K^+ currents produce an intracellular environment that enables DNA fragmentation, caspase activation, and apoptosis (Redman et al., 2007; Yao et al., 2009; Shah et al., 2014). Kv2.1 may play a similar pro-apoptotic role in DRG neurons, and Dfe by suppressing Kv2.1 expression or inhibiting Kv2.1 current may protect DRGs from apoptosis.

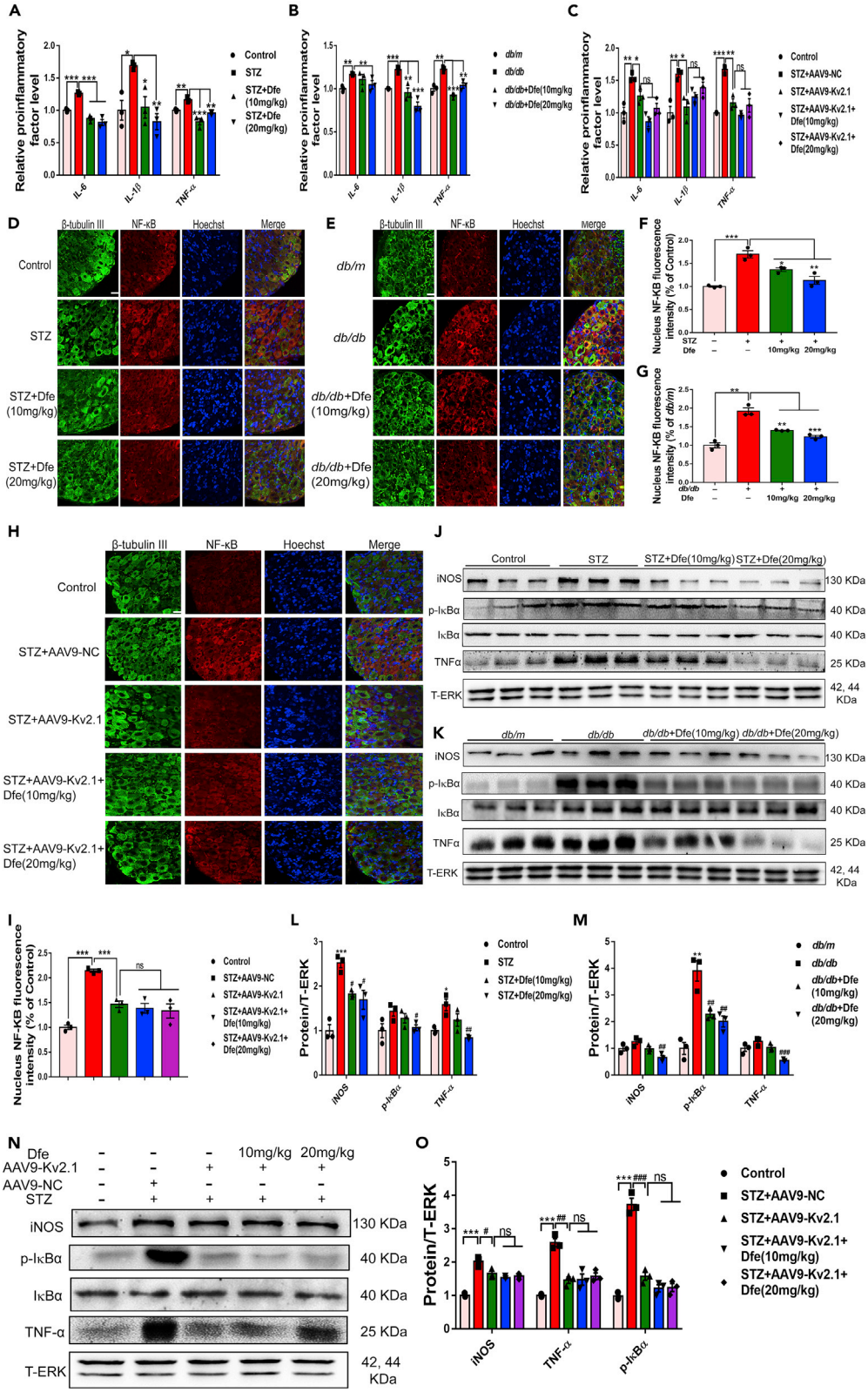
A
B
C
Relative proinflammatory factor level
IL-6
IL-1β
TNF-α
Control
STZ
STZ+Dfe (10mg/kg)
STZ+Dfe (20mg/kg)
db/m
db/db
db/db+Dfe(10mg/kg
db/db+Dfe(20mg/kg
STZ+AAV9-NC
STZ+AAV9-Kv2.1
STZ+AAV9-Kv2.1+ Dfe(10mg/kg)
STZ+AAV9-Kv2.1+ Dfe(20mg/kg)
D
E
β-tubulin III
NF-κB
Hoechst
Merge
Control
STZ
STZ+Dfe (10mg/kg)
STZ+Dfe (20mg/kg)
db/m
db/db
db/db+Dfe (10mg/kg)
db/db+Dfe (20mg/kg)
F
G
Nucleus NF-KB fluorescence intensity (% of Control)
Nucleus NF-KB fluorescence intensity (% of db/m)
STZ
Dfe
10mg/kg
20mg/kg
H
J
K
iNOS
p-IκBα
IκBα
TNFα
T-ERK
130 KDa
40 KDa
25 KDa
42, 44 KDa
I
L
M
Protein/T-ERK
N
O
AAV9-Kv2.1
AAV9-NC
Dfe
10mg/kg
20mg/kg

Figure 7. Dfe Treatment Reduced Inflammation in DPN Mice by Inhibiting Kv2.1 Channel

(A and B) ELISA analysis of proinflammatory cytokines IL-6, IL-1β, and TNF-α in the serum from (A) Control, STZ or Dfe (10, 20 mg/kg)-treated STZ mice (STZ + Dfe) and (B) db/m, db/db or Dfe (10, 20 mg/kg)-treated db/db mice (db/db + Dfe). N = 3. IL-6 (STZ versus Control by Student's t test: ***p < 0.001, Dfe (10, 20 mg/kg) versus STZ by one-way ANOVA with Dunnett's post hoc test: F (2, 6) = 55.44. ***p < 0.001; db/db versus db/m by Student's t test: **p < 0.01, Dfe (10, 20 mg/kg) versus db/db by one-way ANOVA with Dunnett's post hoc test: F (2, 6) = 1.884. **p < 0.01), IL-1β (STZ versus Control by Student's t test: *p < 0.05, Dfe (10, 20 mg/kg) versus STZ by one-way ANOVA with Dunnett's post hoc test: F (2, 6) = 13.92. *p < 0.05, **p < 0.01; db/db versus db/m by Student's t test: ***p < 0.001, Dfe (10, 20 mg/kg) versus db/db by one-way ANOVA with Dunnett's post hoc test: F (2, 6) = 23.84. **p < 0.01, ***p < 0.001), TNF-α (STZ versus Control by Student's t test: *p < 0.05, Dfe (10, 20 mg/kg) versus STZ by one-way ANOVA with Dunnett's post hoc test: F (2, 6) = 25.92. **p < 0.01, ***p < 0.001; db/db versus db/m by Student's t test: **p < 0.01, Dfe (10, 20 mg/kg) versus db/db by one-way ANOVA with Dunnett's post hoc test: F (2, 6) = 45.48. **p < 0.01, ***p < 0.001).

(C) ELISA analysis of proinflammatory cytokines IL-6, IL-1β, and TNF-α in the serum from Control, AAV9-NC or AAV9-Kv2.1-RNAi-injected STZ (STZ + AAV9-NC, STZ + AAV9-Kv2.1) and Dfe (10, 20 mg/kg)-treated AAV9-Kv2.1-RNAi-injected STZ mice (STZ + AAV9-Kv2.1 + Dfe). N = 3. IL-6 (STZ + AAV-NC versus Control by Student's t test: **p < 0.01. STZ + AAV-Kv2.1 versus STZ + AAV-NC by Student's t test: *p < 0.05. Dfe (10, 20 mg/kg) versus STZ + AAV-Kv2.1 by one-way ANOVA with Dunnett's post hoc test: F (2, 6) = 7.015. ns), IL-1β (STZ + AAV-NC versus Control by Student's t test: **p < 0.01. STZ + AAV-Kv2.1 versus STZ + AAV-NC by Student's t test: *p < 0.05. Dfe (10, 20 mg/kg) versus STZ + AAV-Kv2.1 by one-way ANOVA with Dunnett's post hoc test: F (2, 6) = 2.671. ns), TNF-α (STZ + AAV-NC versus Control by Student's t test: ***p < 0.001. STZ + AAV-Kv2.1 versus STZ + AAV-NC by Student's t test: **p < 0.01. Dfe (10, 20 mg/kg) versus STZ + AAV-Kv2.1 by one-way ANOVA with Dunnett's post hoc test: F (2, 6) = 2.023. ns).

(D and E) Paraffin sections of DRG tissue from (D) Control, STZ or Dfe (10, 20 mg/kg)-treated STZ mice (STZ + Dfe) and (E) db/m, db/db or Dfe (10, 20 mg/kg)-treated db/db mice (db/db + Dfe) for NF-κB immunostaining. Scale bar: 25 μm.

(F and G) Quantitative analyses for (D, E). N = 3. STZ versus Control by Student's t test: ***p < 0.001. Dfe (10, 20 mg/kg) versus STZ by one-way ANOVA with Dunnett's post hoc test: F (2, 6) = 16.15. *p < 0.05, **p < 0.01; db/db versus db/m by Student's t test: **p < 0.01. Dfe (10, 20 mg/kg) versus db/db by one-way ANOVA with Dunnett's post hoc test: F (2, 6) = 42.06. **p < 0.01, ***p < 0.001).

(H and I) Paraffin sections of DRG tissue from Control, AAV9-NC or AAV9-Kv2.1-RNAi-injected STZ (STZ + AAV9-NC, STZ + AAV9-Kv2.1) and Dfe (10, 20 mg/kg)-treated AAV9-Kv2.1-RNAi-injected STZ mice (STZ + AAV9-Kv2.1 + Dfe) for NF-κB immunostaining and quantitative analysis. N = 3. STZ + AAV-NC versus Control by Student's t test: ***p < 0.001. STZ + AAV-Kv2.1 versus STZ + AAV-NC by Student's t test: ***p < 0.001. Dfe (10, 20 mg/kg) versus STZ + AAV-Kv2.1 by one-way ANOVA with Dunnett's post hoc test: F (2, 6) = 0.3936. ns.

(J and K) Western blot results indicating the expressions of iNOS, TNF-α, phosphorylated IκBα and IκBα in DRG tissue from (J) Control, STZ or Dfe (10, 20 mg/kg)-treated STZ mice (STZ + Dfe) and (K) db/m, db/db or Dfe (10, 20 mg/kg)-treated db/db mice (db/db + Dfe). N = 3.

(L and M) Quantitative analyses for (J, K). iNOS (STZ versus Control by Student's t test: ***p < 0.001, Dfe (10, 20 mg/kg) versus STZ by one-way ANOVA with Dunnett's post hoc test: F (2, 6) = 9.918. *p < 0.05; db/db versus db/m by Student's t test: ns, Dfe (10, 20 mg/kg) versus db/db by one-way ANOVA with Dunnett's post hoc test: F (2, 6) = 12.43. ns. **p < 0.01), p-IκBα (STZ versus Control by Student's t test: ns, Dfe (10, 20 mg/kg) versus STZ by one-way ANOVA with Dunnett's post hoc test: F (2, 6) = 3.739. *p < 0.05; db/db versus db/m by Student's t test: **p < 0.01, Dfe (10, 20 mg/kg) versus db/db by one-way ANOVA with Dunnett's post hoc test: F (2, 6) = 15.79. **p < 0.01), TNF-α (STZ versus Control by Student's t test: *p < 0.05, Dfe (10, 20 mg/kg) versus STZ by one-way ANOVA with Dunnett's post hoc test: F (2, 6) = 11.13. ns, **p < 0.01; db/db versus db/m by Student's t test: ns, Dfe (10, 20 mg/kg) versus db/db by one-way ANOVA with Dunnett's post hoc test: F (2, 6) = 25.83. ns, ***p < 0.001).

(N and O) Western blot assays in DRG tissue from Control, AAV9-NC or AAV9-Kv2.1-RNAi-injected STZ (STZ + AAV9-NC, STZ + AAV9-Kv2.1) and Dfe (10, 20 mg/kg)-treated AAV9-Kv2.1-RNAi-injected STZ mice (STZ + AAV9-Kv2.1 + Dfe). DRG tissue from three mice per group were mixed and homogenized. iNOS (STZ + AAV-NC versus Control by Student's t test: ***p < 0.001. STZ + AAV-Kv2.1 versus STZ + AAV-NC by Student's t test: *p < 0.05. Dfe (10, 20 mg/kg) versus STZ + AAV-Kv2.1 by one-way ANOVA with Dunnett's post hoc test: F (2, 6) = 1.224. ns), p-IκBα (STZ + AAV-NC versus Control by Student's t test: ***p < 0.001. STZ + AAV-Kv2.1 versus STZ + AAV-NC by Student's t test: ***p < 0.001. Dfe (10, 20 mg/kg) versus STZ + AAV-Kv2.1 by one-way ANOVA with Dunnett's post hoc test: F (2, 6) = 3.089. ns), TNF-α (STZ + AAV-NC versus Control by Student's t test: ***p < 0.001. STZ + AAV-Kv2.1 versus STZ + AAV-NC by Student's t test: **p < 0.01. Dfe (10, 20 mg/kg) versus STZ + AAV-Kv2.1 by one-way ANOVA with Dunnett's post hoc test: F (2, 6) = 0.2739. ns). All data were presented as means ± SEM.

Dfe Treatment Reduced Inflammation in DPN Mice Involving IκBα/NF-κB Signaling by Inhibiting Kv2.1 Channel

Dfe treatment suppressed proinflammatory cytokines in DPN mice by inhibiting Kv2.1 channel: Given the close linkage of inflammation to DPN, we inspected the potential anti-inflammation effect of Dfe treatment on DPN mice by ELISA assay.

As indicated in Figures 7A and 7B, the levels of proinflammatory factors (IL-6, IL-1β, and TNF-α) were increased in the serum of DPN mice (STZ, *db/db*) compared with those of control mice (Control, *db/m*) but repressed in the serum of Dfe-treated DPN mice (STZ + Dfe, *db/db* + Dfe) compared with those of vehicle-treated DPN mice (STZ, *db/db*) (for IL-6, F (2, 6) = 55.44 in STZ mice, 1.884 in *db/db* mice; for IL-1β, F (2, 6) = 13.92 in STZ mice, 23.84 in *db/db* mice; for TNF-α, F (2, 6) = 25.92 in STZ mice, 45.48 in *db/db* mice). As indicated in Figure 7C, the levels of the proinflammatory cytokines (IL-6, IL-1β, and TNF-α) were all decreased in the serum of AAV9-Kv2.1-RNAi-injected STZ mice (STZ + AAV9-Kv2.1) compared with those of AAV9-NC-injected STZ mice (STZ + AAV9-NC). All these results thus demonstrated that either Kv2.1 inhibition or Dfe treatment could alleviate proinflammatory cytokines in DPN mice.

Notably, no significant difference was determined in the levels of any proinflammatory cytokines of the serum between Dfe-treated AAV9-Kv2.1-RNAi-injected STZ mice (STZ + AAV9-Kv2.1 + Dfe) and vehicle-treated AAV9-Kv2.1-RNAi-injected STZ mice (STZ + AAV9-Kv2.1) (F (2, 6) = 7.015 for IL-6, 2.671 for IL-1β, and 2.023 for TNF-α).

Together, all results demonstrated that Dfe treatment suppressed proinflammatory cytokines in DPN mice by inhibiting Kv2.1 channel.

Dfe treatment repressed NF-κB nuclear translocation by inhibiting Kv2.1 channel: NF-κB is a widely influential transcriptional regulator in chronic inflammatory process and, NF-κB dimer can be activated by various post-translational modifications to translocate into the nucleus, which is thought to be indicative of inflammation (Liu et al., 2018; Tak et al., 2001). With these facts, we inspected the potential regulation of Dfe treatment against NF-κB nuclear translocation in DRG neuron from DPN mice by immunostaining assay.

As shown in Figures 7D–7G, the number of NF-κB translocated into nuclei of DRG neuron was increased from DPN mice (STZ, *db/db*) compared with that from normal mice (Control, *db/m*) and decreased from the Dfe-treated DPN mice (STZ + Dfe, *db/db* + Dfe) compared with that from the vehicle-treated DPN mice (STZ, *db/db*) (F (2, 6) = 16.15 for STZ mice, 42.06 for *db/db* mice). Notably, the number of NF-κB translocated into the nuclei of DRG neuron from AAV9-Kv2.1-RNAi-injected STZ mice (STZ + AAV9-Kv2.1) was slightly decreased compared with that from AAV9-NC-injected STZ mice (STZ + AAV9-NC) (Figures 7H and 7I), and no significant difference was found in this number between Dfe-treated AAV9-Kv2.1-RNAi-injected STZ mice (STZ + AAV9-Kv2.1 + Dfe) and vehicle-treated AAV9-Kv2.1-RNAi-injected STZ mice (STZ + AAV9-Kv2.1) (Figures 7H and 7I) (F (2, 6) = 0.3936).

Therefore, all results indicated that Dfe treatment repressed NF-κB nuclear translocation by inhibiting Kv2.1 channel.

Dfe treatment suppressed inflammatory factors of DRG tissue in DPN mice by inhibiting Kv2.1 channel: Given that IκBα phosphorylation displays IκBα degradation and activates NF-κB dimer release into nucleus (Kumar et al., 2012), we detected the potential of Dfe treatment in regulating key inflammatory factors iNOS, TNF-α, and p-IκBα in DRG tissue of DPN mice by western blot assay.

As indicated in Figures 7J–7M, the protein levels of iNOS, TNF-α, and p-IκBα in DRG tissue were increased from DPN mice (STZ, *db/db*) compared with those from normal mice (Control, *db/m*) and decreased from Dfe-treated DPN mice (STZ + Dfe, *db/db* + Dfe) compared with vehicle-treated DPN mice (STZ, *db/db*) (for iNOS, F (2, 6) = 9.918 in STZ mice, 12.43 in *db/db* mice; for p-IκBα, F (2, 6) = 3.739 in STZ mice, 15.79 in *db/db* mice; for TNF-α, F (2, 6) = 11.13 in STZ mice, 25.83 in *db/db* mice). Thus, these results demonstrated that Dfe treatment suppressed inflammatory factors of DRG tissue in DPN mice.

Notably, we also determined that the protein levels of the above-mentioned inflammatory factors were repressed in DRG tissue from AAV9-Kv2.1-RNAi-injected STZ mice (STZ + AAV9-Kv2.1) compared with those from AAV9-NC-injected STZ mice (STZ + AAV9-NC), and no significant difference was found in any levels of these inflammatory factors of DRG neuron between Dfe-treated AAV9-Kv2.1-RNAi-injected STZ mice (STZ + AAV9-Kv2.1 + Dfe) and vehicle-treated AAV9-Kv2.1-RNAi-injected STZ mice (STZ + AAV9-Kv2.1) (Figures 7N and 7O) (F (2, 6) = 1.224 for iNOS, 3.089 for p-IκBα, and 0.2739 for TNF-α).

Together, all results implied that Dfe treatment suppressed inflammatory factors of DRG tissue in DPN mice by inhibiting Kv2.1 channel.

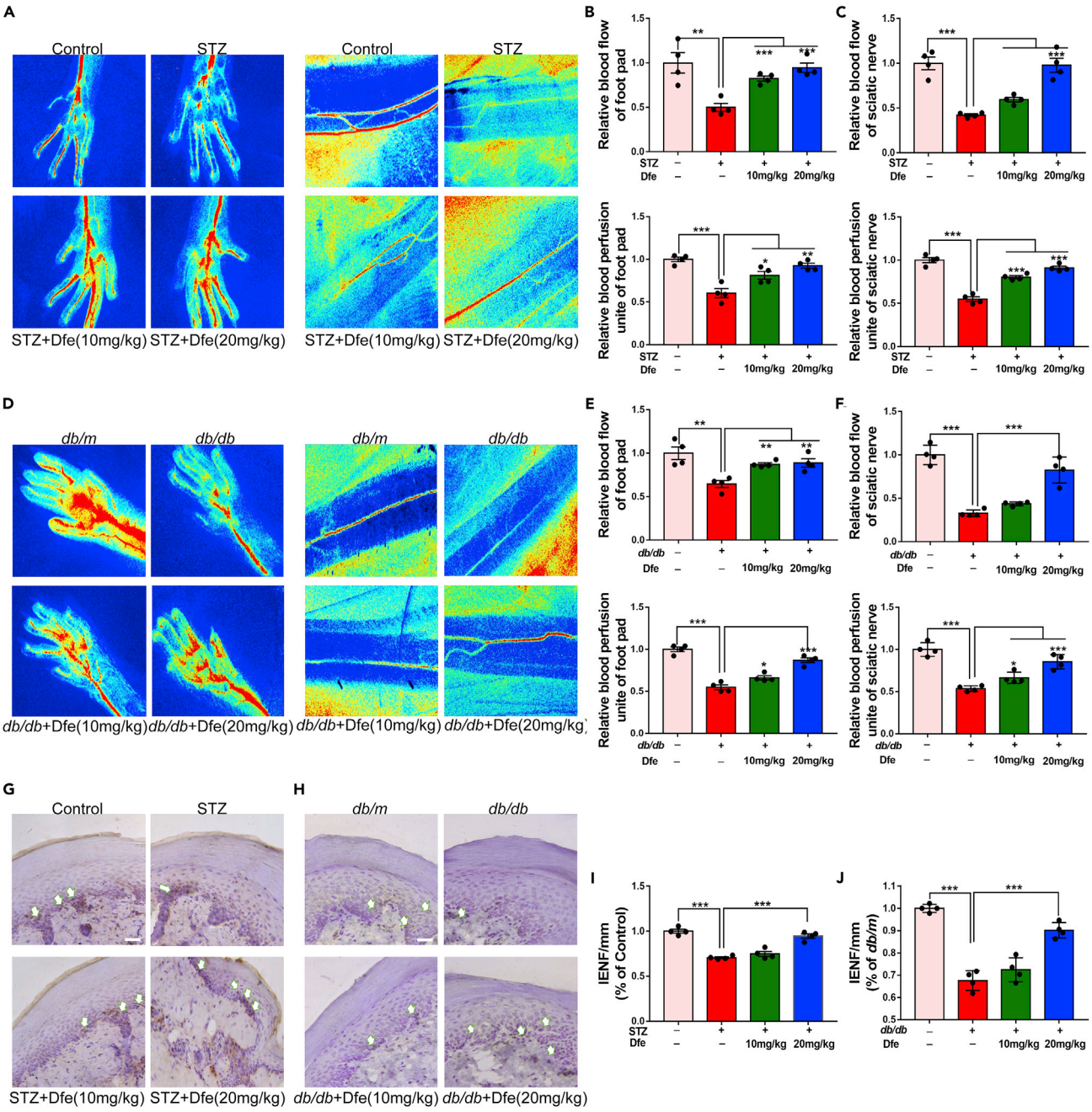

Figure 8. Dfe Treatment Improved Neurovascular Dysfunction in DPN Mice

(A and D) Representative images of blood flow velocity and blood perfusion unite of foot pad and sciatic nerve in (A) Control, STZ or Dfe (10, 20 mg/kg)-treated STZ mice (STZ + Dfe) and (D) db/m, db/db or Dfe (10, 20 mg/kg)-treated db/db mice (db/db + Dfe). N = 4.

(B, C, E, and F) Quantitative analyses of blood flow and blood perfusion of foot pad and sciatic nerve for (A, D). For blood flow of foot pad, STZ versus Control by Student's t test: **p < 0.01, Dfe (10, 20 mg/kg) versus STZ by one-way ANOVA with Dunnett's post hoc test: F (2, 9) = 28.2. ***p < 0.001; db/db versus db/m by Student's t test: **p < 0.01, Dfe (10, 20 mg/kg) versus db/db by one-way ANOVA with Dunnett's post hoc test: F (2, 9) = 12.95. **p < 0.01. For blood perfusion of foot pad, STZ versus Control by Student's t test: ***p < 0.001, Dfe (10, 20 mg/kg) versus STZ by one-way ANOVA with Dunnett's post hoc test: F (2, 9) = 14. *p < 0.05, **p < 0.01; db/db versus db/m by Student's t test: ***p < 0.001, Dfe (10, 20 mg/kg) versus db/db by one-way ANOVA with Dunnett's post hoc test: F (2, 9) = 37.14. *p < 0.05, ***p < 0.001. For blood flow of sciatic nerve, STZ versus Control by Student's t test: ***p < 0.001, Dfe (10, 20 mg/kg) versus STZ by one-way ANOVA with Dunnett's post hoc test: F (2, 9) = 34.78. ns, ***p < 0.001; db/db versus db/m by Student's t test: ***p < 0.001, Dfe (10, 20 mg/kg) versus db/db by one-way ANOVA with Dunnett's post hoc test: F (2, 9) = 33.6. ns, ***p < 0.001. For blood perfusion of sciatic nerve, STZ versus Control by Student's t test: ***p < 0.001, Dfe (10, 20 mg/kg) versus STZ by one-way ANOVA with Dunnett's post hoc test: F (2, 9) = 73.09. ***p < 0.001; db/db versus db/m by Student's t test: ***p < 0.001, Dfe (10, 20 mg/kg) versus db/db by one-way ANOVA with Dunnett's post hoc test: F (2, 9) = 24. *p < 0.05, ***p < 0.001.

Figure 8. *Continued*

(G and H) Representative sections of mice paw skin for PGP9.5 immunostaining (white arrows) in (G) Control, STZ or Dfe (10, 20 mg/kg)-treated STZ mice (STZ + Dfe) and (H) db/m, db/db or Dfe (10, 20 mg/kg)-treated db/db mice (db/db + Dfe). Scale bar: 100 μm. N = 4.

(I and J) Quantitative analysis results for (G, H). STZ versus Control by Student's t test: ***$p < 0.001$. Dfe (10, 20 mg/kg) versus STZ by one-way ANOVA with Dunnett's post hoc test: $F(2, 9) = 34.68$. ns, ***$p < 0.001$; db/db versus db/m by Student's t test: ***$p < 0.001$. Dfe (10, 20 mg/kg) versus db/db by one-way ANOVA with Dunnett's post hoc test: $F(2, 9) = 27.84$. ns, ***$p < 0.001$. All data were presented as means ± SEM.

Dfe Treatment Improved Neurovascular Impairment in DPN Mice

Dfe treatment improved peripheral tissue perfusion in DPN mice: Considering that neurovascular impairment is one of the leading causes for DPN (Nguyen et al., 2012; Van et al., 2013; Demiot et al., 2006), we inspected the potential amelioration of Dfe on neurovascular impairment in DPN mice. In the assay, Laser Speckle Contrast Imaging system was applied. As indicated in Figures 8A–8F, Dfe treatment increased the blood flow velocity and blood perfusion area of sciatic nerve and footpad in DPN mice (for blood flow of footpad, $F(2, 9) = 28.2$ in STZ mice, 12.95 in *db/db* mice; for blood flow of sciatic nerve, $F(2, 9) = 34.78$ in STZ mice, 33.6 in *db/db* mice; for blood perfusion of footpad, $F(2, 9) = 14$ in STZ mice, 37.14 in *db/db* mice; for blood perfusion of sciatic nerve, $F(2, 9) = 73.09$ in STZ mice, 24 in *db/db* mice).

Dfe treatment improved intraepidermal nerve fiber density in DPN mice: Neurovascular function is closely related to peripheral nerves and intradermal nerve fibers (IENFs) innervating dermis and epidermis, whereas skin biopsy-based IENF density measurement has been widely used in clinical testing of peripheral nerve function (Cameron et al., 2001; Lauria et al., 2010). With these facts, immunostaining assay was performed to examine the density of PGP9.5-positive IENF. As indicated in Figure 8, Dfe-treated DPN mice (STZ + Dfe, *db/db* + Dfe) exhibited increased density of PGP9.5-positive IENF in the plantar skin tissue compared with vehicle-treated DPN mice (STZ, *db/db*) ($F(2, 9) = 34.68$ for STZ mice, and 27.84 for *db/db* mice). Therefore, these results demonstrated that Dfe treatment improved intraepidermal nerve fiber density in DPN mice.

DISCUSSION

DPN is a long-term complication of diabetes with complicated pathogenesis, and there has yet been no efficient treatment against this disease. It is actually full of challenges to develop effective medication to treat DPN by new target and strategy. In the present work, we determined that inhibition of Kv2.1 channel is an effective therapeutic strategy for DPN and Dfe as an inhibitor of Kv2.1 is expected to find its valuable application in new generation of anti-DPN drug design. Dfe was found to efficiently alleviate DPN-like pathology by counteracting multiple risk factors including mitochondrial dysfunction, apoptosis, and inflammation in DPN mice. Additionally, Dfe is currently a clinically drug, its efficient amelioration of DPN-like pathology in the current work may provide valuable references for further anti-DPN drug discovery.

Mitochondrial dysfunction and apoptosis are mainly pathogenetic features of DPN (Srinivasan et al., 2000), and improvement of mitochondrial dysfunction is believed to be a promising strategy for DPN (Roy Chowdhury et al., 2012). Kv2.1 overexpression in β cell was reported to enhance cell response to mitochondrial dysfunction and endoplasmic reticulum stress thus promoting cell apoptosis (Kim et al., 2012; Pal et al., 2003). Here, we found that Dfe as a Kv2.1 inhibitor was capable of improving mitochondrial bioenergetics profiles in DRG neuron. Consistent with the previous report that AMPK activation in sensory neuron was related to the transient elevation of intracellular Ca^{2+} concentration (Calcutt et al., 2017), we also determined that Dfe stimulated extracellular calcium influx in DRG neuron (Figure S5) and activated Ca^{2+}-dependent kinase CaMKKβ activity in DPN mice (Figure 5). We found that Dfe improved mitochondrial dysfunction of DRG neuron by Kv2.1/CaMKKβ/AMPK/PGC-1α signaling. Bcl-2 family proteins are central regulators of apoptosis with either anti-apoptotic or pro-apoptotic function (Chan et al., 2004), and Caspase-3 is indispensable for apoptotic chromatin condensation and DNA fragmentation (Porter et al., 1999). Here, we determined that Dfe alleviated apoptosis of DRG neuron involving regulation of Bcl-2 family proteins and Caspase-3 by inhibiting Kv2.1 channel. All these findings have further strengthened the potential of Kv2.1 inhibition as a therapeutic strategy for DPN.

Notably, neurovascular function damage is tightly associated with inflammation in DPN, and inflammation reduction promotes the recovery of vascular function (Liu et al., 2017; Nguyen et al., 2012). Here, we determined that Kv2.1 inhibition improved peripheral blood perfusion and alleviated the loss of intraepithelial

nerve fibers. It is suggested that the neurovascular function improvement should be ascribed to the Dfe-mediated anti-inflammatory effect through Kv2.1 inhibition.

Although the detailed mechanism underlying the beneficial effect of Dfe on DPN-like pathology relating to potassium flux could not be well presented, we tentatively suggested that Dfe repressed Kv2.1 expression on the surface of cell membrane causing the opening of potassium channels and reducing of potassium conductance. As indicated in Figure S9, Dfe reduced the post-polarization potential and shortened the latency of DRG neuron action potential release, thus facilitating action potential release. As a result, the level of opening of potassium ion channels and the difference between the resting potential and the threshold potential decreased, resulting in an increase in the conduction velocity of the action potential. In addition, neuronal excitability changes led to an improvement in DPN-like pathology including neuropathic pain. Moreover, by considering that Kv2 downregulation augments firing by limiting the Kv2 inhibitory effect on spike frequency and Kv2 blocker against DRG neuron promotes myelinated neuron hyperexcitability (Tsantoulas et al., 2014), we here tentatively proposed that the beneficial effect of Dfe on DPN-like pathology in our work might be also related to the Dfe-mediated regulation of myelinated neuron hyperexcitability.

It was noticed that the densities of total Kv, IA, and IK currents were reduced in medium and large-diameter DRG neurons in DPN rats (Cao et al., 2010) and K^+ channel expression was also reduced in sensory neurons of other models of chronic peripheral pain at early pathological stage (Tsantoulas et al., 2014; Tsantoulas et al., 2012; Tsantoulas et al., 2014; Ishikawa et al., 1999; Uchida et al., 2010; Ritter et al., 2012; Chien et al., 2007; Cao et al., 2010). In contrast, our current work mainly involved the study on the late stage of DPN mice with evident hypersensitivity, demonstrating different result concerning Kv2.1 expression. Thus, our finding that Dfe could effectively improve the late stage of the DPN-like pathology might highlight its potential in preventing the occurrence of diabetic foot.

Finally, in the current work, apart from Kv2 (Kv2.1 and Kv2.2), we also assayed the mRNA levels of other Kv channels Kv1.1, Kv1.2, Kv1.4, Kv3.4, Kv4.2, and Kv4.3 in DRG tissue from DPN mice (Figures S7K–S7P), and the results indicated that the mRNA levels of the tested Kv channels were all upregulated in DRG tissue of type 1 diabetic mice but there were no obvious changes of mRNA levels for the other tested Kv genes except for the upregulations of Kv3.4 and Kv4.2 in DRG tissue of type 2 diabetic mice compared with those of Control and *db/m* mice. These results thus revealed the DPN-like pathology difference in Kv channel expression between type 1 and type 2 DPN model mice.

Based on the literature that elevated expression of channel protein may lead to the amplification of whole-cell current, we speculated that the decrease of Kv2.1 expression could reduce the whole-cell current (Leung et al., 2005; Wang et al., 2014). Thus, we tentatively hypothesized that the functional consequences caused by Kv2.1 current inhibition were in response to the functional consequences caused by the decrease of Kv2.1 channel protein expression.

In summary, we reported that antispasmodic drug Dfe as a Kv2.1 inhibitor ameliorated DPN-like pathology and the underlying mechanisms have been investigated by assay against the DPN mice with *in vivo* Kv2.1 knockdown by injection of adeno associated virus AAV9-Kv2.1-RNAi. As summarized in the Graphical Abstract, Dfe ameliorated mitochondrial dysfunction through the Kv2.1/CaMKKβ/AMPK/PGC-1α pathway, suppressed inflammation by IκBα/NF-κB signaling, and alleviated apoptosis by regulating Bcl-2 family proteins and Caspase-3.

Limitations of the Study

In our study, we determined that Dfe as a Kv2.1 inhibitor efficiently ameliorated DPN-like pathology and the underlying mechanism has been intensively investigated. As Dfe is a clinical drug for treating spasmolysis, the structure of Dfe needs to be rationally modified and optimized for developing Dfe-based anti-DPN reagents with high specificity and low side effects.

Resource Availability

Lead Contact

Further information and requests should be directed to and will be fulfilled by the Lead Contact, Xu Shen (xshen@njucm.edu.cn).

Materials Availability

This study did not generate new unique reagents.

Data and Code Availability

The authors confirm that the data supporting the findings of this study are available within the article and its Supplemental Information. Original data have been deposited to Mendeley Data: [https://doi.org/10.17632/gmxth7wsh8.1]

METHODS

All methods can be found in the accompanying Transparent Methods supplemental file.

SUPPLEMENTAL INFORMATION

Supplemental Information can be found online at https://doi.org/10.1016/j.isci.2020.101617.

ACKNOWLEDGMENTS

This work was supported by National Science & Technology Major Project "Key New Drug Creation and Manufacturing Program" China (Number:2018ZX09711002), the National Natural Science Foundation of China for Young Scientists of China (81703806), Postgraduate Research & Practice Innovation Program of Jiangsu Province (KYCX18_1600), the Open Project Program of Jiangsu Key Laboratory for Pharmacology and Safety Evaluation of Chinese Materia Medica (No. JKLPSE201801), the Project of the Priority Academic Program Development of Jiangsu Higher Education Institutions of Jiangsu Higher Education Institutions (PAPD), Priority Academic Program Development of Jiangsu Higher Education Institutions (Integration of Chinese and Western Medicine) and Innovative Research Team of Six Talent Peaks Project in Jiangsu Province (TD-SWYY-013).

AUTHOR CONTRIBUTIONS

Xiaoju Xu and X.S. designed the study. X.S. reviewed the manuscript. Xiaoju Xu and X.Z. performed the animal experiments. Y.H. conducted the patch clamp experiment. Xiaoju Xu analyzed and interpreted data. Xiaoju Xu and Xu Xu wrote the manuscript. Xiaoju Xu, X.S., Y.Li., and J.W. are the guarantors of this work and, as such, have full access to all data in the study and take responsibility for the integrity of the data and the accuracy of the data analysis. All authors approved the manuscript.

DECLARATION OF INTERESTS

The authors declare no competing interests.

Received: December 26, 2019
Revised: July 22, 2020
Accepted: September 23, 2020
Published: October 23, 2020

REFERENCES

Bodur, E., Cokuğraş, A.N., and Tezcan, E.F. (2001). Inhibition effects of benactyzine and drofenine on human serum butyrylcholinesterase. Arch. Biochem. Biophys. *386*, 25–29.

Bönhof, G.J., Herder, C., Strom, A., Papanas, N., Roden, M., and Ziegler, D. (2019). Emerging biomarkers, tools, and treatments for diabetic polyneuropathy. Endocr. Rev. *40*, 153–192.

Boulton, A.J.M., Vinik, A.I., Arezzo, J.C., Bril, V., Feldman, E.L., Freeman, R., Malik, R.A., Maser, R.E., Sosenko, J.M., Ziegler, D., et al. (2005). Diabetic neuropathies: a statement by the american diabetes association. Diabetes Care *28*, 956–962.

Calcutt, N.A., Smith, D.R., Frizzi, K., Sabbir, M.G., Chowdhury, S.K., Mixcoatlzecuatl, T., Saleh, A., Muttalib, N., Van, P.R., Ochoa, J., et al. (2017). Selective antagonism of muscarinic receptors is neuroprotective in peripheral neuropathy. J. Clin. Invest. *127*, 608–622.

Cameron, N.E., Eaton, S.E.M., Cotter, M.A., and Tesfaye, S. (2001). Vascular factors and metabolic interactions in the pathogenesis of diabetic neuropathy. Diabetologia *44*, 1973–1988.

Cao, X.H., Byun, H.S., Chen, S.R., Cai, Y.Q., and Pan, H.L. (2010). Reduction in voltage-gated k+ channel activity in primary sensory neuron in painful diabetic neuropathy: role of brain-derived neurotrophic factor. J. Neurochem. *114*, 1460–1475.

Chan, S.L., and Yu, V.C. (2004). Proteins of the bcl-2 family in apoptosis signalling: from mechanistic insights to therapeutic opportunities. Clin. Exp. Pharmacol. Physiol. *31*, 119–128.

Chao, R.Y., Cheng, C.H., Wu, S.N., and Chen, P.C. (2017). Defective trafficking of kv2.1 channels in mptp-induced nigrostriatal degeneration. J. Neurochem. *144*, 483–497.

Chien, L.Y., Cheng, J.K., Chu, D., Cheng, C.F., and Tsaur, M.L. (2007). Reduced expression of A-type potassium channels in primary sensory neurons induces mechanical hypersensitivity. J. Neurosci. *27*, 9855–9865.

Chowdhury, S.K., Smith, D.R., and Fernyhough, P. (2013). The role of aberrant mitochondrial

bioenergetics in diabetic neuropathy. Neurobiol. Dis. *51*, 56–65.

Demiot, C., Tartas, M., Fromy, B., Abraham, P., Saumet, J.L., and Sigaudo-Roussel, D. (2006). Aldose reductase pathway inhibition improved vascular and c-fiber functions, allowing for pressure-induced vasodilation restoration during severe diabetic neuropathy. Diabetes *55*, 1478–1483.

Deering-Rice, C.E., Mitchell, V.K., Romero, E.G., Abdel Aziz, M.H., Ryskamp, D.A., Križaj, D., Gopal, V.R., and Reilly, C.A. (2014). Drofenine: a 2-APB analogue with greater selectivity for human TRPV3. Pharmacol. Res. Perspect. *2*, e00062.

Duksal, T., Tiftikcioglu, B.I., Bilgin, S., Kose, S., and Zorlu, Y. (2016). Role of inflammation in sensory neuropathy in prediabetes or diabetes. Acta Neurol. Scand. *133*, 384–390.

Frazzini, V., Guarnieri, S., Bomba, M., Navarra, R., Morabito, C., Mariggiò, M.A., Mariggi, and Sensi, S.L. (2016). Altered Kv2.1 functioning promotes increased excitability in hippocampal neurons of an Alzheimer's disease mouse model. Cell Death Dis *7*, e2100.

Frolov, R.V., and Singh, S. (2014). Celecoxib and ion channels: a story of unexpected discoveries. Eur. J. Pharmacol. *730*, 61–71.

Hashem, R.M., Rashed, L.A., Hassanin, K.M.A., Hetta, M.H., and Ahmed, A.O. (2017). Effect of 6-gingerol on AMPK-NF-κB axis in high fat diet fed rats. Biomed. Pharmacother. *88*, 293–301.

Hermanstyne, T.O., Kalpana, S., Wei, L.W., Hoffman, G.E., Meredith, A.L., Mong, J.A., and Misonou, H. (2013). Kv2.2: a novel molecular target to study the role of basal forebrain gabaergic neuron in the sleep-wake cycle. Sleep *36*, 1839–1848.

Herzig, S., and Shaw, R.J. (2018). AMPK: guardian of metabolism and mitochondrial homeostasis. Nat. Rev. Mol. Cell. Biol. *19*, 121–135.

Hotta, N., Akanuma, Y., Kawamori, R., Matsuoka, K., Oka, Y., Shichiri, M., Toyota, T., Nakashima, M., Yoshimura, I., Sakamoto, N., et al. (2006). Long-term clinical effects of epalrestat, an aldose reductase inhibitor, on diabetic peripheral neuropathy. Diabetes Care *29*, 1538.

Hur, J., Dauch, J.R., Hinder, L.M., Hayes, J.M., Backus, C., Pennathur, S., Kretzler, M., Brosius, F.C., III, and Feldman, E.L. (2015). The metabolic syndrome and microvascular complications in a murine model of type 2 diabetes. Diabetes *64*, 3294–3304.

Ishikawa, K., Tanaka, M., Black, J.A., and Waxman, S.G. (1999). Changes in expression of voltage-gated potassium channels in dorsal root ganglion neurons following axotomy. Muscle Nerve *22*, 502–507.

Jacobson, D.A., Kuznetsov, A., Lopez, J.P., Kash, S., and Philipson, L. (2007). Kv2.1 ablation alters glucose-induced islet electrical activity, enhancing insulin secretion. Cell Metab. *6*, 229–235.

Jensen, C.S., Watanabe, S., Stas, J.I., Klaphaak, J., Yamane, A., Schmitt, N., Olesen, S.P., Trimmer, J.S., Rasmussen, H.B., and Misonou, H. (2017). Trafficking of kv2.1 channels to the axon initial segment by a novel non-conventional secretory pathway. J. Neurosci. *37*, 11523–11536.

Jia, L., Wang, L., Chopp, M., Zhang, Y., Szalad, A., and Zhang, Z.G. (2016). MicroRNA 146a locally mediates distal axonal growth of dorsal root ganglia neuron under high glucose and sildenafil conditions. Neuroscience *329*, 43–53.

Jiang, D.Q., Li, M.X., Ma, Y.J., Wang, Y., and Wang, Y. (2016). Efficacy and safety of prostaglandin e1 plus lipoic acid combination therapy versus monotherapy for patients with diabetic peripheral neuropathy. J. Clin. Neurosci. *27*, 8–16.

Jiang, D.Q., Li, M.X., Wang, Y., and Wang, Y. (2015). Effects of prostaglandin e1 plus methylcobalamin alone and in combination with lipoic acid on nerve conduction velocity in patients with diabetic peripheral neuropathy: a meta-analysis. Neurosci. Lett. *594*, 23–29.

Johnson, B.T., Ashley, L., Michael, K., Emily, M., and James, T. (2018). The kv2.1 potassium channel forms endoplasmic reticulum/plasma membrane junctions via interaction with vap-a and vap-b. Biophys. J. *114*, 295a.

Kim, S.J., Widenmaier, S.B., Choi, W.S., Nian, C., Ao, Z., Warnock, G., and Mclntosh, C.H. (2012). Pancreatic beta-cell prosurvival effects of the incretin hormones involve post-translational modification of Kv2.1 delayed rectifier channels. Cell Death Differ *19*, 333–344.

Kumar, A., Negi, G., and Sharma, S.S. (2012). Suppression of NF-κB and NF-κB regulated oxidative stress and neuroinflammation by BAY 11-7082 (IκB phosphorylation inhibitor) in experimental diabetic neuropathy. Biochimie *94*, 1158–1165.

Kunysz, E.L., Michel, A.D., and Whiting, R.L. (1988). Functional and direct binding studies using subtype selective muscarinic receptor antagonists. Br. J. Pharmacol. *93*, 491–500.

Lauria, G., Hsieh, S.T., Johansson, O., Kennedy, W.R., Leger, J.M., Mellgren, S.I., Nolano, M., Merkies, I.S., Polydefkis, M., and Smith, A.G. (2010). European federation of neurological societies/peripheral nerve society guideline on the use of skin biopsy in the diagnosis of small fiber neuropathy. Report of a joint task force of the European Fe-deration of neurological societies and the peripheral nerve society. Eur. J. Neurol. *17*, 903–E49.

Lee, S., Milescu, M., Jung, H.H., Lee, J.Y., Bae, C.H., Lee, C.W., Kim, H.H., Swartz, K.J., and Kim, J.I. (2010). Solution structure of GXTX-1E, a high-affinity tarantula toxin interacting with voltage sensors in kv2.1 potassium channels. Biochemistry *49*, 5134–5142.

Leung, Y.M., Kang, Y., Xia, F., Sheu, L., Gao, X., Xie, H., Tsushima, R.G., and Gaisano, H.Y. (2005). Open form of syntaxin-1A is a more potent inhibitor than wild-type syntaxin-1A of Kv2.1 channels. Biochem. J. *387*, 195–202.

Liu, H.W., and Chang, S.J. (2018). Moderate exercise suppresses NF-κB signaling and activates the SIRT1-AMPK-PGC1alpha Axis to attenuate muscle loss in diabetic *db/db* mice. Front. Physiol. *9*, 636.

Liu, X.S., Fan, B., Szalad, A., Jia, L., Wang, L., Wang, X., Pan, W., Zhang, L., Zhang, R., Hu, J., et al. (2017). Microrna-146a mimics reduce the peripheral neuropathy in type II diabetic mice. Diabetes *66*, 3111–3121.

MacDonald, P.E. (2002). Inhibition of Kv2.1 voltage-dependent K+ channels in pancreatic beta-cell enhances glucose-dependent insulin secretion. J. Biol. Chem. *277*, 44938–44945.

Nguyen, D.V., Shaw, L.C., and Grant, M.B. (2012). Inflammation in the pathogenesis of microvascular complications in diabetes. Front. Endocrinol. *3*, 170.

Pal, S., Hartnett, K.A., Nerbonne, J.M., Levitan, E.S., and Aizenman, E. (2003). Mediation of neuronal apoptosis by Kv2.1-encoded potassium channels. J. Neurosci. *23*, 4798–4802.

Pathak, D., Guan, D., and Foehring, R.C. (2016). Roles of specific Kv channel types in repolarization of the action potential in genetically identified subclasses of pyramidal neuron in mouse neocortex. J. Neurophysiol. *115*, 2317–2329.

Porter, A.G., and JaÈnicke, R.U. (1999). Emerging roles of caspase-3 in apoptosis. Cell Death Differ. *6*, 99–104.

Ramírez, A., Vázquez-Sánchez, A.Y., Carrión-Robalino, N., and Javier, C. (2016). Ion channels and oxidative stress as a potential link for the diagnosis or treatment of liver diseases. Oxid. Med. Cell. Longev. *2016*, 3928714.

Redman, P.T., He, K., Hartnett, K.A., Jefferson, B.S., Hu, L., Rosenberg, P.A., Levitan, E.S., and Aizenman, E. (2007). Apoptotic surge of potassium currents is mediated by p38 phosphorylation of Kv2.1. Proc. Natl. Acad. Sci. *104*, 3568–3573.

Ritter, D.M., Ho, C., O'Leary, M.E., and Covarrubias, M. (2012). Modulation of Kv3.4 channel N-type inactivation by protein kinase C shapes the action potential in dorsal root ganglion neurons. J. Physiol. *590*, 145–161.

Romer, S.H., Deardorff, A.S., and Fyffe, R.E. (2016). Activity-dependent redistribution of Kv2.1 ion channels on rat spinal motoneuron. Physiol. Rep. *4*, e13039.

Roy Chowdhury, S.K., Smith, D.R., Saleh, A., Schapansky, J., Marquez, A., Gomes, S., Akude, E., Morrow, D., Calcutt, N.A., and Fernyhough, P. (2012). Impaired adenosine monophosphate-activated protein kinase signalling in dorsal root ganglia neurons is linked to mitochondrial dysfunction and peripheral neuropathy in diabetes. Brain *135*, 1751–1766.

Shah, N.H., and Aizenman, E. (2014). Voltage-gated potassium channels at the crossroads of neuronal function, ischemic tolerance, and neurodegeneration. Transl. Stroke. Res. *5*, 38–58.

Shaw, R.J. (2005). The kinase LKB1 mediates glucose homeostasis in liver and therapeutic effects of metformin. Science *310*, 1642–1646.

Srinivasan, S., Stevens, M., and Wiley, J.W. (2000). Diabetic peripheral neuropathy: evidence for apoptosis and associated mitochondrial dysfunction. Diabetes *49*, 1932–1938.

Tak, P.P., and Firestein, G.S. (2001). NF-κB: a key role in inflammatory diseases. J. Clin. Invest. *107*, 7–11.

Tesfaye, S., and Selvarajah, D. (2012). Advances in the epidemiology, pathogenesis and management of diabetic peripheral neuropathy. Diabetes Metab. Res. Rev. *28*, 8–14.

Tsantoulas, C., Zhu, L., Shaifta, Y., Grist, J., Ward, J.P.T., Raouf, R., Michael, G.J., and Mcmahon, S.B. (2012). Sensory neuron downregulation of the Kv9.1 potassium channel subunit mediates neuropathic pain following nerve injury. J. Neurosci. *32*, 17502–17513.

Tsantoulas, C., Zhu, L., Yip, P., Grist, J., and Mcmahon, S.B. (2014). Kv2 dysfunction after peripheral axotomy enhances sensory neuron responsiveness to sustained input. Exp. Neurol. *251*, 115–126.

Uchida, H., Ma, L., and Ueda, H. (2010). Epigenetic gene silencing underlies C-Fiber dysfunctions in neuropathic pain. J. Neurosci. *30*, 4806–4814.

Van, D.P.S., Cotter, M.A., Bravenboer, B., and Cameron, N.E. (2013). Pathogenesis of diabetic neuropathy: focus on neurovascular mechanisms. Eur. J. Pharmacol. *719*, 180–186.

Vincent, A.M., Callaghan, B.C., Smith, A.L., and Feldman, E.L. (2011). Diabetic neuropathy: cellular mechanisms as therapeutic targets. Nat. Rev. Neurol. *7*, 573–583.

Wang, C.Y., Huang, A.Q., Zhou, M.H., and Mei, Y.A. (2014). GDF15 regulates Kv2.1-mediated outward K+ current through the Akt/mTOR signalling pathway in rat cerebellar granule cells. Biochem. J. *460*, 35–47.

Wei, Y., Shin, M.R., and Sesti, F. (2018). Oxidation of KCNB1 channels in the human brain and in mouse model of Alzheimer's disease. Cell Death Dis. *9*, 820.

Wilson, N.M.W.D. (2011). Inflammatory mediators in diabetic neuropathy. J. Diabetes Metab. *S5*, 004.

Yang, C.T., Lu, G.L., Hsu, S.F., Macdonald, I., Chiou, L.C., Hung, S.Y., and Chen, Y.H. (2018). Paeonol promotes hippocampal synaptic transmission: the role of the kv2.1 potassium channel. Eur. J. Pharmacol. *827*, 227–237.

Yao, H., Zhou, K., Yan, D., Li, M., and Wang, Y. (2009). The Kv2.1 channels mediate neuronal apoptosis induced by excitotoxicity. J. Neurochem. *108*, 909–919.

Zhao, M., Chen, J.Y., Chu, Y.D., Zhu, Y.B., and Bu, S.Z. (2018). Efficacy of epalrestat plus α-lipoic acid combination therapy versus monotherapy in patients with diabetic peripheral neuropathy: a meta-analysis of 20 randomized controlled trials. Neural Regen. Res. *13*, 1087.

Zhou, T.T., Quan, L.L., Chen, L.P., Du, T., Sun, K.X., Zhang, J.C., Yu, L., Li, Y., Wan, P., Chen, L.L., et al. (2016). Sp6616 as a new kv2.1 channel inhibitor efficiently promotes β-cell survival involving both PKC/Erk1/2 and CaM/PI3K/Akt signaling pathways. Cell Death Dis *7*, e2216.

iScience, Volume *23*

Supplemental Information

Antispasmodic Drug Drofenine as an Inhibitor of Kv2.1 Channel Ameliorates Peripheral Neuropathy in Diabetic Mice

Xiaoju Xu, Xu Xu, Yanping Hao, Xialin Zhu, Jian Lu, Xingnan Ouyang, Yin Lu, Xi Huang, Yang Li, Jiaying Wang, and Xu Shen

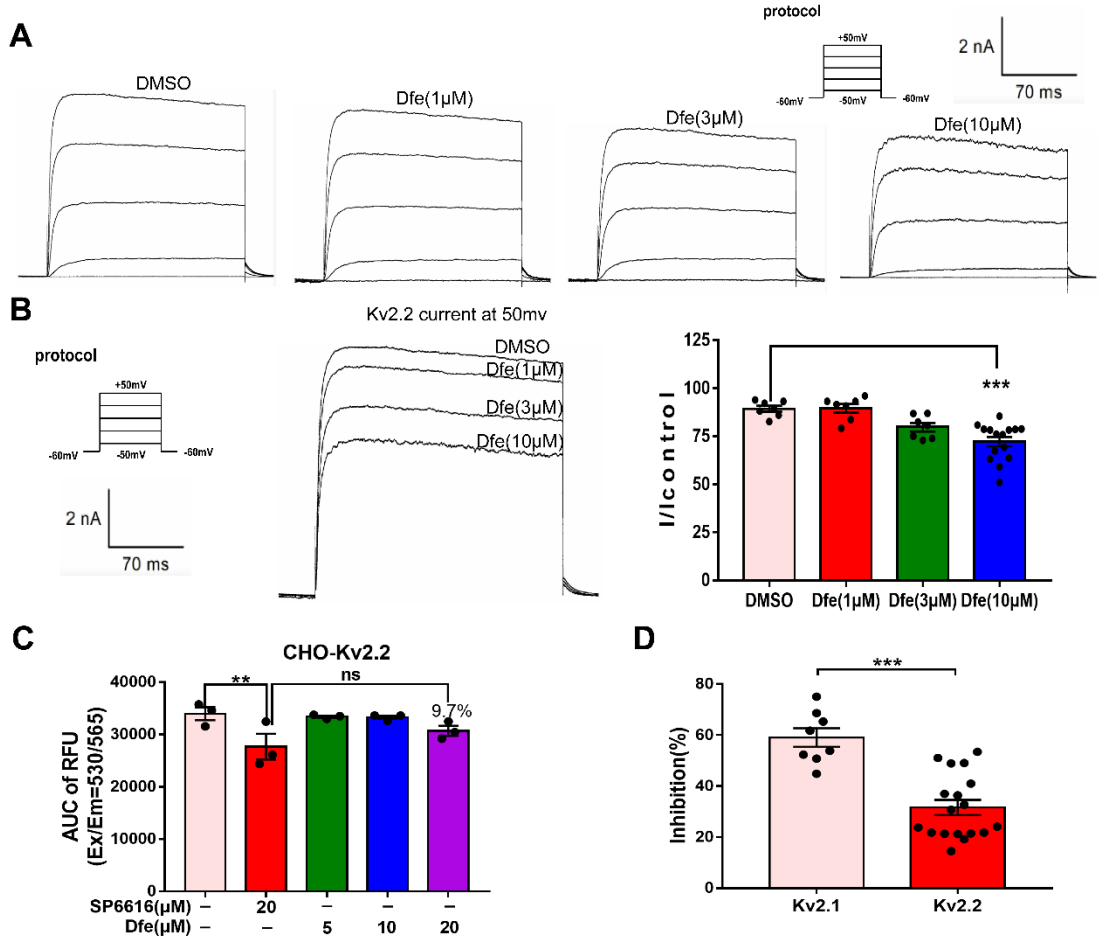

Supplemental Fig. S1. Dfe exhibits selectivity for Kv2.1 over Kv2.2, related to Figure 1.

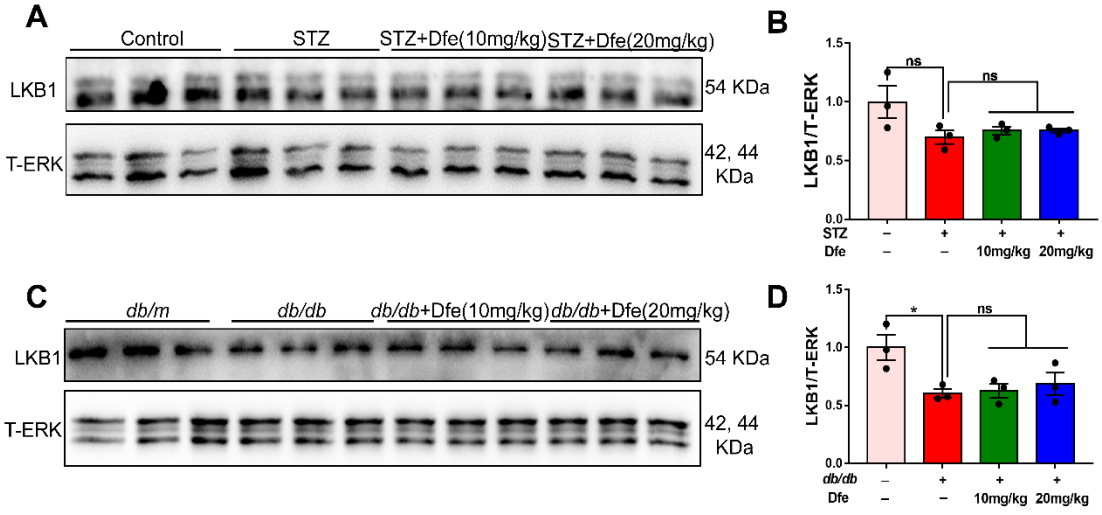

Supplemental Fig. S2. Western blot results of LKB1 protein expression in DPN

mice, related to Figure 5.

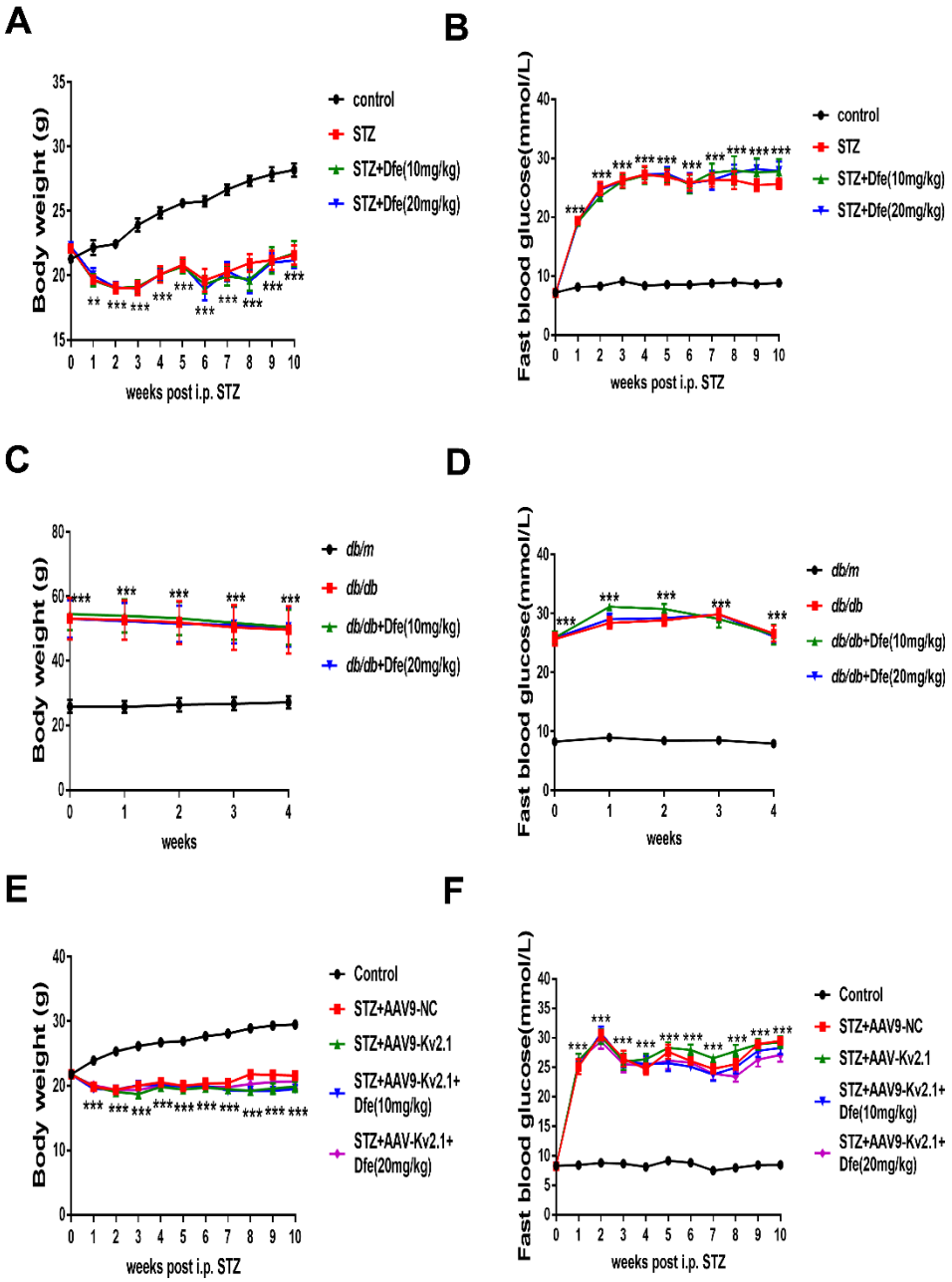

Supplemental Fig. S3. Time course of body weight and fast blood glucose in DPN mice, related to Figure 4.

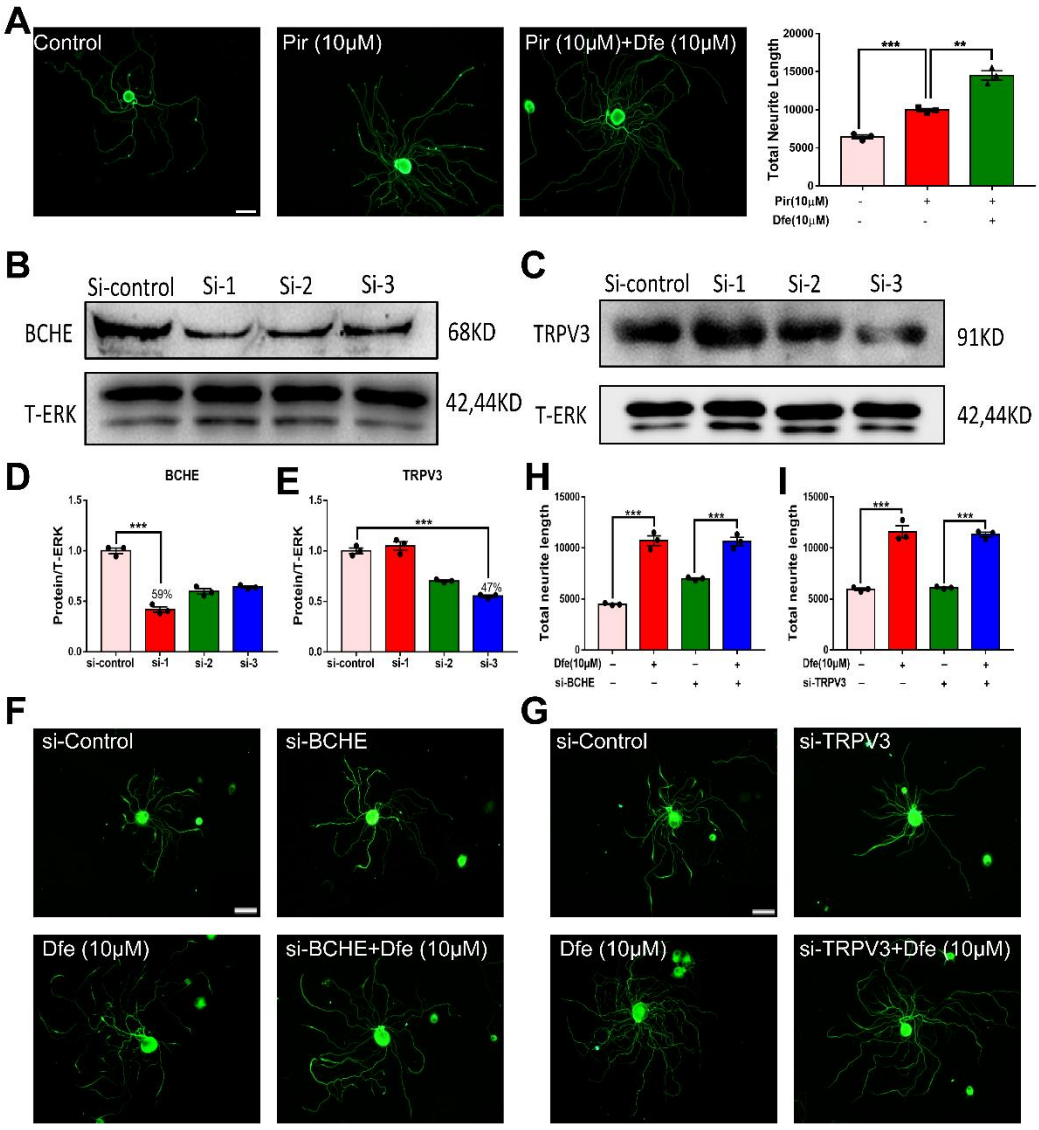

Supplemental Fig. S4. Dfe did not promoted neurite outgrowth of DRG neuron in DPN mice through BCHE and TRPV3, related to Figure 3.

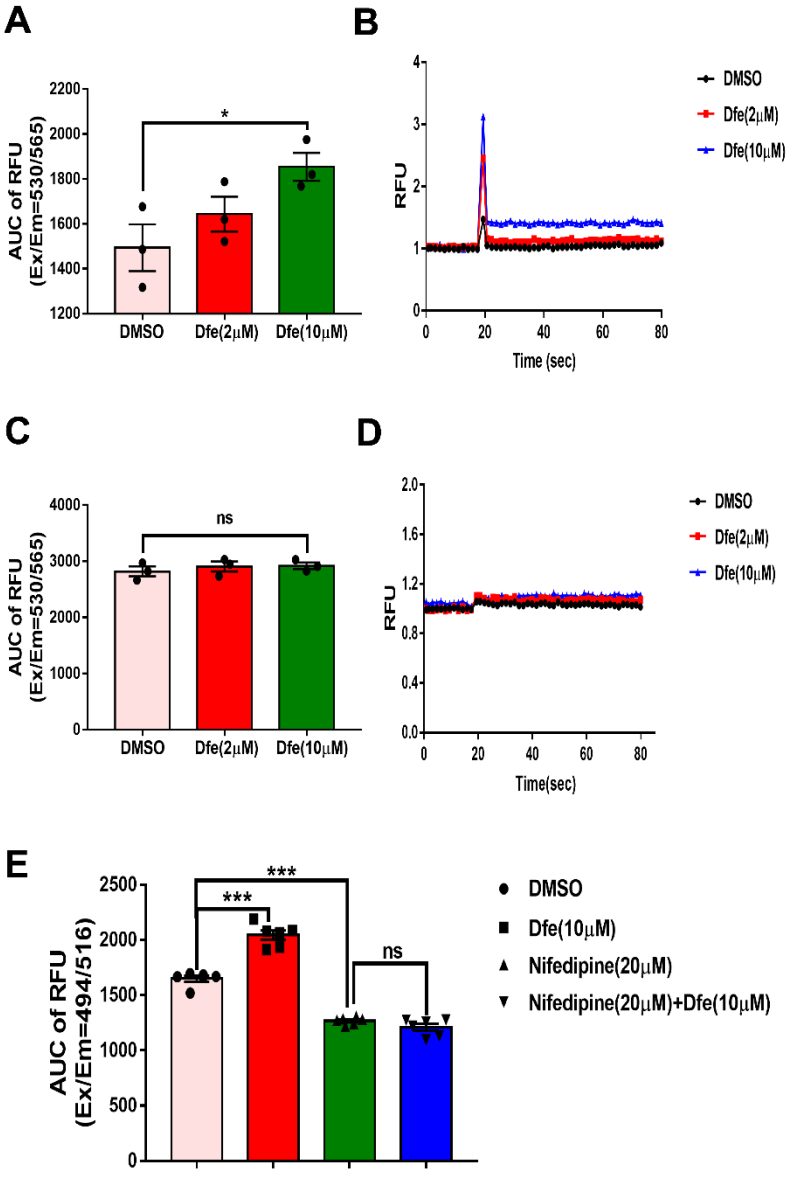

Supplemental Fig. S5. Dfe increased calcium influx in DRG neuron, related to Figure 5.

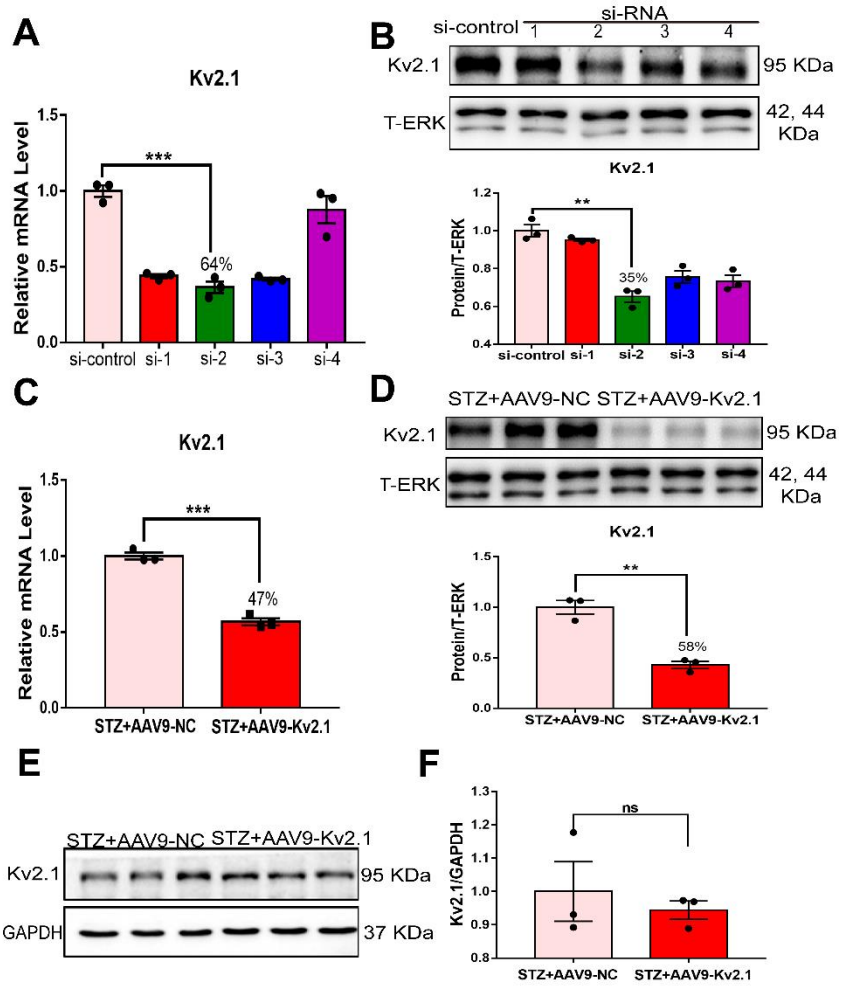

Supplemental Fig. S6. Screen of Kv2.1 interference sequence and identification of Kv2.1 protein expression, related to Figure 3-8.

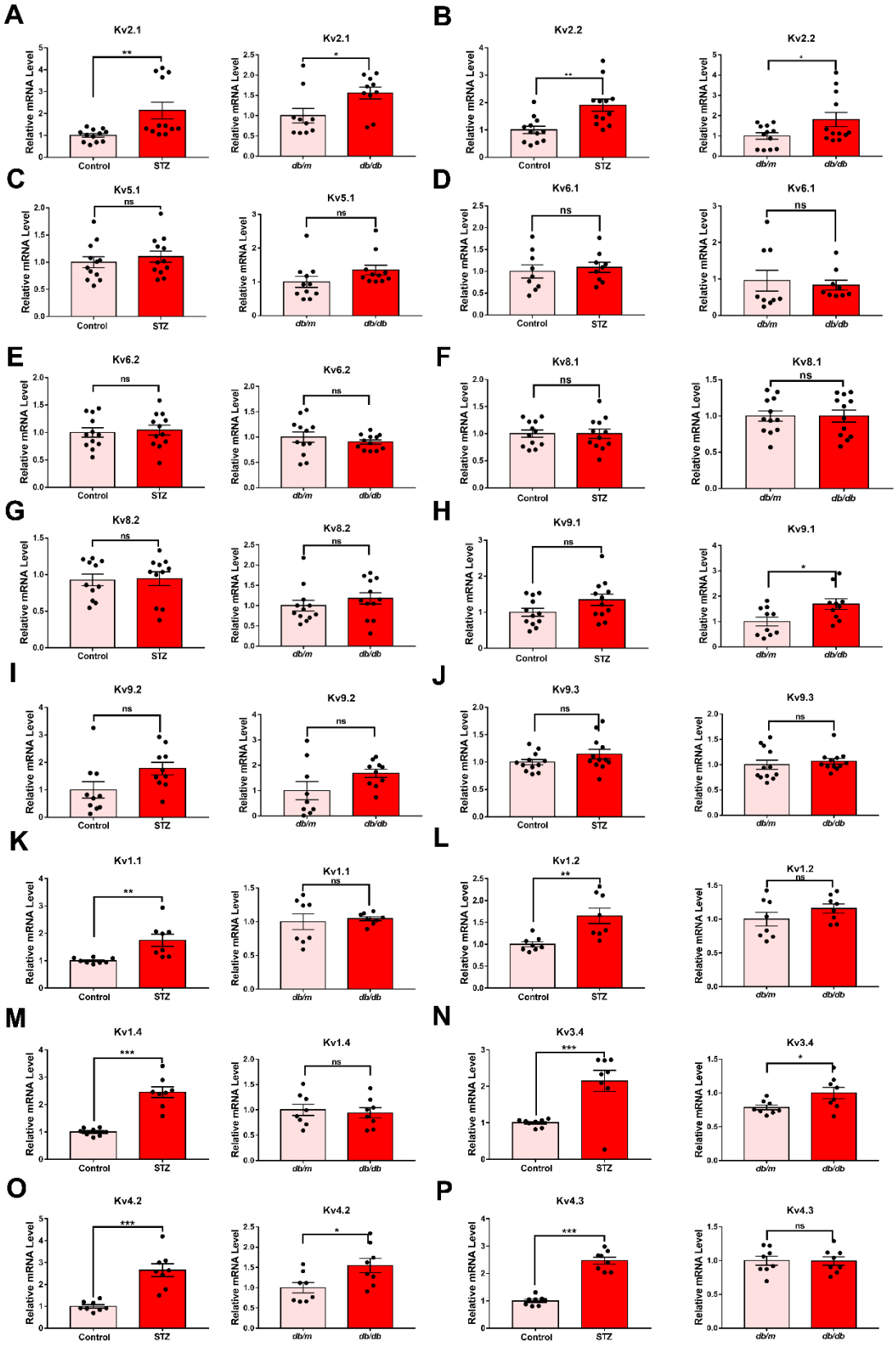

Supplemental Fig. S7. Transcription analyses of Kv channel in DRG tissue of DPN mice, related to Figure 2.

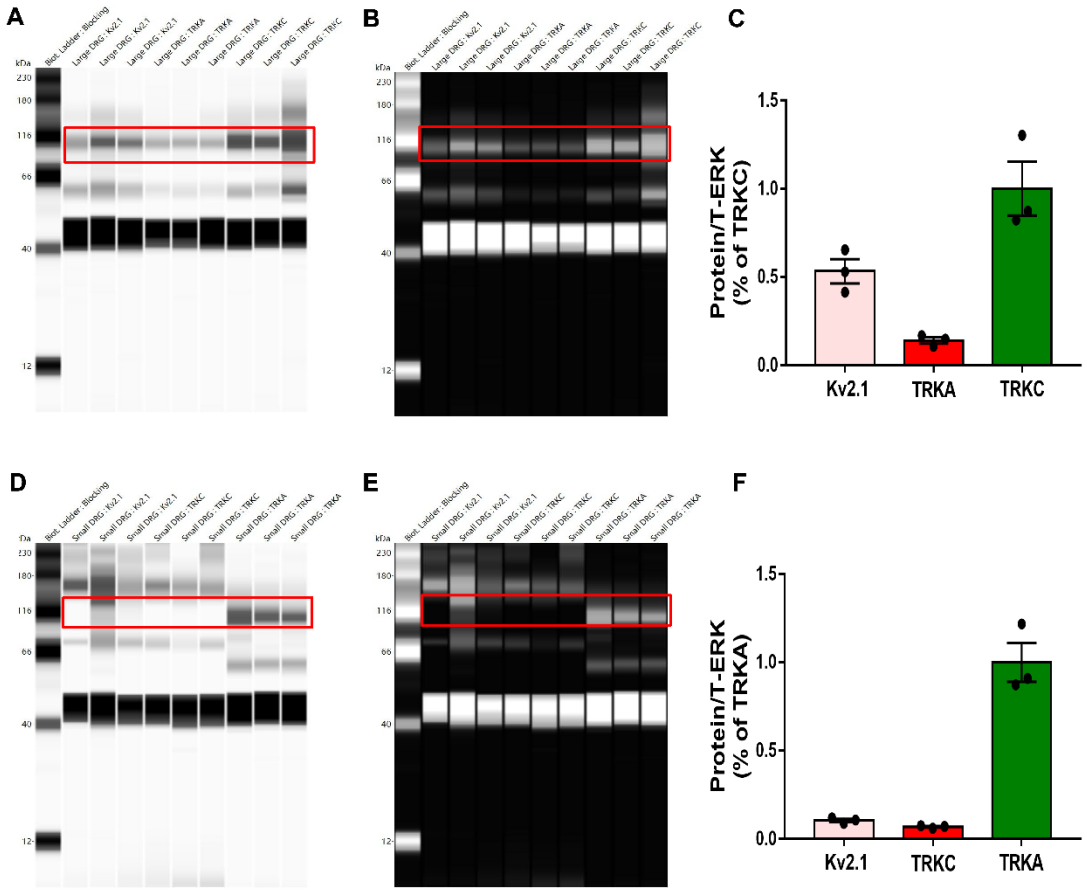

Supplemental Fig. S8. Kv2.1 expression in small, medium and large DRG neurons of DPN mice, related to Figure 2.

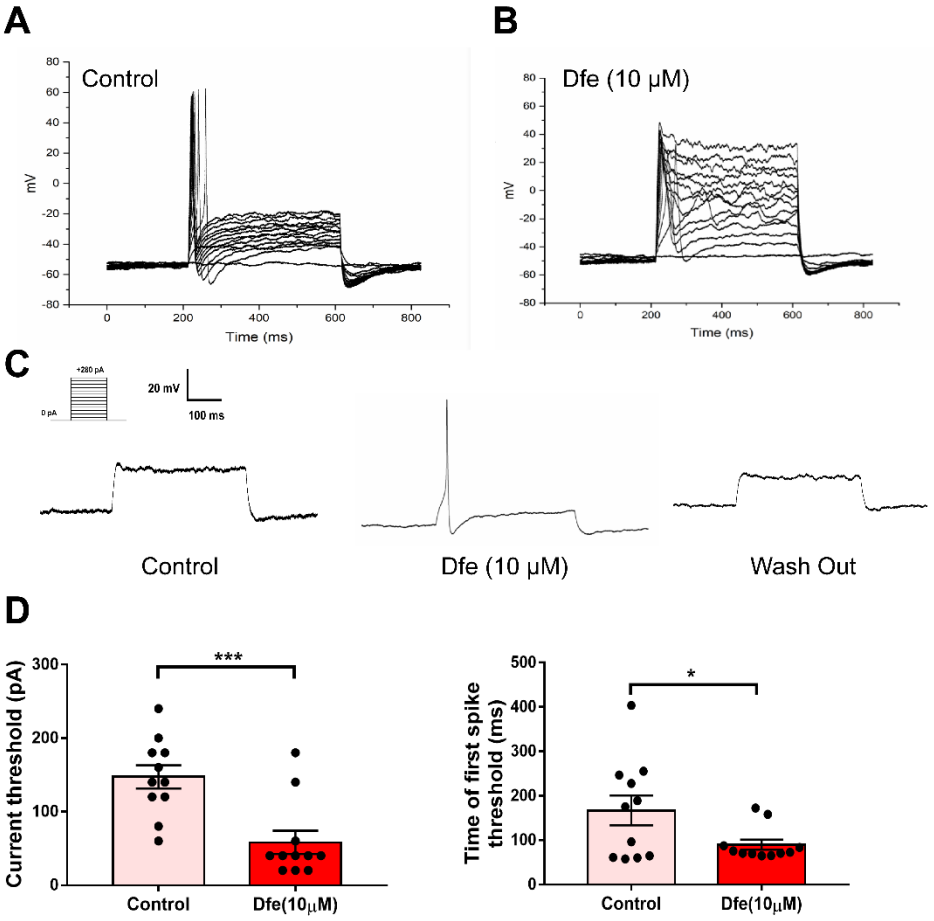

Supplemental Fig. S9. Example traces of the action potential and distribute images of single action potential of Dfe, related to Figure 2.

A

Time (h)	Concentration of Dfe in plasma (ng/ml)
0.25	22.14
1.5	30.38
4	2.46
8	-1.64
12	-1.86
24	-2.28

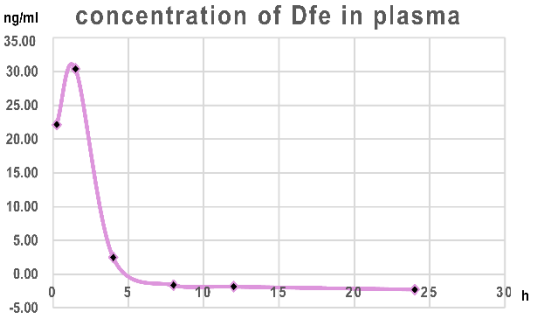

B

Time (h)	Concentration of Dfe in DRG (ng/ml)
0.25	7.96
1.5	8.76
4	3.33
8	0.55
12	-0.31
24	-0.38

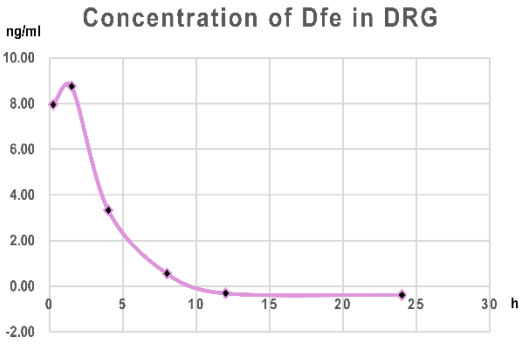

Supplemental Fig. S10. The concentration of Dfe in plasma and DRG tissue, related to Figure 1.

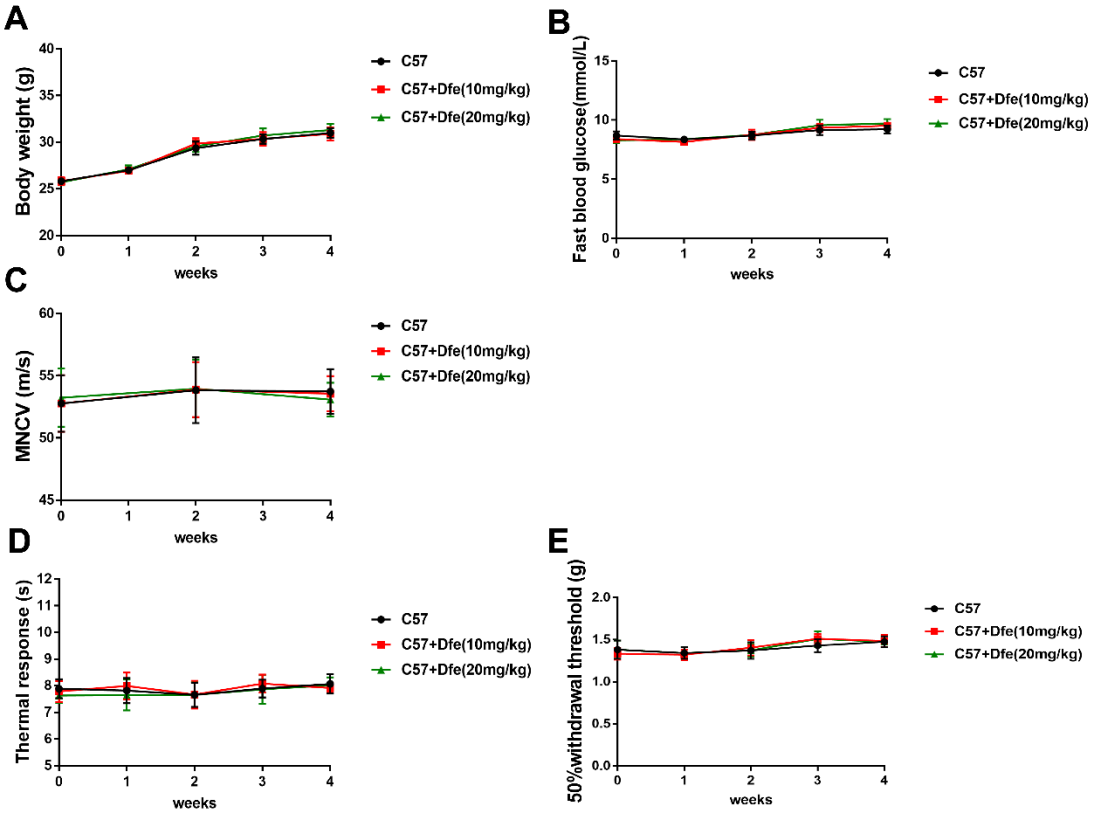

Supplemental Fig. S11. Time course of body weight and fast blood glucose in normal mice, related to Figure 4.

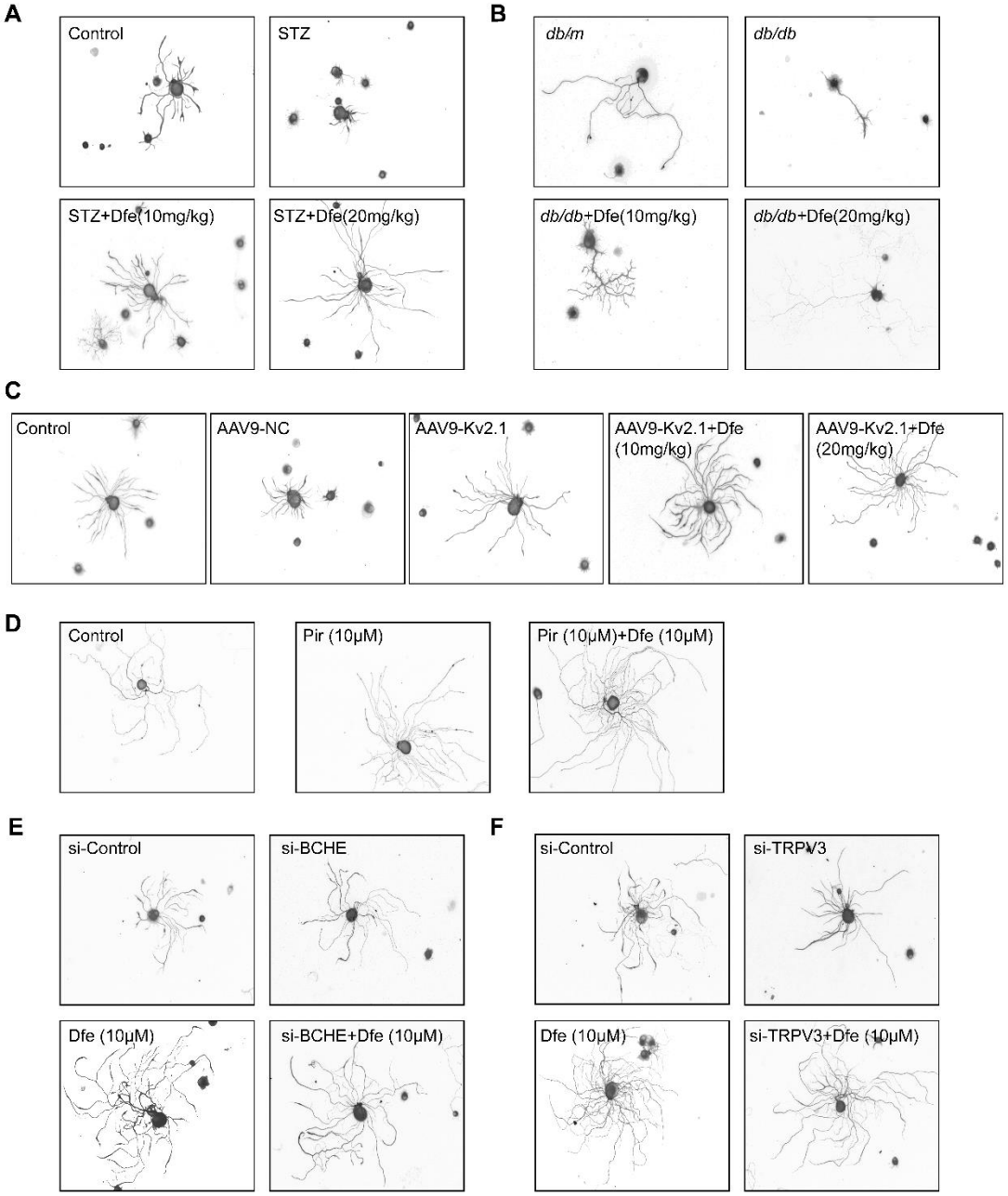

Supplemental Fig. S12. Grayscale images of neurites in DRG neurons from DPN mice, related to Figure 3.

Supplemental Table 1. List of Kv2.1-siRNA interference sequences used in real-time RT-PCR, related to Figure 3-8.

si-RNA	Target sequence
si-RNA1(si-1)	AGCAGAGGTAATTATAATCCA
si-RNA2(si-2)	CAGAGTCTGACAGAACTCCTA
si-RNA3(si-3)	TGGGTGGGTTATATGCTCATA
si-RNA4(si-4)	TACCCGAACCACTATCTTCTA

Supplemental Table 2. List of BCHE-siRNA interference sequences used in Western Blot, related to Figure 3.

si-RNA	Target sequence
si-RNA1(si-1)	CCGCAACCCUUAAACAAAUTT AUUUGUUUAAGGGUUGCGGTT
si-RNA2(si-2)	GCUCGUGUUGAAAGAGUUATT UAACUCUUUCAACACGAGCTT
si-RNA3(si-3)	GGGAGUUAACAAAGAUGAATT UUCAUCUUUGUUAACUCCCTT

Supplemental Table 3. List of TRPV3-siRNA interference sequences used in Western Blot, related to Figure 3.

si-RNA	Target sequence
si-RNA1(si-1)	CCAAGAAGAGUGCACACUUTT AAGUGUGCACUCUUCUUGGTT
si-RNA2(si-2)	GCUCCUAGGGAGGAUGUUUTT AAACAUCCUCCCUAGGAGCTT
si-RNA3(si-3)	CCUGUCAGAUGCCUGGUUUTT AAACCAGGCAUCUGACAGGTT

Supplemental Table 4. List of primers used in real-time RT-PCR, related to Figure 2.

Gene	Forward Primer	Reverse Primer
Kv1.1	GGAGCGCCCCCTACCCGAGAAG	GGTGAATGGTGCCCGTGAAGTCCT

Kv1.2	TCCCGGATGCCTTCTGGTG	GGCCTGCTCCTCTCCCTCTGT
Kv1.4	TTGTGAACGCGTGGTAATAAATGTGT	GGCGGCCTCCTGACTGGTAATAATA
Kv2.1	TCGACAACACGTGCTGTGCT	GGCCAACTTCAGGATGCGC
Kv2.2	TTGATAACACCTGCTGCCCG	TGGCGAGTTTCAGTATCCTGA
Kv3.4	CCACGGGGCAATGACCACACC	ACACAGCGCACCCACCAGCATTCCT
Kv4.2	GCCGCAGCGCCTAGTCGTTACC	TGATAGCCATTGTGAGGGAAAAGAGCA
Kv4.3	CTCCCTAAGCGGCGTCCTGGTCATT	CTTCTGTGCCCTGCGTTTATCTGCTCTC
Kv5.1	CTGGTGGGCTATCATCACCA	CGGGTCCTATGATGCTTCTC
Kv6.1	GTCCGTTCTGTTTGTCACCG	GGATCAGCACCCGTTCTTGT
Kv6.2	GGCTCTTCGCCTACGTCTC	CATCACGCGTGCTGTCCTC
Kv8.1	TCTGCGCATGCTGAAACTGG	AGTACTTGCTCTCTCCCTGC
Kv8.2	CTTCCGAATCCTCAAGCTGG	GTTGACCTTTCCTCGTTCCC
Kv9.1	AGGTAGTGCAAGTGTTCCGC	AAGTCCTCAAACTCGCGCTG
Kv9.2	TTCTCAAGCTGGCCAGACAC	TGACCGAAGGGACCTCTTTC
Kv9.3	TGTAGGGCTTCGGTCTCTTG	AGTACGGTAGCTCATGGCAC

KEY RESOURCES TABLE

REAGENT or RESOURCE	SOURCE	IDENTIFIER
Antibodies		
Rabbit anti-phospho AMPK(Thr172)	Cell Signaling Technology	Cat# 8208; RRID: AB_1658160
Rabbit anti-total AMPK (T-AMPK)	Cell Signaling Technology	Cat# 5831; RRID: AB_10622186
Rabbit anti-CaMKKβ	Santa Cruz Biotechnology	Cat# SC-50341; RRID: AB_2068532
Rabbit anti-phospho ACC	Cell Signaling Technology	Cat# 11818; RRID: AB_2687505
Rabbit anti-PGC-1α	Abcam	Cat# ab54481; RRID: AB_881987
Mouse anti-Kv2.1	Abcam	Cat# ab192761; RRID: N/A
Rabbit anti-PGP9.5	Abcam	Cat# ab108986; RRID: AB_10891773
Rabbit anti-Bcl-xl	Cell Signaling Technology	Cat# 2764; RRID: AB_2228008
Rabbit anti-Bax	Cell Signaling Technology	Cat# 5023; RRID: RRID: AB_10557411
Rabbit anti-Caspase-3	Cell Signaling Technology	Cat# 14220; RRID: AB_2798429
Rabbit anti-Cleaved caspase-3	Cell Signaling Technology	Cat# 9664; RRID: AB_2070042
Rabbit anti-iNOS	Cell Signaling Technology	Cat# 13120; RRID: AB_2687529
Rabbit anti-P-IκBα	Cell Signaling Technology	Cat# 2859; RRID: AB_561111

Rabbit anti-P-Bad	Cell Signaling Technology	Cat# 5284; RRID: AB_560884
Mouse anti-Bad	Cell Signaling Technology	Cat# 9239; RRID: AB_2062127
Rabbit anti-TNF-α	Cell Signaling Technology	Cat# 11948; RRID: AB_2687962
Rabbit anti-Total extracellular regulated protein kinase (T-ERK)	Cell Signaling Technology	Cat# 9102; RRID: AB_330744
Rabbit anti-NeuN	Cell Signaling Technology	Cat# 24307; RRID: AB_2651140
Anti-mouse IgG, HRP-linked Antibody	Cell Signaling Technology	Cat# 7076; RRID: AB_330924
Anti-rabbit IgG, HRP-linked Antibody	Cell Signaling Technology	Cat# 7074; RRID: AB_2099233
fluorescein 596-conjugated secondary antibody	Proteintech	Cat# SA00013-4; RRID: AB_2810984
fluorescein 488-conjugated secondary antibody	Proteintech	Cat# SA00013-1; RRID: AB_2810983
Virus Strains		
AAV9-Kcnb1-RNAi	GENECHEM	Cat# 77626-1
AAV9-CON400	GENECHEM	N/A
Chemicals, Peptides, and Recombinant Proteins		
Fetal Bovine Serum (FBS)	ThermoFischer Scientific	Cat# 10100
B27 serum-free supplement	ThermoFischer Scientific	Cat# 17504044
Drofenine Hydrochloride	Absin	Cat# 819384
Ham's F-12 Nutrient Mix	ThermoFischer Scientific	Cat# 11765054
REAGENT or RESOURCE	SOURCE	IDENTIFIER
Penicillin-Streptomycin	ThermoFischer Scientific	Cat# 15140148
Dulbecco's Modified Eagle's Medium	Hyclone	Cat# SH30022.01B
Puromycin	Beyotime	Cat# ST551
RIPA Lysis Buffer	Beyotime	Cat# P0013D
Collagenase from Clostridium histolyticum	Sigma-Aldrich	Cat# C0130
Poly-d-Lysine (PDL)	Solarbio	Cat# D6790
4% paraformaldehyde	Solarbio	Cat# P1110
Toluidine Blue O	Solarbio	Cat# G3661
Dimethylsulfoxide	Sigma-Aldrich	Cat# D2650
Streptozotocin	Sigma-Aldrich	Cat# S0130
Polysorbate 80	Sigma-Aldrich	Cat# 59924
viscous liquid	Sigma-Aldrich	Cat# P7949
Sodium pyruvate	Sigma-Aldrich	Cat# 792500
L-Glutamine	Sigma-Aldrich	Cat# G3126
Thiazolyl Blue Tetrazolium Bromide	Sigma-Aldrich	Cat# M2128
Carbonyl cyanide 4-(trifluoromethoxy) phenylhydrazone	Sigma-Aldrich	Cat# C2920
Rotenone	Sigma-Aldrich	Cat# R8875
Lipofectamine 2000 Transfection Reagent	ThermoFischer Scientific	Cat# 11668019

Protease Inhibitor Cocktail (100X)	ThermoFischer Scientific	Cat# 78430
Protease and Phosphatase Inhibitor Cocktail (100X)	ThermoFischer Scientific	Cat# 78444
Oligomycin A	Broadway	Cat# 325839
PrimeScript (R) RT Master Mix	Takara Bio	Cat# RR036B
RNAiso Plus	Takara Bio	Cat# 9109
Dispase II	ThermoFischer Scientific	Cat# 17105041
Critical Commercial Assays		
BCA protein assay kit	Beyotime	Cat# P0012
Mitochondrial membrane potential assay kit with JC-1	Beyotime	Cat# C2006
Seahorse XF Cell Mito Stress Test kit	Agilent Technologies	Cat# 102416-100
One Step TUNEL Apoptosis Assay Kit	Beyotime	Cat# C1088
TNFα ELISA Kit	Nanjing Jiancheng Bioengineering Institute	Cat# H052
IL-6 ELISA Kit	Nanjing Jiancheng Bioengineering Institute	Cat# H007
IL-1β ELISA Kit	Nanjing Jiancheng Bioengineering Institute	Cat# H002
REAGENT or RESOURCE	SOURCE	IDENTIFIER
HE Staining Kit	Solarbio	Cat# G1120
DAB Kit	ZSGB-BIO	Cat# ZLI-9017
Experimental Models: Cell Lines		
CHO-Kv2.1	CLS	Cat# 603480/p693; RRID: CVCL_0214
CHO-K1	CLS	Cat# 603480/p693; RRID: CVCL_0214
Experimental Models: Mouse		
Mouse: C57BL/6	Beijing Vital River Laboratory Animal Technology Co., Ltd.	N/A
Mouse: BKS Cg-*m*$^{+/+}$*Lepr*^{db}/*J*	Model Animal Research Center of Nanjing University	N/A
Oligonucleotides		
Primers: mouse Kv2.1 Forward: TCGACAACACGTGCTGTGCT Reverse: GGCCAACTTCAGGATGCGC	Sangon Biotech	N/A

Primers: mouse β-actin Forward: TCATCACTATTGGCAACGAGC Reverse: AACAGTCCGCCTAGAAGCAC	Sangon Biotech	N/A
Kv2.1 si-RNA	QIAGEN	Cat# 1027416
Recombinant DNA		
Plasmid: pLV-EYFP-N-Kv2.1	Yao XG et al., 2013	N/A
Plasmid: pcDNA3.1a-Kv2.2	Zhou TT et al., 2016	N/A
Software and Algorithms		
GraphPad Prism 7 software	GraphPad Inc.	https://www.graphpad.com
Image J	Image J	RRID: SCR_003070

Transparent methods

1. Animals

All animals were received humane care and housed in standard cages and maintained on a 12-h light/dark cycle at an ambient temperature of 22°C. Animal-related protocols were approved by the Institutional Animal Care and Use Committees at Nanjing University of Chinese Medicine. Male C57BL/6 mice at 7 weeks of age were purchased from Beijing Vital River Laboratory Animal Technology Co., Ltd., and male BKS Cg-m+/+Leprdb/J *db/db* mice aged 17 weeks were purchased from Model Animal Research Center of Nanjing University.

Type 1 diabetic mice with DPN-Type 1 diabetic mice with DPN (STZ) were prepared according to the literature approach (Emiri et al., 2019). Briefly, seven-week-old male C57BL/6 mice were fed adaptively for one week and then induced by a single

intraperitoneal injection of STZ (Sigma Aldrich) at 150 mg/kg. Nondiabetic mice (Control, used as control animals in STZ mice-related assay. N = 12) were injected with 200 μl vehicle buffer (Na-Citrate Buffer, pH 4.5). Type 1 diabetic mice were defined as a fasting blood glucose level >16 mmol/L after STZ injection one week (Ma et al., 2014). Motor nerve conduction velocity (MNCV) was detected at Week 0, 4 and 10 post STZ injection, tactile allodynia and thermal sensitivity were detected every week and Drofenine was administrated at Week 7, 8, 9 and 10. DPN mice were defined at 12 weeks of age (4 weeks after STZ injection) through behavioral tests (insensitivity to mechanical stimulation, thermal hypoalgesia and decreased motor nerve conduction velocity, *etc*.).

Type 2 diabetic mice with DPN-Type 2 diabetic mice with DPN were prepared according to the published approach (Menichella et al., 2014) and *db/db* mice aged 18 weeks were used as type 2 diabetic mice with DPN (*db/db*). Age-matched heterozygotes mice (*db*/m) with nonpenetrant genotype were used as control animals in *db/db* mice-related assay. MNCV was detected at Week 0, 2 and 4, tactile allodynia and thermal sensitivity were detected every week and Drofenine was administrated at Week 1, 2, 3, and 4.

Normal mice-Fifteen-week-old male C57BL/6 mice were applied for the experiment. Dfe (10, 20 mg/kg) was administered by intraperitoneal injection for four weeks. Body weight and fast blood glucose of mice were measured every week, and tactile allodynia, MNCV and thermal sensitivity were monitored every week.

2. AAV9-Kv2.1-RNAi vector injection

In the current work, AAV was used in knockdown related experiments for its safety and high infection efficiency *in vivo* (Fang et al; 2012). By considering that type 1

diabetic mice may exhibit more obvious DPN-like symptoms compared with type 2 diabetic mice (Otto-Buczkowska et al., 2008; Sima et al., 2006), type 1 diabetic mice were here chosen for AAV-related assay.

For constructing adeno-associated-virus (AAV) 9-Kv2.1-RNAi, a gene sequence (5' to 3': (RNA)-CAG AGT CTG ACA GAA CTC CTA) able to significantly knock down the protein expression of Kv2.1 channel was at first *in vitro* screened in DRG neuron (Fig. S5A and B). AAV carrying the target gene was constructed in Shanghai Genechem Co., Ltd. Shanghai, China. The titer of AAV9-Kv2.1-RNAi vector was 1.29 $\times 10^{13}$ vector genomes/ml. It was diluted with saline to reach the titer of 1.7×10^{11} vector genomes/mouse. Two weeks after tail vein injection of the virus into STZ mice, mRNA and protein expression levels of Kv2.1 channel in DRG tissue were detected by RT-PCR and western blot (Fig. S5C and D).

3. Animal administration

Dfe was dissolved in physiological saline with 2% DMSO and 8% tween 80 (Vehicle buffer). STZ, *db/db* or AAV9-Kv2.1-RNAi injected STZ mice (N = 12) were daily administrated with 10 or 20 mg/kg of Dfe by intraperitoneal injection for 4 weeks. Control (N = 12) or *db/m* (N = 12) mice were administrated with the same volume of the vehicle buffer as that for DPN mice. Mice were sacrificed 4 weeks after the last administration of Dfe under sodium pentobarbital (5 mg/100g) anesthesia.

4. Weight and glucose measurements

Measurements of body weight and blood glucose levels in mice were conducted weekly according to published methods (Roy Chowdhury et al., 2012). Fasting blood glucose was obtained from tail vein using a blood glucose meter (Roche).

5. Tactile allodynia test

Tactile allodynia test was carried out according to the published approach

(Chaplan et al., 1994). Von Frey filaments were purchased from Ugo Basile, Comerio VA, Italy. A paw withdrawal of mice in response to each irritation was recorded. Each mouse was measured six times to determine the threshold, and 50% withdrawal threshold was calculated according to 50% threshold= (10^ (xf + kδ)/10,000.

6. Thermal sensitivity measurement

Thermal sensitivity measurement was carried out according to the published approach (Wang et al., 2011). Plantar thermal stimulation meter was purchased from Ugo Basile, Comerio VA, Italy. Briefly, mice were placed in a perspex enclosure with a metal mesh floor, and a movable radiant heat source was placed directly under the plantar surface of the hind paw. The paw withdrawal latency was automatically recorded from the onset of irradiation (Lamp 40 W, distance lamp to paw 40 mm, 24°C room temperature) to the withdrawal of the hind paw. The average withdrawal time of the left and right hind paws was used for statistical analysis.

7. Neurophysiological measurement

Neurophysiological measurement was carried out according to the published approaches (Wang et al., 2012; McGuire et al., 2009; Kumar et al., 2007). Mice were placed on a heated pad in a room maintained at 25°C to ensure a constant rectal temperature at 37°C. After mice were treated with intraperitoneal injection of sodium pentobarbital (5 mg/100g), the motor nerve conduction velocity (MNCV) of sciatic nerve ranging from ankle to sciatic notch was measured via bipolar electrodes with a supramaximal stimulus (3V) of 0.05 ms duration. MNCV was measured by dividing the distance between the distal and proximal ends. Calculation formula was set by: nerve conduction velocity (m/s) = distance between two points (cm) *10/latency difference between two points.

8. Measurement of regional blood flow velocity and perfused blood vessel area

Mice in each group were anesthetized with isoflurane inhalation (small animal anesthetic machine, RWD, China). The real-time regional velocity, blood flow distribution and perfused blood vessel of sciatic nerve and foot pads were detected by Laser Speckle Contrast Imaging/LSCI (RFLSI Pro, RWD, China). Regional sciatic nerve and foot pad blood flow ratios from control mice were used as baseline values. The imaging system presented blood perfusion signal with a color-coded image ranging from dark blue (low perfusion) to bright red (high perfusion). When observing the blood flow of sciatic nerve, the signal interference of surrounding tissue should be avoided as much as possible. 100 consecutive photographs were taken, and blood flow velocity and blood perfusion area were analyzed by BFI software and Image J.

9. Cell Culture

CHO cell was cultured in Dulbecco's Modified Eagle Medium (DMEM) with 10% FBS, 100 U/ml penicillin and 100 μg/ml streptomycin with 5% CO_2 at 37°C. CHO-Kv2.1 cell was cultured in DMEM medium containing 0.25 μg/ml purinomycin, 10% FBS, 100 U/ml penicillin and 100 g/ml streptomycin with 5% CO_2 at 37°C.

Primary sensory neuron (dorsal root ganglion, DRG) from adult male mice were cultured in Ham's F-12 containing 1% PS and 2% B27 based on the published approach (Roy Chowdhury et al., 2012). In all studies, neuron from normal mice was grown in defined Hams F12 medium with B27 additive including 10 mM D-glucose and 10 nM insulin, and neuron from DPN mice was maintained in medium containing 25 mM D-glucose (Gavazzi et al., 1999; Roy Chowdhury et al., 2012).

10. Kv2.1 channel inhibitor screening

Kv2.1 channel inhibitor screening was performed based on our previously published approach (Zhou et al., 2016). Briefly, the CHO cell overexpressing Kv2.1

was co-incubated with compounds in voltage-sensitive fluorescent indicators and membrane dyes. Fluorescent indicators were attached to the outside of the cell membrane and covered by membrane dyes. In the process of screening compounds, compounds were added into cell at 1:1000 and then dyed at 1:1. The compounds, dyes and cells were incubated for 30 minutes before addition of KCl (100 mM). Membrane potential assay was conducted by Flex station III instrument (Molecular Devices). The changes of potential energy were observed. Kv2.1 inhibitor was evaluated by comparison with negative control (DMSO). To exclude the effect of the discovered inhibitor on the other ion channels, the effects of compounds on potential energy were detected in normal CHO cell.

11. Electrophysiological recording assay

The whole-cell patch clamp recordings against cultured CHO-Kv2.1 cell or DRG neuron were performed at room temperature with Axopatch-200B amplifier (Molecular Devices) as described previously (Li et al., 2005). The microelectrodes fashioned from 1.5 mm thin-walled borosilicate glass with filament were pulled from Flaming/Brown type micropipette puller (P-97; SUTTER INSTRUMENT). Pipettes had resistances of 3-7 MΩ when filled with a solution as following composition: for CHO-Kv2.1 cell, 140 mM KCl, 2 mM $MgCl_2$, 10 mM EGTA, 1 mM $CaCl_2$, 10 mM HEPES (pH 7.3); for DRG neuron, 135 KCl, 3 Mg-ATP, 0.5 Na_2-ATP, 1 $CaCl_2$, 2 EGTA, 5 Glucose (pH7.3-7.4). Cell was bath perfused with a solution of the following composition: for CHO-Kv2.1 cell, 150 mM NaCl, 5 mM KCl, 0.5 mM $CaCl_2$, 1.2 mM $MgCl_2$, 10 mM HEPES (pH 7.3); for DRG neuron, 140 mM NaCl, 4 mM KCl, 2 mM $CaCl_2$, 2 mM $MgCl_2$, 10

mM HEPES, 10 mM Glucose (pH 7.3-7.4). The current signals were filtered at 1 kHz and digitized at a 10 kHz sampling frequency by using DigiData 1440 A (Molecular Devices) and analyzed with the software of pClamp 10.2 (Molecular Devices). Whole-cell currents were recorded using the protocol as follows: the holding potential was set at -80mV (for CHO-Kv2.1 cell) or -100 mV (for DRG neuron), and stepwise depolarized from -80 to 120 mV in 20 mV (for CHO-Kv2.1 cell) or -60 to +50 mV in 10 mV (for DRG neuron) increments and then repolarized to -60 mV (for CHO-Kv2.1 cell) or -100 mV (for DRG neuron). For large cell, we further performed the correction offline by recording much of empty control CHO cell (Li et al., 2002). Liquid junction potentials were less than 2 mV, and calculated using JPCalc software (Barry et al., 1994).

To record action potential, a current clamp protocol delivered several hyperpolarizing steps of increasing amplitude (20 pA increments, 400 ms duration, -50 mV holding potential) from 0 pA to 280 pA.

12. Liposome transfection assay

CHO cell was inoculated in 96-well plates, after 24 hours of culture the original culture medium was replaced by that without serum and antibiotics. Lipofectamine 2,000 was used to transfect pcDNA3.1a-Kv2.2 plasmid (1,000 ng/well) into CHO cell. Then, the cell culture medium was replaced by complete medium after 6 hours of transfection followed by overnight incubation in incubator, and subsequent experiments were carried out.

The liposome transfection assay procedures for BCHE si-RNA and TRPV3 si-RNA (1,000 ng/well) in DRG neuron were similar to those above-mentioned

approaches.

13. MTT assay

Viability of cultured cell was detected by MTT assay. Briefly, CHO-Kv2.1 cell was seeded overnight in 96-well plates at a density of 10^5 cell/well in 100 μL medium, and co-incubated with different concentrations of Dfe (5, 10, 20 μM) for 24 h. The medium was removed and added with 0.5 mg/μL MTT. After incubation at 37°C for 4 h, 100 μL of dimethyl sulfoxide (DMSO) was added to each well, and the mixture was shaken at a low speed for 10 min on a shaker to fully dissolve the formazan crystals, followed by the measurement of absorbance at 490 nm using an MI3X spectrophotometer (Molecular Devices).

14. Total neurite outgrowth assessment

Detection of neurite outgrowth was carried out by the published approach (Roy Chowdhury et al., 2012). DRG neuron from adult male mice was inoculated into a 12-well plate at 100 cell per well. After overnight adherence, cell was incubated with different concentrations of Dfe (5, 10, 20 μM) for 24 hours. The original culture medium was removed and fixed with 4% polyformaldehyde for 15 minutes, and 0.3% Triton was permeated for 5 minutes, then washed by PBS and sealed at room temperature for 1 hour. β-tubulin III antibody (1:1000; Sigma Aldrich) was incubated overnight (1:1000) at 4°C and then incubated with goat anti-mouse (1:200; Proteintech) at room temperature for 1 hour. Finally, imaging was captured under a fluorescence microscope. As shown in Fig. S11, Image J (Meijering et al., 2010) was used to quantify the neurite outgrowth of DRG neuron based on the grayscale images. Neurite picture

was at first converted to grayscale, and the background signal was subtracted. All neurites were traced and measured by freehand using Image J.

15. Mitochondrial membrane potential assay

Mitochondrial membrane potential (MMP) assay was carried out by the manufacturer's protocol (Srinivasan et al., 2000). Briefly, DRG neurons from normal mice, DPN mice or Dfe-treated DPN mice were plated in 96-well plates at a density of 20,000 cell/well and incubated for 24 h, followed by incubation with JC-1 solution (Beyotime) at 37°C in an environment protected from light for 20 min. Then, cells were washed with Hams F12 without FBS, and fluorescence data were analyzed with Microplate Reader (MD, USA). Ratio of green/red (530/590 nm) fluorescence was used as an indicator of MMP.

16. Measurement of mitochondrial respiration in DRG neuron

DRG neuron was seeded into a specialized 96-well microplates allowing for oxygen consumption rates (OCR) monitored in real time at 20,000 cell per well (Hill et al., 2009). An XF96 Analyzer (Seahorse Biosciences) was preheated at 37°C overnight the day before, and calibration solution was added into the Utility plate, followed by hydration overnight in an incubator (CO_2 free) at 37°C. Base Medium and detection solution were prepared the next day, and the required substrates (Glutamine, Glucose, Pyruvic Acid) were added. ATP synthase inhibitor Oligomycin (1 μM), uncoupling agent carbonyl cyanideptrifluorocarbonyl-cyanide methoxyphenyl hydrazine (FCCP) (0.75 μM) and respiratory chain inhibitor rotenone/antimycin A (ROT/AA) (1 μM, 1:1) were injected sequentially after medium exchange. The results were obtained after

approximately 80 minutes and analyzed using wave software. The difference of control values might be caused by the calibration of the instrument itself (Calcutt et al., 2017; Chowdhury et al., 2013).

17. Immunofluorescence

Cultured cell-based assay

DRG neuron from STZ or *db/db* mice was cultured in 12-well plate at 37°C for 24h and then fixed in 4% paraformaldehyde for 24 hours at room temperature. Annexin V/PI double staining was used to detect cell apoptosis. Images were collected under a 10-fold microscope using fluorescence microscope (Leica), Leica quantitative software was used to analyze and quantify the results.

Tissue-based assay

Sciatic nerve, epidermal foot pad and DRG tissues of mice were used for immunohistochemistry assay according to the published approach (Wang et al., 2011).

Measurement of density of intraepidermal nerve fibers (IENFs)- The epidermal foot pad tissue of mice was removed and fixed in 4% paraformaldehyde for 24 hours at room temperature. The foot pad tissue was embedded in paraffin and then cut into 6 μm-thick sections in microtome. Sections were incubated overnight at 4°C with primary antibody PGP 9.5 (1:1000; Abcom) diluted in blocking solution of 3% goat serum, followed by incubation with HRP (Horseradish peroxidase)-conjugated secondary antibody (Yeasen Biotech Co., Ltd) the next day at 37°C for 1h. Sections were washed in PBS, and DAB staining (Zsbio) was then applied to label positive intraepidermal nerve fibers. Nuclei were counter-stained with Hematoxylin (Solarbio). Images were collected under a light

microscope at 40 × magnification (Leica). Morphometric analyses were performed by IHC-Toolbox in Image J (Abramoff et al., 2004).

Measurement of myelin sheath of sciatic nerves- Sciatic nerve tissue of mice was removed and fixed in Glutaraldehyde (Solarbio) for 24 hours at room temperature. It was embedded in paraffin and then cut into 2 μm-thick sections in microtome. Sections were stained with toluidine blue to analyze the area of myelin sheath. The fields were chosen randomly, and images were collected under a light microscope at 100 × magnification (Leica). Morphometric analyses were performed by IHC-Toolbox in Image J (Abramoff et al., 2004).

Detection of apoptosis in DRG tissue-DRG tissue of mice was removed and fixed in 4% paraformaldehyde for 24 hours at room temperature. It was embedded in paraffin and then cut into 6 μm-thick sections in microtome. Sections were incubated overnight at 4°C with primary antibody NeuN (1:1000; Cell Signaling Technology) diluted in blocking solution of 3% goat serum, followed by incubation with fluorescein 596-conjugated secondary antibody (1:200, anti-rabbit, Proteintech) and tunnel (Beyotime) the next day at 37°C for 1h. Images were collected under a 63-fold microscope using laser scanning confocal microscope (Leica), leica quantitative software was used to analyze and quantify the results.

Detection of the number of NF-kB entering nuclei in DRG tissue-DRG tissue of mice was removed and fixed in 4% paraformaldehyde for 24 hours at room temperature. It was embedded in paraffin and then cut into 6 μm-thick sections in microtome. Sections were incubated overnight at 4°C with primary antibody β-tubulin III (1:1000;

Sigma Aldrich) and NF-κB (1:1000; Abcam), followed by incubation with fluorescein 596-conjugated secondary antibody and fluorescein 488-conjugated secondary antibody the next day at 37°C for 1h. Hoechst was used as a marker of nucleus. Images were collected under a 63-fold microscope using laser scanning confocal microscope (Leica). A single channel-based quantification was performed by using Leica software and the fluorescence intensity in the nucleus was focused.

Detection of the area of Kv2.1 expression in DRG tissue- DRG tissue of mice was removed and fixed in 4% paraformaldehyde for 24 hours at room temperature. It was embedded in paraffin and then cut into 6 μm-thick sections in microtome. Sections were incubated overnight at 4°C with primary antibody Kv2.1, followed by incubation with HRP (Horseradish peroxidase)-conjugated secondary antibody was carried out at 37°C for 1h. DAB staining was then applied to label Kv2.1. Nuclei were counter-stained with Hematoxylin. Images were collected under a light microscope at 100 × magnification (Leica). Morphometric analyses were performed by IHC-Toolbox in Image J (Abramoff et al., 2004).

18. RT-PCR analysis

Total RNA of DRG tissue in mice was extracted by TRIzol reagent. 1 μg mRNA was used to reverse transcribe into cDNA, and the reverse transcriptional procedure was at 37°C for 15 min. cDNA was detected using SYBR Premix Ex Taq kit and a Bio-Rad CFX connect real-time system machine. Results were normalized to mRNA levels of β-actin.

19. Western blot assay

Protein samples were obtained from DRG tissue of mice. SDS-PAGE sampling buffer (25% SDS, 62.5mM Tris, 25% glycerol, 0.1% bromofenblue, pH 6.8) was used for protein collection. Proteins were electrophoretized, transferred and blocked, while incubated with antibodies to the following proteins (KEY RESOURCES TABLE). Total extracellular regulated protein kinase (T-ERK) was used as a loading control for its good stability in DRG tissue (Fernyhough et al., 1999; Calcutt et al., 2017). Finally, the horseradish peroxidase (HRP) substrate was incubated for 5 minutes, and the signals were collected using the Tanon-5200 Multi luminescent imaging system. Quantity One software was used for all protein band quantification.

20. Jess-based analysis of protein

Protein samples were obtained from DRG tissue of STZ mice. After digestion, DRG neuron was filtered by 40 μM cell sieve, and large and small DRG neurons were isolated. Samples were run undilutedly on a 12-230 kDa separation module according to the manufacturer's instructions. Data were analyzed with Compass software version 4.0.0 (ProteinSimple). For analysis on the Jess system from ProteinSimple, antibodies of anti-Kv2.1 (Abcam; ab192761; 1:50), anti-TRKA (Bioss; bs-0193R; 1:50), anti-TRKC (Proteintech; 111999-1-AP; 1:50) and anti-ERK (Cell Signaling Technology; 9102; 1:200) were used.

21. Pharmacokinetic analysis of Dfe

Dfe level in DRG tissue or plasma of mice was detected by using a Thermo TSQ Vantage tandem mass spectrometer coupled with an HPLC model U3000 apparatus (Dionex, San Jose, CA). Dfe was administered intraperitoneally (20 mg/kg) in normal

mice. Blood was taken from the orbit at 0 min, 15 min, 90 min, 4 h, 8 h, and 12 h after administration. DRG tissue was taken at 0 min, 15 min, 90 min, 4 h, 8 h, 12 h, and 24 h after administration. Blood was placed in a tube prepared in advance with heparin sodium (0.3% heparin sodium, 10 μL), and then centrifuged at 8,000 rpm at 4°C for 5 min. The upper plasma was transferred to a pre-cooled EP tube and stored at 4°C for testing. DRG tissue was taken into a 1.5 mL EP tube containing 1 mL of saline in advance, and then centrifuged at 4,000 rpm for 2 minutes to discard the upper saline. DRG tissue in each tube was weighted and stored at -20°C. Methanol was used to precipitate protein and extract analyte, and Dfe concentration in plasma or DRG tissue was assessed by LC-MS/MS.

22. ELISA assay

Inflammatory cytokines IL-6, IL-1β and TNFα in the serum of mice were quantified according to mouse ELISA kit instructions (Nanjing Jiancheng Bioengineering Institute). Samples of mouse serum were separately incubated in a plate coated with TNFα, IL-6, IL-1β antibody at 37°C for 30 minutes, and then HRP secondary antibody was added and incubated at 37°C for 30 minutes. Next, solution A and solution B were added and incubated for 10 minutes, and finally the stop solution was added to stop the reaction. Normal color development and reading protocol as per ELISA plate reader manufacturer's directions were followed.

23. Data analysis

All experiments performed were blind to group assignment. All data in the current work were plotted, analyzed by GraphPad Prism 7 software (except for special

instructions) and shown as mean ± sem. Unpaired 2-tailed Student's t test was used for two-group comparison. One-way ANOVA with post hoc comparisons using Tukey's or Dunnett's post hoc tests was used for at least three groups' comparisons. P value of less than 0.05 was considered statistically significant.

Supplemental References

Abramoff, M.D., Magelhaes, P.J., and Ram, S.J. (2004). Image Processing with ImageJ. Brief. Bioinform. *11*, 36-42.

Barry, P.H. (1994). JPCalc, a software package for calculating liquid junction potential corrections in patch-clamp, intracellular, epithelial and bilayer measurements and for correcting junction potential measurements. J. Neurosci. Methods. *51*, 107-116.

Chaplan, S.R., Bach, F.W., Pogrel, J.W., Chung, J.M., and Yaksh, T.L. (1994). Quantitative assessment of tactile allodynia in the rat paw. J. Neurosci. Methods. *53*, 55-63.

Emiri MiuraTELura, Tsunekawa, S., Naruse, K., Nakamura, N., and Kamiya, H. (2019). Secreted factors from cultured dental pulp stem cell promoted neurite outgrowth of dorsal root ganglion neuron and ameliorated neural functions in streptozotocin-induced diabetic mice. J. Diabetes. Investig. DOI: 10.1111/jdi.13085.

Fang, H.F., Lai, N.C., Gao, M.H., Miyanohara, A., Roth, D.M., Tang, T., Hammond, H.K. (2012). Comparison of Adeno-Associated Virus Serotypes and Delivery Methods for Cardiac Gene Transfer. Hum Gene Ther Methods. *23(4)*: 234-241.

Gavazzi, I., Kumar, R.D.C., Mcmahon, S.B., and Cohen, J. (1999). Growth responses of different subpopulations of adult sensory neuron to neurotrophic factors. Eur. J. Neurosci. *11*, 3405-3414.

Hill, B.G., Dranka, B.P., Zou, L., Chatham, J.C., and Darley-Usmar, V.M. (2009). Importance of the bioenergetic reserve capacity in response to cardiomyocyte stress induced by 4-hydroxynonenal. Biochem. J. *424*, 99-107.

Kumar, A., Kaundal, R.K., Iyer, S., and Sharma, S.S. (2007). Effects of resveratrol on nerve functions, oxidative stress and DNA fragmentation in experimental diabetic neuropathy. Life. Sci. *80*, 1236-1244.

Li, Y., Gamper, N., Hilgemann, D.W., and Shapiro, M.S. (2005). Regulation of Kv7 (KCNQ) K+ channel open probability by phosphatidylinositol 4,5-bisphosphate. J. Neurosci. *25*, 9825-9835.

Li, Y., Hu, G.Y., and Huperzine, A. (2002). A nootropic agent, inhibits fast transient potassium current in rat dissociated hippocampal neuron. Neurosci. Lett. *324*, 25-28.

Ma, J., Farmer, K.L., Pan, P., Urban, M.J., Zhao, H., Blagg, B.S., and Dobrowsky, R.T. (2014). Heat shock protein 70 is necessary to improve mitochondrial bioenergetics and reverse diabetic sensory neuropathy following ku-32 therapys. J. Pharmacol. Exp. Ther. *348*, 281-292.

McGuire, J.F., Rouen, S., Siegfreid, E., Wright, D.E., and Dobrowsky, R.T. (2009). Caveolin-1 and altered neuregulin signaling contribute to the pathophysiological progression of diabetic peripheral neuropathy. Diabetes *58*, 2677-2686.

Meijering, E. (2010). Neuron Tracing in Perspective. Cytometry A. *77*, 693-704.

Menichella, D.M., Abdelhak, B., Ren, D., Shum, A., Frietag, C., and Miller, R.J. (2014). CXCR4 chemokine receptor signaling mediates pain in diabetic neuropathy. Mol. Pain. *10*, 42.

Otto-Buczkowska, E., Kazibutowska, Z., Sołtyk, J., Machnica, Łukasz. Neuropathy and type 1 diabetes mellitus. (2008). J. Pediatr. Endocr. Met. *4(2)*, 109-116.

Roy Chowdhury, S.K., Smith, D.R., Saleh, A., Schapansky, J., Marquez, A., Gomes, S., Akude, E., Morrow, D., Calcutt, N.A., and Fernyhough, P. (2012). Impaired adenosine monophosphate-activated protein kinase signalling in dorsal root ganglia neuron is linked to mitochondrial dysfunction and peripheral neuropathy in diabetes. Brain *135*, 1751-1766.

Sima, A.A.F., and Kamiya, H. Diabetic Neuropathy Differs in Type 1 and Type 2 Diabetes. (2006). Ann. Ny. Acad. Sci. *1084*, 235-249.

Wang, L., Chopp, M., Szalad, A., Liu, Z., and Zhang, Z.G. (2011). Phosphodiesterase-5 is a therapeutic target for peripheral neuropathy in diabetic mice. Neuroscience *193*, 399-410.

Wang, L., Chopp, M., and Zhang, Z.G. (2012). Thymosin β4 Promotes the Recovery of Peripheral Neuropathy in Type II Diabetic Mice. Neurobiol. Dis. *48*, 546-55.

Zhou, T.T., Quan, L.L., Chen, L.P., Du, T., Sun, K.X., Zhang, J.C., Yu, L., Li, Y., Wan, P., Chen, L.L., et al. (2016). Sp6616 as a new kv2.1 channel inhibitor efficiently promotes β-cell survival involving both PKC/Erk1/2 and CaM/PI3K/Akt signaling

pathways. Cell Death Dis. *7*, e2216.